

CONSOLIDATION CHARACTERISTICS OF UNSATURATED SOIL

A THESIS SUBMITTED TO
THE DEPARTMENT OF BUILDING AND
CONSTRUCTION ENGINEERING OF THE UNIVERSITY
OF TECHNOLOGY IN PARTIAL FULFILLMENT OF THE
REQUIREMENTS FOR THE DEGREE OF MASTER
OF SCIENCE IN CIVIL ENGINEERING
(GEOTECHNICAL ENGINEERING)

BY
FIRAS JAWAD KADHIM
(B.Sc Building and Construction Eng. 2003)

Supervised By
Asst. Prof. Dr. Mohammed Yousif Fattah

MAY 2008

Jumada Al-Awal 1429

بِسْمِ اللَّهِ الرَّحْمَنِ الرَّحِيمِ

وَمَا أَوْتَيْتُمْ مِنَ الْعِلْمِ ۖ إِلَّا قَلِيلًا

صدق الله العظيم

سورة الإسراء الآية 85

This is to certify that I have read this thesis titled (Consolidation Characteristics of Unsaturated Soil). The thesis is now qualified for debate as far as Language is concerned.

Signature:

Name: Eyad shamsadden

Title: Ass. Prof.

Date:

Certification

I certify that this thesis titled (**Consolidation Characteristics of Unsaturated Soil**) was prepared by **Firas Jawad Kadhim** under my supervision at the Building and Construction Engineering Department, University of Technology, in a partial fulfillment of the requirements for the Degree of Master in Geotechnical Engineering.

Signature:

Dr. Mohammed Y. Fattah

Date: / /

In a view of the available recommendation, I forward this thesis for debate by the examining committee.

Signature:

Dr. Mohammed Y. Fattah

Head of the Highway and Bridge Engineering Branch

Data: / /

Abstract

The most common two-phase problem in porous media is the flow of air and water. This is for example found in the unsaturated zone, where water infiltrates through partly saturated pores to the groundwater. Liquid flow in the unsaturated zone is controlled by a combination of gravitational, capillary, and viscous forces.

The mechanical behaviour of partially saturated soils can be very different from that of fully saturated soils. It has long been established that for such soils, changes in suction do not have the same effect as changes in the applied stresses, and consequently the effective stress principle is not applicable. Conventional constitutive models, which are based on this principle, are therefore of limited use when analyzing geotechnical problems that involve the presence of partially saturated soil zones.

In this thesis, Al-Mdaina trial embankment was the problem this work deals with. The finite element programs SIGMA/W and SEEP/W was used, and eight noded isoparametric quadrilateral elements are used for modelling both the soil skeleton and pore water pressure. Parametric study was carried out and different parameters were changed to find their effects on behaviour of partially saturated soil. These parameters include the modulus of elasticity of the soil (E), hydraulic conductivity (k) and the unsaturated soil modulus (H).

It is concluded that the effect of modulus of elasticity on the behaviour of unsaturated soil is apparent at early stages of consolidation and diminishes when the time proceeds. When the clay layer consists of soft clay ($E_{\text{soil}} < 10000 \text{ kN/m}^2$), the effect of unsaturated soil is apparent, while effect of the modulus of elasticity diminishes when the soil is stiff.

And it is also concluded that the excess pore water pressure of fully saturated soil is greater than that of partially saturated soil and dissipation starts at fast rate and becomes slow with time. In addition the vertical displacement of fully saturated soil is greater than that of partially saturated soil.

It can be concluded that the failure potential of unsaturated soil is less than that for fully saturated soil since that the deviatoric stress ($\sigma_1 - \sigma_3$) at all stages of consolidation is smaller.

Acknowledgements

In the name of God the Most Compassionate and the Most Merciful. All my praise be to Allah, the Lord of the world.

I would like to thank my supervisor Dr. Mohammed Y. Fattah for his guidance, encouragement and assistance until this thesis is finished.

I would like to thank my parents for their support and understanding without which I would not have managed to complete this thesis.

Finally I would like to thank my uncle for his encouragement and support.

CONTENTS

	<u>Page</u>
Abstract	I
Acknowledgements	III
Contents	IV
Notation	VIII
List of Figures	XII
List of Tables	XXII

CHAPTER ONE- INTRODUCTION

1.1 General.	1
1.2 Consolidation Process.	2
1.3 Settlement.	3
1.3.1 Immediate settlement.	3
1.3.2 Primary consolidation.	4
1.3.3 secondary compression.	4
1.4 Consolidation theory.	4
1.4.1 One dimensional consolidation theory (Terzaghi's theory).	4
1.4.2 Biot's Theory.	6
1.5 Scope of Thesis.	6
1.6 Thesis Layout.	7

CHAPTER TWO- LITERATURE REVIEW

1 Introduction.	8
2.2 Subsurface Water.	9
2.2.1 Saturation zone.	9
2.2.2 Aeration zone.	10
2.2.2.1 Capillary fringe.	10

2.2.2.2 Intermediate belt.	11
2.2.2.3 Soil belt.	11
2.3 Gradual Emergence of Unsaturated Soil Mechanics.	11
2.4 Unsaturated Soil as a Four-Phase Mixture.	13
2.5 Distinctive Features of the Contractile Skin.	14
2.6 Previous Works on Unsaturated Soils.	16

CHAPTER THREE- FUNDAMENTAL CONSTITUTIVE
RELATIONS FOR UNSATURATED SOILS

Introduction.	34
3.2 Water Seepage Constitutive Relations.	35
3.3 Ability of an Unsaturated Soil for Storage	40
3.4 Air Flow Constitutive Relations.	40
3.5 Shear Strength Constitutive Relations.	43
3.5.1 State surfaces.	43
3.6 Volume–Mass Constitutive Relations.	50
3.7 Definition of Unsaturated Soil in the Present Work	56

CHAPTER FOUR-FINITE ELEMENT FORMULATION FOR
CONSOLIDATION PROBLEMS

Introduction.	57
4.2 Element Shape.	57
4.3 Higher Order Elements.	59
4.4 Consolidation Analysis.	59
4.4.1 Coordinate Systems.	60
4.4.2 Field Variable Model.	62
4.4.3 Derivatives of Interpolating Functions.	63
4.4.4 Finite Element Equations.	64

4.4.5 Strain-Displacement Matrix.	66
4.4.6 Elastic Constitutive Relationship.	67
4.4.7 Body Forces.	68
4.5 Soil-Pore Fluid Interaction (The problem and the governing equations).	68
4.6 Additional Material Properties for Unsaturated Coupled Analysis.	71
CHAPTER FIVE - TECHNICAL OVERVIEW ON THE COMPUTER PROGRAM AND VERIFICATIONS	
5.1 Introduction.	73
5.2 The program SIGMA/W.	73
5.3 The Program Applications.	73
5.3.1 Deformation Analysis.	74
5.3.2 Embankment/Excavation Construction.	74
5.3.3 Excess Pore-Water Pressures.	74
5.3.4 Soil-Structure Interactions.	74
5.3.5 Consolidation Analyses.	75
5.4 Load and Deformation Analysis.	75
5.4.1 Constitutive Models.	75
5.4.2 Material Models in an Unsaturated Consolidation Analysis.	77
5.4.3 H-Modulus Function in a Consolidation Analysis.	77
5.4.4 Total and Effective Stresses.	78
5.4.5 Boundary Conditions.	80
5.4.6 Finite Element Implementation.	81
5.5 KeyIn Initial Water Table.	81
5.6 KeyIn Functions Conductivity.	82

5.7 Negative Pore-Water Pressure	84
5.8 Verification.	84
CHAPTER SIX – RESULTS AND DISCUSSIONS	
6.1 Introduction.	89
6.2 Problem Description.	89
6.3 Problem Profile .	89
6.4 Modelling and Material Properties.	90
6.5 Analysis and Results.	91
6.5.1 Pore Water Pressure.	92
6.5.2 Vertical displacement.	99
6.5.3 Horizontal displacement.	103
6.5.4 Contour Lines of Pore Water Pressure.	108
6.5.5 Contour Lines of Vertical displacement.	113
6.5.6 Contour Lines of Deviatoric Stress.	120
6.5.7 Vertical displacement along center line of the embankment.	125
6.5.8 Pore water pressure vs. hydraulic conductivity.	128
6.5.9 Vertical displacement vs. hydraulic conductivity.	133
6.5.10 Pore water vs. time with H- modulus.	137
6.5.11 Vertical displacement vs. time with H- modulus.	140
CHAPTER SEVEN - CONCLUSIONS AND RECOMMENDATIONS	
7.1 Conclusions.	142
7.2 Recommendations.	143
REFERENCES	145

NOTATION

<u>Symbol</u>	<u>Definition</u>
A	Area along the boundary of an element.
{a}	Column vector of nodal incremental x- and y-displacements.
[B]	Strain-displacement matrix.
b	Unit body force intensity.
b_v	The body force in the vertical direction.
C	damping.
[C]	Constitutive matrix.
C_v	Coefficient of consolidation.
C_3	The coefficient of consolidation under three-dimensional strain condition.
C_c	Compressive index.
c'	Effective cohesion intercept.
[D]	The constitutive (element property) matrix.
D_{ax} , D_{ay} , and D_{az}	Air diffusivity in the x, y, and z directions, respectively.
dV_s	The change in volume of the soil particles.
dV_v	The change in the volume of voids.
E	The stiffness of the material.
E	Young's modulus.
e_o	Initial void ratio.
{F}	Applied nodal incremental force.
{ F_b }	Incremental body forces.
{ F_n }	Concentrated nodal incremental loads.
{ F_s }	Force due to surface boundary incremental pressures
f	Force matrices.

f_1	Soil property function defining the relationship between shear strength and soil suction.
g	Acceleration due to gravity.
H	The unsaturated modulus.
h	Hydraulic head.
[J]	The Jacobian matrix.
[J] ⁻¹	The inverse of the Jacobian.
K	The standard stiffness matrix.
[K]	Element characteristic (or stiffness) matrix.
k	The permeability.
k_a	The air coefficient of permeability.
k	A soil constant.
$k_{wx}, k_{wy}, \text{ and } k_{wz}$	Coefficients of permeability for each of the cartesian coordinate directions.
M	A material characteristic independent of stresses.
M	Mass.
$m_{ax}, m_{ay}, \text{ and } m_{az}$	Flow rate in the x, y, and z directions, respectively.
M_s	A functions of matric suction.
<N>	Interpolation functions evaluated at the given point.
n	The porosity of the soil.
p	Incremental surface pressure.
p	The pressure of the fluid.
p	Any total stress state under consideration.
p_o	Initial total stress.
Q	Related to the compressibility of the fluid.
R	Radial distance.
S_r	Degree of saturation.
t	Time.
t	Thickness.

$\{U\}$	x-displacement at the nodes of the element.
\tilde{u}	The displacement discretization parameters.
u	x-displacement at the given location.
u_a	The pore pressure of the air in the soil.
u_w	The pore pressure of the water.
$\{V\}$	y-displacement at the nodes of the element.
v	Volume of an element.
v	y-displacement at the given location.
v_a	Velocity of flow.
$v_{wx}, v_{wy}, \text{ and } v_{wz}$	Velocity of water flow in the x, y, and z directions, respectively.
$v_{ax}, v_{ay}, \text{ and } v_{az}$	Velocity of air flow in the x, y, and z directions, respectively.
W	Water content.
$\{X\}$ and $\{Y\}$	The global x y coordinates of the element nodes.
Y	Elevation head.

Greek

ϵ	Strain.
ϵ_v	The volumetric strain.
ϵ_x, ϵ_y	Longitudinal strain in the (x, y) directions, respectively.
γ_s	Unit weight of soil.
γ_{xy}	Shear strain in the x-y plane.
ρ	Mass density.
ρ_w	Density of water.
K	Slope of unload-reload lines in $v:\ln(p')$.
μ_s	A functions of matric suction.
ν	Poisson's ratio.

σ	The stress.
σ'	Effective stress.
σ_n	Total normal stress on the failure plane at failure.
$\sigma_x, \sigma_y, \sigma_z$	The total stress increment in x, y and z direction, respectively.
$\sigma_1, \sigma_2, \text{ and } \sigma_3$	The principal stresses.
τ	Shear strength.
ϕ'	Effective angle of internal friction.
ϕ^b	The angle of friction with respect to change in suction.
λ	Slope of isotropic compression line in $v:\ln(p')$.

LIST OF FIGURES

<u>Figure</u>	<u>Page</u>
Fig. (2.1) Tendency of the water table to follow the earth's surface (Smith and Smith, 1998).	10
Fig. (2.2) Diagram illustrating types of subsurface water (Smith and Smith, 1998).	11
Fig. (2.3) Density distribution across the contractile skin reprinted from liquid–fluid interface, (Lyklema , 2000).	15
Fig. (2.4) Geometry of the steady state flows problem a) Dam with horizontal drain b) Dam with no horizontal drain.	24
Fig. (2.5) Permeability function for analyzing steady state seepage through a dam.	25
Fig. (2.6) Seepage through an isotropic earth dam with a horizontal drain under steady state infiltration ,(Abdul Kareem Asmat Zainai, 2002)	26
Fig. (2.7) Results obtained from the saturated/unsaturated flow regime analysis (Abdul Kareem Asmat Zainai, 2002).	27
Fig. (2.8) Finite element mesh (after Saif , 2006).	30
Fig. (2.9) Lateral movement predicted of the wall for different degrees of saturated.	32
Fig. (2.10) Predicted wall bending moment for different degrees of saturation.	32
Fig. (2.11) Surface movement predicted of the soil for different degrees of saturation.	33
Fig. (3.1) Shape of the drying and wetting permeability function for glass beads tested by Mualem (1976).	37
Fig.(3.2) The soil–water characteristic curve for the glass beads showing hysteresis during drying and wetting (Mualem, 1976).	37

Fig.(3.3) Example of permeability and water storage functions for an anisotropic soil (Fredlund,2006).	39
Fig. (3.4) Air permeability function estimated from the SWCC (Ba-Te et al., 2005).	42
Fig.(3.5) Extended Mohr-Coulomb failure surface written as a function of the stress state (Fredlund et al. 1978).	44
Fig.(3.6) Curvature to the shear strength envelope with respect to matric suction.	45
Fig.(3.7) Shear strength results showing the relationship between the SWCC and the peak shear strength of a soil (Melinda et al., 2004).	46
Fig.(3.8) Critical state shear strength results on compacted kaolin (Wheeler and Sivakumar, 1995).	47
Fig. (3.9) State surface plots (based on Matyas and Radhakrishna , 1968).	49
Fig.(3.10) Reference compression curves for a saturated soil (Fredlund, 2006).	51
Fig. (3.11) Illustration of the limiting or bounding relationships for a typical clayey silt soil (Fredlund, 2006).	52
Fig. (3.12) Volume–mass constitutive surfaces for Beaver Creek sand (Pham, 2005).	54
Fig. (3.13) Volume–mass constitutive surfaces for Regina clay(Pham ,2005).	55
Fig. (3.14) A Typical H-modulus function (Manual user's guide of SIGMA/W).	56
Fig. (4.1) Element Slopes and Performance.	58
Fig. (4.2) Global and Local Coordinate Systems.	61
Fig.(5.1) Linear Elastic.	76
Fig.(5.2) Nonlinear Elastic (Hyperbolic).	76
Fig.(5.3) Anisotropic Linear Elastic.	76

Fig.(5.4) Strain-Softening.	76
Fig.(5.5) Elastic Plastic (Mohr-Coulomb or Tresca).	76
Fig.(5.6) Cam-Clay model (Critical state).	77
Fig.(5.7) Modified Cam-clay model (Critical State).	77
Fig. (5.8) H-Modulus as a Function of Pore-Water Pressure (Manual user's guide of SIGMA/W, 2002).	78
Fig. (5.9) Example of Pore Pressure B Function (Manual user's guide of SIGMA/W, 2002).	79
Fig. (5.10) Examples of Pore Pressure A Function (Manual user's guide of SIGMA/W, 2002).	79
Fig. (5.11) Sample of Boundary Conditions (Manual user's guide of SIGMA/W, 2002).	80
Fig. (5.12) Calculation of Initial Pore-Water Pressure (Manual user's guide of SIGMA/W, 2002).	82
Fig. (5.13) A Conductivity Function (Manual user's guide of SEEP/W, 2002).	83
Fig. (5.14) Problem geometry (Lambe and Whitman, 1979).	84
Fig. (5.15) Finite element mesh of the problem.	86
Fig. (5.16) The relationship between the pore water pressure and depth.	86
Fig. (5.17) The relationship between the total stress and depth.	86
Fig. (5.18) Contour lines of vertical settlement.	87
Fig. (5.19) Contour lines of vertical stress.	87
Fig. (5.20) Contour lines of volumetric strain.	88
Fig. (6.1) Cross-section of Al-Mdaina trial embankment.	90
Fig. (6.2) Finite element mesh of Al-Mdaina trial embankment.	92
Fig. (6.3) The relation between (u_p/u_f) and soil modulus of elasticity at point (A) with water table at (2 m) from the ground level.	93
Fig. (6.4) The relation between (u_p/u_f) and soil modulus of elasticity	

at point (A) with water table at (4 m) from the ground level.	93
Fig. (6.5) The relation between (u_p/u_f) and soil modulus of elasticity at point (A) with water table at (6 m) from the ground level.	94
Fig. (6.6) The relation between (u_p/u_f) and soil modulus of elasticity at point (A) with water table at (8 m) from the ground level.	94
Fig. (6.7) The relation between (u_p/u_f) and soil modulus of elasticity at point (B) with water table at (2 m) from the ground level.	94
Fig. (6.8) The relation between (u_p/u_f) and soil modulus of elasticity at point (B) with water table at (4 m) from the ground level.	95
Fig. (6.9) The relation between (u_p/u_f) and soil modulus of elasticity at point (B) with water table at (6 m) from the ground level.	95
Fig. (6.10) The relation between (u_p/u_f) and soil modulus of elasticity at point (B) with water table at (8 m) from the ground level.	95
Fig. (6.11) The relation between $(\delta_{vp}/\delta_{vf})$ and soil modulus of elasticity at point (A) with water table at (2 m) from the ground level.	100
Fig. (6.12) The relation between $(\delta_{vp}/\delta_{vf})$ and soil modulus of elasticity at point (A) with water table at (4 m) from the ground level.	100
Fig. (6.13) The relation between $(\delta_{vp}/\delta_{vf})$ and soil modulus of elasticity at point (A) with water table at (6 m) from the ground level.	101
Fig. (6.14) The relation between $(\delta_{vp}/\delta_{vf})$ and soil modulus of elasticity at point (A) with water table at (8 m) from the ground level.	101
Fig. (6.15) The relation between $(\delta_{vp}/\delta_{vf})$ and soil modulus of elasticity at point (B) with water table at (2 m) from the ground level.	101
Fig. (6.16) The relation between $(\delta_{vp}/\delta_{vf})$ and soil modulus of elasticity at point (B) with water table at (4 m) from the ground level.	102
Fig. (6.17) The relation between $(\delta_{vp}/\delta_{vf})$ and soil modulus of elasticity at point (B) with water table at (6 m) from the ground level.	102
Fig. (6.18) The relation between $(\delta_{vp}/\delta_{vf})$ and soil modulus of elasticity at point (B) with water table at (8 m) from the ground level.	102

Fig. (6.19) The relation between $(\delta_{hp}/\delta_{hf})$ and soil modulus of elasticity at point (A) with water table at (2 m) from the ground level.	105
Fig. (6.20) The relation between $(\delta_{hp}/\delta_{hf})$ and soil modulus of elasticity at point (A) with water table at (4 m) from the ground level.	105
Fig. (6.21) The relation between $(\delta_{hp}/\delta_{hf})$ and soil modulus of elasticity at point (A) with water table at (6 m) from the ground level.	106
Fig. (6.22) The relation between $(\delta_{hp}/\delta_{hf})$ and soil modulus of elasticity at point (A) with water table at (8 m) from the ground level.	106
Fig. (6.23) The relation between $(\delta_{hp}/\delta_{hf})$ and soil modulus of elasticity at point (B) with water table at (2 m) from the ground level.	106
Fig. (6.24) The relation between $(\delta_{hp}/\delta_{hf})$ and soil modulus of elasticity at point (B) with water table at (4 m) from the ground level.	107
Fig. (6.25) The relation between $(\delta_{hp}/\delta_{hf})$ and soil modulus of elasticity at point (B) with water table at (6 m) from the ground level.	107
Fig. (6.26) The relation between $(\delta_{hp}/\delta_{hf})$ and soil modulus of elasticity at point (B) with water table at (8 m) from the ground level.	107
Fig. (6.27) Contour lines of pore water pressure (kPa) of fully saturated soil after 1 day.	108
Fig. (6.28) Contour lines of pore water pressure (kPa) of fully saturated soil after 190 days.	108
Fig. (6.29) Contour lines of pore water pressure (kPa) of fully saturated soil after 2000 days.	109
Fig. (6.30) Contour lines of pore water pressure (kPa) of partially saturated soil with water table at (2 m) from the ground level after 1 day.	109
Fig. (6.31) Contour lines of pore water pressure (kPa) of partially saturated soil with water table at (2 m) from the ground level after 190 days.	110
Fig. (6.32) Contour lines of pore water pressure (kPa) of partially	

saturated soil with water table at (2 m) from the ground level after 2000 days.	110
Fig. (6.33) Contour lines of pore water pressure (kPa) of partially saturated soil with water table at (6 m) from the ground level after 1 day.	111
Fig. (6.34) Contour lines of pore water pressure (kPa) of partially saturated soil with water table at (6 m) from the ground level after 190 day.	111
Fig. (6.35) Contour lines of pore water pressure (kPa) of partially saturated soil with water table at (6 m) from the ground level after 2000 day.	112
Fig. (6.36) Contour lines of vertical displacement (m) of fully saturated soil after 1 day.	113
Fig. (6.37) Contour lines of vertical displacement (m) of fully saturated soil after 190 days.	114
Fig. (6.38) Contour lines of vertical displacement (m) of fully saturated soil after 1500 days.	114
Fig. (6.39) Contour lines of vertical displacement (m) of fully saturated soil after 5000 days.	115
Fig. (6.40) Contour lines of vertical displacement (m) of partially saturated soil with water table at (2 m) from the ground level after 1 day.	115
Fig. (6.41) Contour lines of vertical displacement (m) of partially saturated soil with water table at (2 m) from the ground level after 190 days.	116
Fig. (6.42) Contour lines of vertical displacement (m) of partially saturated soil with water table at (2 m) from the ground level after 1500 days.	116
Fig. (6.43) Contour lines of vertical displacement (m) of partially	

saturated soil with water table at (2 m) from the ground level after 5000 days.	117
Fig. (6.44) Contour lines of vertical displacement (m) of partially saturated soil with water table at (6 m) from the ground level after 1 day.	117
Fig. (6.45) Contour lines of vertical displacement (m) of partially saturated soil with water table at (6 m) from the ground level after 190 days.	118
Fig. (6.46) Contour lines of vertical displacement (m) of partially saturated soil with water table at (6 m) from the ground level after 1500 days.	118
Fig. (6.47) Contour lines of vertical displacement(m) of partially saturated soil with water table at (6 m) from the ground level after 5000 days.	119
Fig. (6.48) Contour lines of deviatoric stress (kN/m^2) at fully saturated soil after 1 day.	121
Fig. (6.49) Contour lines of deviatoric stress (kN/m^2) at fully saturated soil after 190 days.	121
Fig. (6.50) Contour lines of deviatoric stress (kN/m^2) at fully saturated soil after 1500 days.	122
Fig. (6.51) Contour lines of deviatoric stress (kN/m^2) of partially saturated soil with water table at (2 m) from the ground level after 1 day.	122
Fig. (6.52) Contour lines of deviatoric stress (kN/m^2) of partially saturated soil with water table at (2 m) from the ground level after 190 days.	123
Fig. (6.53) Contour lines of deviatoric stress (kN/m^2) of partially saturated soil with water table at (2 m) from the ground level after 1500 days.	123

- Fig. (6.54) Contour lines of deviatoric stress (kN/m^2) of partially saturated soil with water table at (6 m) from the ground level after 1 day. 124
- Fig. (6.55) Contour lines of deviatoric stress (kN/m^2) of partially saturated soil with water table at (6 m) from the ground level after 190 day. 124
- Fig. (6.56) Contour lines of deviatoric stress (kN/m^2) of partially saturated soil with water table at (6 m) from the ground level after 1500 day. 125
- Fig. (6.57) Distribution of the vertical displacement along the center line of the embankment with time (fully saturated). 126
- Fig. (6.58) Distribution of the vertical displacement along the center line of the embankment with time (W.T. 2 m from the ground level). 126
- Fig. (6.59) Distribution of the vertical displacement along the center line of the embankment with time (W.T. 6 m from the ground level). 127
- Fig. (6.60) The relation between (u_p/u_f) and soil hydraulic conductivity at point (A) when water table is at (2 m) from the ground level. 129
- Fig. (6.61) The relation between (u_p/u_f) and soil hydraulic conductivity at point (A) when water table is at (4 m) from the ground level. 129
- Fig. (6.62) The relation between (u_p/u_f) and soil hydraulic conductivity at point (A) when water table is at (6 m) from the ground level. 130
- Fig. (6.63) The relation between (u_p/u_f) and soil hydraulic conductivity at point (B) when water table is at (2 m) from the ground level. 130
- Fig. (6.64) The relation between (u_p/u_f) and soil hydraulic conductivity at point (B) when water table is at (4 m) from the

ground level.	131
Fig. (6.65) The relation between (u_p/u_f) and soil hydraulic conductivity at point (B) when water table is at (6 m) from the ground level.	131
Fig. (6.66) The relation between $(\delta_{vp}/\delta_{vf})$ and soil hydraulic conductivity at point (A) when water table is at (2 m) from the ground level.	134
Fig. (6.67) The relation between $(\delta_{vp}/\delta_{vf})$ and soil hydraulic conductivity at point (A) when water table is at (4 m) from the ground level.	134
Fig. (6.68) The relation between $(\delta_{vp}/\delta_{vf})$ and soil hydraulic conductivity at point (A) when water table is at (6 m) from the ground level.	135
Fig. (6.69) The relation between $(\delta_{vp}/\delta_{vf})$ and soil hydraulic conductivity at point (B) when water table is at (2 m) from the ground level.	135
Fig. (6.70) The relation between $(\delta_{vp}/\delta_{vf})$ and soil hydraulic conductivity at point (B) when water table is at (4 m) from the ground level.	136
Fig. (6.71) The relation between $(\delta_{vp}/\delta_{vf})$ and soil hydraulic conductivity at point (B) when water table is at (6 m) from the ground level.	136
Fig. (6.72) H1-modulus function.	138
Fig. (6.73) H2-modulus function.	138
Fig. (6.74) H3-modulus function.	139
Fig. (6.75) The variation of pore water pressure with time at point (A) considering different H-modulus functions.	139
Fig. (6.76) The variation of pore water pressure with time at point (B) considering different H-modulus functions.	140

Fig. (6.77) The relation between vertical displacement and time at point (A) considering different H-modulus functions.	140
Fig. (6.78) The relation between vertical displacement and time at point (B) considering different H-modulus functions.	141

LIST OF TABLES

<u>Table</u>	<u>Page</u>
Table (4.1) Local Element Node Numbering System.	60
Table (5.1) Soil Properties.	85
Table (6.1) Material Properties for the Mdaina trial embankment (after Al-Hamrany, 1980).	91

CHATER ONE

INRODUCTION

CHAPTER ONE

INTRODUCTION

1.1 General

Partially saturated soil is the most common material encountered in the field of geotechnical engineering. Yet, mechanics of partially saturated soil lags far behind that of saturated soil. A partially saturated soil is a complex multi-phase system consisting of air, water and solid material whose response is a function of the stress state, moisture condition and other internal variables present within the soil. From a thermodynamic viewpoint, the problem amounts to deriving a free energy for the composite soil and water system.

The classical definition of soil for the purposes of numerical analysis is one in which the volume of material is comprised of two phases, incompressible solid grains and a pore volume consisting of solely air or water known as a saturated soil. However, the more realistic state of soil is one consisting of four phases: solid, liquid, air and an air-water interface that all interact with one another within a matrix of soil grains known as a partially saturated soil (PSS). The former soil definition is used extensively for the design of soil structures, however the latter is necessary in the prediction of actual response of soil structures and their effects with changes in environment.

Conventional soil mechanics theory treats soil as either fully saturated (pores filled with water) or dry (pores filled with air). However, a large number of geotechnical problems involve the presence of partially saturated soil zones where the voids between the soil particles are filled with a mixture of air and water. These zones are usually ignored in

practice and the soil is assumed to be either fully saturated or completely dry. It has long been established however that behaviour of partially saturated soils can be very different from that of fully saturated or completely dry soils.

Experimental and theoretical difficulties (e.g. direct measurement of suction, large number of influencing factors) delayed considerably the development of an understanding of the behaviour of partially saturated soils. It is only during the last few years that theoretical frameworks and constitutive models have been proposed to describe the mechanical behaviour of such soils.

Although the existing constitutive models are capable of reproducing important feature of the behaviour of partially saturated soils, most models are basic, compared to those available for fully saturated soils, and often soil type specific. There is therefore need for improvement and an increasing number of researchers around the working on improving the understanding and constitutive modeling of the mechanical behaviour of partially saturated soils.

Numerical analysis plays an important role in the investigation in to the behaviour of partially saturated soils by highlighting aspects which are important in engineering practice and illustrating the effect of partially soil saturated on the behaviour of geotechnical structures.

1.2 Consolidation Process

Consolidation theory has reached an advanced stage of development, and solutions are now available for most practical problems. Either in closed analytical form or by numerical techniques. However, the predicated consolidation behaviour may be fundamentally affected by the accuracy of the presumed soil profile, and by the

reliability of the sampling and testing procedures used to obtain the soil data.

Thus, a simple analytical procedure using reliable soil parameters will often provide the designer with an adequate prediction of consolidation behaviour.

The variations which result from the use of different consolidation theories will not in general be large. Nonetheless, the differences may be important, and the use of an insufficiently accurate procedure could significantly affect the cost of a structure.

An example of this is the common use of one-dimensional theory in cases where the geometry clearly shows that additional drainage boundaries are present and that a multi-dimensional theory is more appropriate.

Generally, little attention was paid to the consolidation of partially saturated soils.

1.3 Settlement

Any soil consists of solid particles, and takes existing soil skeleton and voids. These voids are either filled with air or with water (completely or partially).

When the soil is subjected to a stress or external load, deformation occurs. Soil settlement consists of three parts:-

1.3.1 Immediate settlement:-

Sometimes called (undrained settlement), in this stage there is no water movement (viz, there is no increase in pore water pressure). Immediate settlement occurs because of the expulsion of air from the voids of unsaturated or partly saturated soil as a result of rearranged soil particles.

1.3.2 Primary consolidation:

Consolidation is a time dependent volume reduction process involving a decrease in water content of the soil due to loading (Lambe and Whitman, 1979).

Primary consolidation results from dissipation of the excess pore water pressure, and it is followed with applied stress transfer from pore water to the soil skeleton. As water is squeezed out, soil particles rearrange themselves in a dense packing resulting in a decrease in void ratio, the vertical components for decrease in volume are called (consolidation settlement) (Scott, 1963).

1.3.3 Secondary compression

This type of settlement is defined as the reduction of volume at influence of continuous effective stress due to adjustment of the soil structure which continues even after the essential dissipation of the excess pore water pressure.

Thus we can interpret the process of consolidation by transfer the stresses from the pore water to the soil skeleton because water movement between boundaries is due to differential pressure between these boundaries.

1.4 Consolidation Theories

1.4.1 One dimensional consolidation theory (Terzaghi's theory)

The consolidation of soil as the result of dissipation of excess pore water pressure has, for many years, been the main concern of both practice and theory in soil mechanics .

Terzaghi's analysis of the phenomenon is often considered as the beginning of modern soil mechanics. Terzaghi presented his theory in

1925 (Terzaghi, 1943) and most of the practical work on the prediction of settlement rate is based upon the differential equation that he derived.

Terzaghi assumed that :-

- a- Isotropy, homogeneous and fully saturated soil.
- b- Compression in one dimension .
- c- Constant total stress .
- d- Darcy's law is valid .
- e- Velocity of water is very small .
- f- One dimensional flow .
- g- Linear stress-strain relationship .
- h- Constant permeability .
- i- Incompressible water and soil particles .
- j- Small strain theory is applicable .

Terzaghi's equation for one dimensional consolidation are (Terzaghi,1943) :-

$$C_v \frac{\partial^2 u}{\partial z^2} = \frac{\partial u}{\partial t} \dots\dots\dots(1.1)$$

where:-

C_v = coefficient of consolidation .

u = excess pore water pressure .

t = time .

The one dimensional consolidation theory was widely applied to the analysis of field situations. It has been found to produce results which generally overestimate the time of consolidation (Skempton and Bjerrum, 1957). This is particularly true in cases where the clays is overconsolidated .

The mathematical simplicity of one dimensional theory permits a variety of extension to cover many situations and to proved solutions (Gibson et al., 1953, 1958) .

1.4.2 Biot's Theory

Biot (1941) developed the three dimensional consolidation theory based on the theory of elasticity. Based on the assumption of Terzaghi-Rendulic theory except that the total stress may vary within the soil mass although the applied load remains constant.

Biot refined his theory to include the compressibility of fluid and soil skeleton and also deal with partly saturated soil (Biot, 1955; 1956). for saturated soil, Biot's theory, for general three-dimensions may be expressed as:

$$\frac{\partial u}{\partial t} = C_3 \left(\frac{\partial^2 u}{\partial x^2} + \frac{\partial^2 u}{\partial y^2} + \frac{\partial^2 u}{\partial z^2} \right) + \frac{1}{3} \frac{\partial}{\partial t} (\sigma_x + \sigma_y + \sigma_z) \dots\dots\dots(1.2)$$

where :

C_3 = is the coefficient of consolidation under three-dimensional strain condition .

$\sigma_x, \sigma_y, \sigma_z$ = are the total stress increments in x, y and z directions, respectively .

u = the excess pore water pressure .

t = the time .

1.5 Scope of Thesis

Unsaturated soil mechanics has rapidly become a part of geotechnical engineering practice as a result of solutions that have emerged to a number of key problems (or challenges). The solutions have emerged from numerous research studies focusing on issues that have a complication to the usage of unsaturated soil mechanics.

The aim of this thesis is studying consolidation characteristics of unsaturated soil. Parametric study was carried out.

Different parameters were changed to find the effect of these changes on behaviour of partially saturated soil. These parameters include the modulus of elasticity of the soil, hydraulic conductivity and the unsaturated soil modulus (H).

1.6 Thesis Layout

Chapter Two: includes review of unsaturated soil studies. The chapter its defines the unsaturated soil and it's phases. Then it presents the work of the researchers that deals with the unsaturated soil.

Chapter Three: presents the fundamental constitutive relations for unsaturated soils.

Chapter Four: covers the finite element formulation for consolidation problems.

Chapter Five: describes the finite element computer program (SIGMA/W) used for analysis of geotechnical problems and the models that are used for unsaturated soil. Verifications problems are solved to validate the problem modeling and analysis methodology.

Chapter Six: The aim of this chapter is to make a comparison between the results of fully saturated soil and unsaturated condition behaviour through solving consolidation problem.

Chapter Seven: includes conclusions and recommendations for future work.

CHAPTER TWO
LITERATURE REVIEW

CHAPTER TWO

LITERATURE REVIEW

2.1 Introduction

The soil is a multi-phase material containing solids and voids which may be filled with air and/or water.

When the voids of a soil contain both air and water the soil is said to be partially saturated or unsaturated.

The pressure of the air in the soil is given the symbol (u_a) and the pressure of the water is given the symbol (u_w).

The degree of saturation is defined by the ratio:

$$S_r = \frac{\text{Volume of water}}{\text{Volume of voids}}$$

Apart from the research field, partially saturated soils, or unsaturated soils, as they are now being called, have not been given as much attention from the civil engineering industry as they deserve.

In 1995, the first international conference on unsaturated soils took place in Paris. Its proceedings, published in three volumes, dramatically illustrate just how important this subject has become. In Britain, seminars on unsaturated soils, held at Imperial College, London in 1995 (in conjunction with the University of Wales) and in 1997, at Edinburgh's Napier University, were well attended and created lively discussions on the type of civil engineering problems that unsaturated soils can create.

Karl Terzaghi is remembered most for providing the “effective stress” variable, ($\sigma - u_w$), that became the key to describing the mechanical of unsaturated soils; where σ = total stress and u_w = pore–water pressure. The effective stress variable became the unifying discovery that elevated geotechnical engineering to a science basis and context.

In his textbook (Theoretical Soil Mechanics), Karl Terzaghi (1943), emphasized the importance of the unsaturated soil portion of the profile and in particular provided an insight into the fundamental nature and importance of the air–water interface (i.e., contractile skin). Considerable attention was given to soils with negative pore– water pressures.

However, his contemporary, Biot (1941), was one of the first to suggest the use of two independent stress state variables when formulating the theory of consolidation for an unsaturated soil.

2.2 Subsurface Water

This is the term used to define all water found beneath the earth's surface. The main source of subsurface water is rainfall, which percolates downwards to fill up the voids and interstices, water can penetrate to a considerable depth, estimated to be as much as (12000) metres, but at depths greater than this, due to the large pressures involved, the interstices have been closed by plastic flow of the rocks. Below this level, water cannot exist in a free state, although it is often found in chemical combination with the rock minerals, so that the upper limit of plastic flow within the rock determines the lower limit of subsurface water.

Subsurface water can be split into two distinct zones: saturation zone and aeration zone, (Smith and Smith, 1998).

2.2.1 Saturation zone

This is the depth throughout which all the fissures, etc., are filled with water under hydrostatic pressure. The upper level of this water is known as the water table, , and water within this zone is called phreatic water or ground water. The water table tends to follow in a more gentle manner the topographical features of the surface above Figure (2.1). At ground water level the hydrostatic

pressure is zero, so another definition of water table is the level to which water will eventually rise in an unlined borehole.

The water table is not constant but rises and falls with variations of rainfall, atmospheric pressure, temperature, etc., whilst coastal regions are affected by tides. When the water table reaches the surface, springs, lakes, swamps, and similar features can be formed.

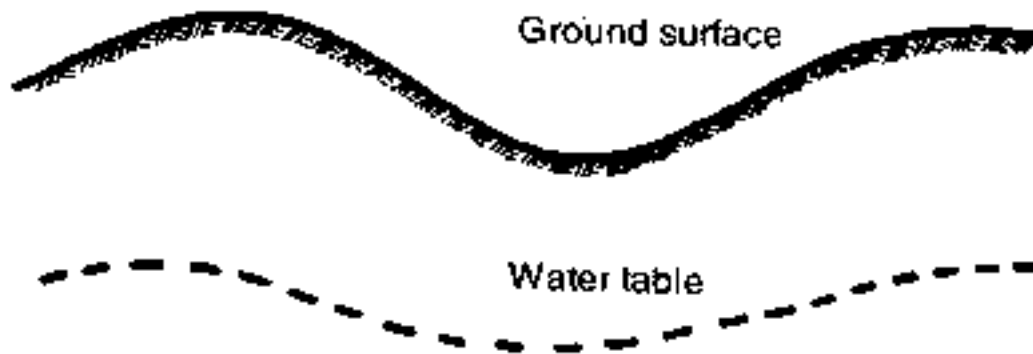


Fig. (2.1) Tendency of the water table to follow the earth's surface (Smith and Smith, 1998).

2.2.2 Aeration zone

Sometimes referred to as the vadose zone, this zone occurs between the water table and the surface, and can be split into three sections.

2.2.2.1 Capillary fringe:

Owing to capillarity, water is drawn up above the water table into the interstices of the soil or rock. Water held in this manner is in a state of suction or negative pressure; its height depends upon the material and in general the finer the voids the greater the capillary rise. In silts, the rise can be as high as two and a half meters and in clays can reach twice that amount.

2.2.2.2 Intermediate belt

As rainwater percolates downward to the water table, a certain amount is held in the soil by the action of surface tension, capillarity, adsorption, chemical action, etc. The water retained in this manner is termed held water and is deep enough not to be affected by plants.

2.2.2.3 Soil belt

This zone is constantly affected by evaporation and plant transpiration. Moist soil in contact with the atmosphere either evaporates water or condenses water into itself until its vapor pressure is equal to atmospheric pressure. Soil water in atmospheric equilibrium is called hygroscopic water, whilst the moisture content which depends upon relative humidity is known as the hygroscopic water content.

The various zones are illustrated in Figure (2.2).

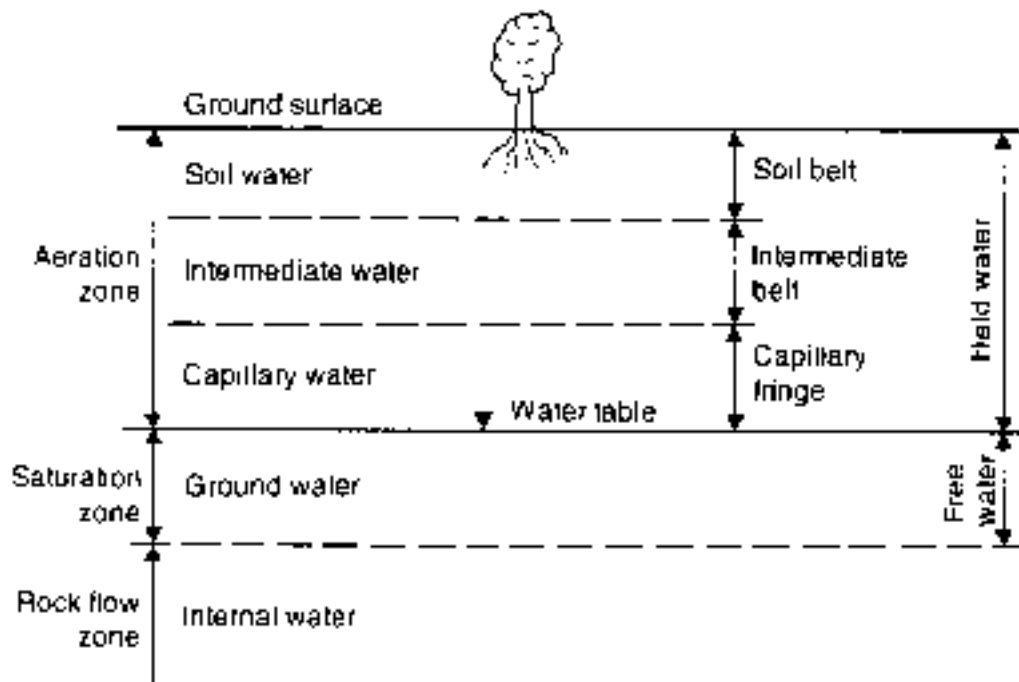


Fig. (2.2) Diagram illustrating types of subsurface water (Smith and Smith, 1998).

2.3 Gradual Emergence of Unsaturated Soil Mechanics

In experimental laboratory studies in the late 1950s, Bishop et al. (1960) showed that it was possible to independently measure (or control) the pore–water and pore–air pressures through the use of high air entry ceramic disks. Laboratory studies were reported over the next decade that revealed fundamental differences between the behavior of saturated and unsaturated soils.

The usual focus on soil property constants was diverted toward the study of nonlinear unsaturated soil property functions. The increased complexity of unsaturated soil was extended from the laboratory to theoretical formulations and solutions.

Originally, there was a search for a single-valued effective stress equation for unsaturated soils but by the late 1960s, there was increasing awareness that the use of two independent stress state variables would provide an approach more consistent with the principles of continuum mechanics (Fredlund and Morgenstern, 1977).

The 1970s was a period when constitutive relations for the classic areas of soil mechanics were proposed and studied with respect to uniqueness (Fredlund and Rahardjo, 1993). Initially, constitutive work focused primarily on the study of seepage, shear strength, and volume change problems. Gradually it became apparent that the behaviour of unsaturated soils could be viewed as a natural extension of saturated soil (Fredlund and Morgenstern, 1976). Later, numerous studies attempted to combine volume change and shear strength in the form of elastoplastic models that were an extension from the saturated soil range to unsaturated soil conditions (Alonso et al., 1990; Wheeler and Sivakumar, 1995; Blatz and Graham, 2003). The study of contaminant transport and thermal soil properties for unsaturated soils also took on the form of nonlinear soil property functions (Newman 1996; Lim et al. 1998; Pentland et al. 2001).

The 1980s was a period when boundary-value problems were solved using numerical, finite element, and finite difference modeling methods. Digital computers were required and iterative, numerical solutions became the norm. The challenge was to find techniques that would ensure convergence of highly nonlinear partial differential equations on a routine basis (Thieu et al., 2001; Fredlund et al., 2002a, b, c). Saturated–unsaturated seepage modeling became the first of the unsaturated soils problems to come into common engineering practice. Concern for stewardship toward the environment further promoted interest in seepage and geoenvironmental, advection-dispersion modeling.

The 1990s and beyond have become a period where there has been an emphasis on the implementation of unsaturated soil mechanics into routine geotechnical engineering practice. A series of international conferences have been dedicated to the exchange of information on the engineering of unsaturated soils and it has become apparent that the time had come for increased usage of unsaturated soil mechanics in engineering practice. Implementation can be defined as “a unique and important step that brings theories and analytical solutions into engineering practice” (Fredlund, 2000).

2.4 Unsaturated Soil as a Four-Phase Mixture

An unsaturated soil is commonly referred to as a three-phase mixture (i.e., solids, air, and water) but there is strong justification for including a fourth independent phase called the contractile skin or the air–water interface. The contractile skin acts like a thin membrane interwoven throughout the voids of the soil, acting as a partition between the air and water phases. It is the interaction of the contractile skin with the soil structure that causes an unsaturated soil to change in volume and shear strength. The unsaturated soil properties change in response to the

position of the contractile skin (i.e., water degree of saturation). It is important to view an unsaturated soil as a four-phase mixture for purposes of stress analysis, within the context of multiphase continuum mechanics. Consequently, an unsaturated soil has two phases that flow under the influence of a stress gradient (i.e., air and water) and two phases that come to equilibrium under the influence of a stress gradient (i.e., soil particles forming a structural arrangement and the contractile skin forming a partition between the fluid phases) (Fredlund and Rahardjo, 1993).

The contractile skin has physical properties differing from the contiguous air and water phases and interacts with the soil structure to influence soil. The contractile skin can be considered as part of the water phase with regard to changes in volume–mass soil properties but must be considered as an independent phase when describing the stress state and phenomenological of an unsaturated soil. Terzaghi (1943) emphasized the important role played by surface tension effects associated with the air–water interface (i.e., contractile skin).

2.5 Distinctive Features of the Contractile Skin

Numerous research studies have been carried out on the nature of the contractile skin point toward its important, independent role in unsaturated soil mechanics. Terzaghi (1943) suggested that the contractile skin might be in the order of 10^{-6} mm in thickness. More recent studies suggest that the thickness of the contractile skin is in the order of 1.5–2 water molecular diameters (i.e., 5 Å) (Israelachvili, 1991; Townsend and Rice, 1991).

A surface tension of approximately 75 mN/m translates into a unit stress in the order of 140,000 kPa. Lyklema (2000) showed that the distribution of water molecules across the contractile skin takes the form

of a hyperbolic tangent function as shown in Figure (2.3) . Properties of the contractile skin are different from that of ordinary water and have a water molecular structure similar to that of ice (Derjaguin and Churaev, 1981; Matsumoto and Kataoka, 1988).

The Young–Laplace and Kelvin equations describe fundamental aspects of the contractile skin but both equations have limitations. The Young–Laplace equation is not able to explain why an air bubble can gradually dissolve in water without any apparent difference between the air pressure and the water pressure. The validity of the Kelvin equation becomes suspect as the radius of curvature reduces to the molecular scale (Adamson and Gast, 1997; Christenson, 1988).

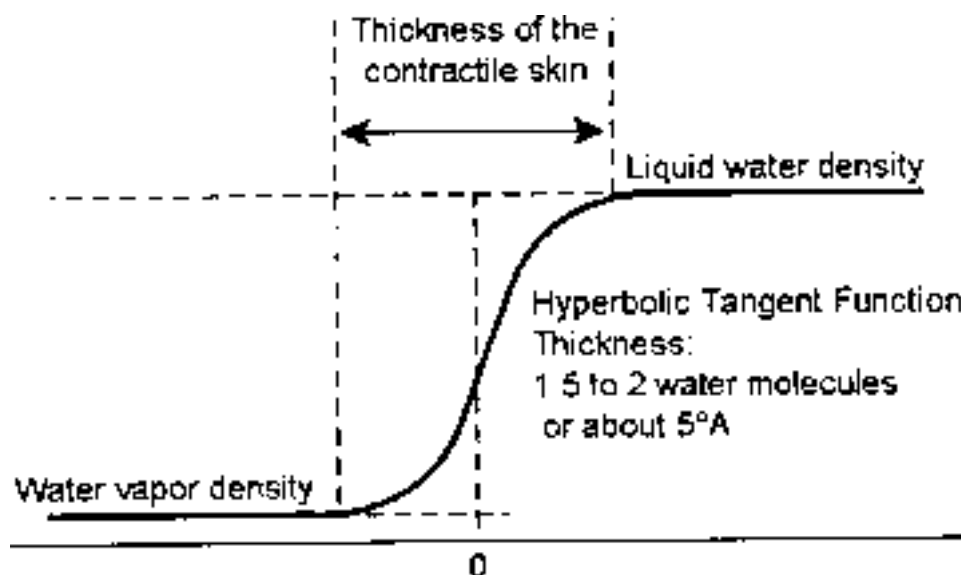


Fig. (2.3) Density distribution across the contractile skin reprinted from liquid–fluid interface, (Lyklema , 2000).

Terzaghi (1943) recognized the limitations of the Kelvin equation and stated that if the radius of a gas bubble approaches zero, the gas pressure approaches infinity. However, within the range of molecular dimensions, the equation loses its validity. Although Terzaghi recognized this limitation, later researchers attempted to incorporate the Kelvin equation into formulations for the compressibility of air–water mixtures,

to no benefit (Schuurman, 1966). The details of the laws describing the behavior of the contractile skin are not fully understood but the contractile skin is known to play a dominant role in unsaturated soil . Terzaghi (1943) stated that surface tension is valid regardless of the physical causes. The views concerning the molecular mechanism which produces the surface tension are still controversial. Yet the existence of the surface film was established during the last century beyond any doubt, (Fredlund, 2006).

2.6 Previous Works on Unsaturated Soils

Lloret and Alonso (1980) were one of the first to attempt to generate a model for unsaturated soil that included consolidation behavior.

They provided a general formulation for three-dimensional behavior that allowed for air and water as separate phases. However, the data for their analyses was determined from one- dimensional tests, and their examples are limited to such. They simulated saturated consolidation, infiltration leading to swelling in an unsaturated soil, and collapse due to loading then wetting of an unsaturated soil, all one-dimensionally.

Their results show the importance of variable permeabilities in governing deformation in unsaturated soil. They appear also to support the use of a three-phase approach, with the air phase explicitly modeled as a separate phase. However, since they did not repeat their analyses with a two-phase model, it is not possible to ascertain the full significance of the three-phase approach.

Additionally, a one-dimensional analysis is not typical of a field situation. Hence, a two-phase, zero air pressure assumption remains a credible approach to the analysis of unsaturated soils.

Lam et al. (1987) presented an approach to modelling “saturated-unsaturated soil systems” using a numerical technique (the finite element

computer program TRASEE), and included three example problems, namely flow through a dam after sudden impounding, vertical flow through an unsaturated soil from a lagoon to the underlying groundwater, and rain-induced infiltration into a slope in a multi-layered soil (in the form of a 1m high experimental model).

No attempt was made to model the strength-strain-stress behavior of the soil, and while a "water coefficient of volume change" is incorporated within their analysis, this represents the change of water storage with suction, and does not reflect consolidation. Moreover, a fixed value is specified, implying a constant slope to the suction-volumetric water content relationship, which is clearly not accurate.

Lam et al. demonstrated that the phreatic surface is not a flow line, with their first, dam, example showing flow across the phreatic surface. This example also shows the importance of flow within the unsaturated region, with a calculated total flow through the dam being 30% greater than that calculated using a traditional flow net, with flow limited to the saturated zone.

Alonso et al. (1988) presented a coupled approach for the stress-strain-flow behavior of partly saturated soils. While not explicitly stated as such, their work appears to be a progression from Lloret and Alonso (1980), and again is a full 3-phase approach.

They used their formulation to look at pore water pressure response and deformation in an earth dam under construction, with either a "dry soil" fill, with an initial degree of saturation of 80%, or a "wet soil" fill, initially at 90% saturation.

Their results show that the wet soil responds to the construction of subsequent layers above, with consolidation and an increase in the pore water pressure occurring. This behavior is not observed in the dry soil.

Alonso et al., (1988) did not give soil water characteristic curve for the material used in their analyses, but rather presented state surfaces to show the behavior of the soil. From this, the air entry value appears to be equal to 0 kPa, with the saturation of the soil decreasing noticeably immediately the soil develops suctions. However, the results of their analyses suggest that the wet soil responds to loading in a manner reminiscent of saturated soil. In contrast, the dry soil shows markedly different behavior compared to a fully saturated soil. This supports the idea that there is some "cut-off " degree of saturation, below 100%, at which point, the soil's behavior changes from a saturated, or at least pseudo-saturated soil to unsaturated behavior.

Forsyth (1988) developed two methods for dealing with transient flow in unsaturated soils, however neither was fully coupled. His work is notable, however, since while one method made the common assumption of zero air pressure, the other allowed for the air phase as a separate phase (i.e. non-zero air pressures possible).

Forsyth showed that the zero air pressure assumption often gives much the same results as the full three phase soil (two-phase flow approach), but that under certain circumstances, significant errors may be given if the air phase is not specifically modeled. Such errors occurred when the air permeability was very low and not changing much, for example when airflow permeability is a power function of air saturation, and air saturation is very low. They also tended to occur if the zone of soil suction was small relative to the mesh element size used in the analysis: where the zone of soil suction lay entirely within the thickness of one element, discrepancies between the standard two phase and more detailed three phase approach occurred. If the element size was adjusted such that the zone of suction was spread over several elements thickness,

and hence changes in the suction between integration points in the mesh were less sharp, both methods gave comparable results.

It is probable, however, that any analysis where the unsaturated zone lay entirely within the thickness of one element would give results of dubious accuracy. Simple good practice would suggest that a finer mesh would be required. Forsyth's work thus emphasizes the need to select element size within a finite element mesh carefully, when dealing with unsaturated soil behavior.

Gioda and Desideri (1988) looked at two-dimensional flow through an earth dam on an impervious base, but with the assumption of a rigid soil (assuming that the deformability of the soil skeleton can be negated). Fundamentally, they approached the problem as a saturated soil problem, but they did provide for unsaturated flow, in that they incorporated a suction permeability relationship that allowed for near-to- but non-zero permeability when pore water pressures were below atmospheric (i.e., when pore water pressures had become suctions). Their work is of little direct relevance to this project, since it involves neither infiltration nor consolidating soil, but the suction-permeability function used is worth noting.

De Campos et al. (1992) undertook stability analysis of a slope in Brazil, using a computer code developed at the Catholic University of Rio de Janeiro. They made the point that the information required to undertake unsaturated analyses, specifically in their case the suction dependent hydraulic conductivity relationship, is frequently scarce, requiring estimates to be made of such properties.

Clearly, the accuracy of a numerical analysis is likely to suffer if parameters are estimated, and this emphasises the need for numerical analysts to work closely with their laboratory-based colleagues in

determining what properties of the soil are needed and ensuring suitable tests are developed to determine them.

Despite using their own software, de Campos et al. still treat the stability problem in two parts, with an initially rigid soil assumed in which the flow analysis is carried out, the results of which are then utilized in the second, limit equilibrium analysis, to determine the factor of safety.

Wong et al. (1998) presented one of the few attempts to develop a fully - coupled approach to the behavior of unsaturated soils. They made use of Biot (1941) and Dakshanamurthy et al. (1984) to generate coupled consolidation equations for unsaturated behavior.

Wong et al. made use of the computer programs SEEP/W and SIGMA/W to undertake their analyses, the first being used to undertake the seepage analyses while the second deals with stress-deformation behavior.

They presented analyses of an unsaturated triaxial test, to investigate the effects of the gradient of the soil water characteristic curve, then go on to model a (2 m) high column of soil, with the phreatic surface at mid-height, subjected to an applied surface load. Their results indicated that while applied loads cause a significant change in the pore water pressure within saturated soil, the effects on the suctions within the unsaturated soil are all but negligible, the most significant effect being the movement of the phreatic surface. Conversely, vertical deformations within the unsaturated zone occur rapidly in response to applied load, whereas in the saturated zone, they occur much more slowly, as the consolidation process occurs.

Wong et al. work included a number of simplifications, such as having a constant permeability, not suction-dependent, and does not attempt to model any part of the infiltration process. However, it is

valuable as an attempt to reproduce coupled behavior in unsaturated soil, and provides a comparison against which the new coding within Imperial College Finite Element Program (ICFEP) can be compared.

Kim (2000) more usefully attempted a fully coupled analysis of an unsaturated soil problem. He looked at the variation in the position of the phreatic surface within a partly saturated / partly unsaturated soil column which was subjected to a surface load.

The results showed that there is an instantaneous rise in the position of the phreatic surface on application of the load. Depending on the initial depth to the phreatic surface, its position may continue to rise with time for a short period, before in all cases the position of the surface begins to drop. The final depth of the phreatic surface lies above its initial position, but below the minimum depth to which it rose.

Vertical displacements of the column surface also reflect the initial position of the phreatic surface. The greater the initial depth to the surface, and hence the more of the column that starts unsaturated, the more rapid is the development of the surface displacements.

Both of these two observations are consistent with the results of Wong et al.'s (1998) work.

Kim stated that "less final steady-state vertical displacement occurs in the partially saturated soil columns. These effects of the unsaturated zone are more conspicuous as the initial water table is located higher and the magnitude of the surface loading increases".

This and the results presented seem to suggest that if the column analyzed is fully unsaturated, vertical displacements are apparently equal to those of a fully saturated column, but as the phreatic surface is raised within the soil, the calculated displacement deviates from the fully saturated value. The biggest deviation between the calculated value for

the saturated and partially saturated column displacements occurs for the case with the phreatic surface at (2 m) below the surface (i.e., for the case where the phreatic surface is closest to the ground surface, without actually being at the surface). Thus the closer the column is to full saturation, the greater the deviation of the calculated displacement from the fully saturated value.

Kim accounted for the displacement behavior by saying "the unsaturated zone absorbs a portion of the mechanical loading stress permanently", but this does not seem to adequately explain the behavior presented.

Ng and Small (2000) used Biot (1941) theory to develop the fully coupled equations for unsaturated soil analysis. However, they are primarily interested in soils that, while unsaturated, have a high degree of saturation, such that the pore water pressure and the pore air pressure are very close in value. They stated that this is typically at degrees of saturation of 80% or higher.

This appears to lead them to make a number of assumptions, most notably that strain can be assumed to be small, and hence that porosity of the soil remains approximately constant. Thus any change in volumetric water content due to a change in suction manifests itself solely as a change in the degree of saturation, with porosity unchanged. Hence, while the soil is not rigid and may undergo normal consolidation through loading, it is effectively rigid in response to changes in matric suction.

Ng and Pang (2000) looked at the dependence of the soil water characteristic curve on the applied stress state, and then considered the implications of this on slope stability. They undertook a numerical analysis of a "typical cut slope" in Hong Kong, using the program SEEP/W to determine the pore water pressure/suction distribution. As they state, the SEEP/W analysis is uncoupled, with soil deformations

ignored. The results of their numerical analysis were then used in a limit-equilibrium analysis to determine factors of safety.

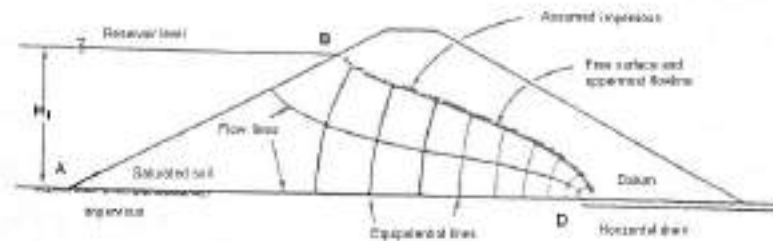
Assouline and Tartakovsky (2001) presented a new two-parameter expression for relative hydraulic conductivity of partially saturated soils. It is based on the premise of Assouline et al. (1998) that soil structures evolve from a uniform random fragmentation process. This assumption allows deriving hydraulic properties of soils (water retention curves and unsaturated hydraulic conductivity) from primary properties, such as pore geometry and soil structure. They tested their relative hydraulic conductivity expression against different soil types and found that it fits data better than the widely used models of Brooks and Corey (1964) and van Genuchten (1980).

A discussion on the general nature of unsaturated soils is followed by a survey of previous attempts to apply numerical modeling to unsaturated soils. The core equations governing the fully coupled constitutive behavior of unsaturated soils are developed and presented, along with details of how these equations were implemented in numerical form. A conceptual model that qualitatively assesses the behavior of unsaturated soils is also presented.

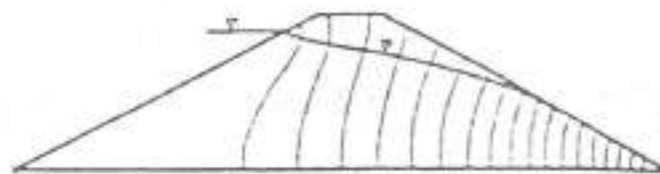
The behavior of unsaturated soil slopes was investigated through numerical simulations of the Tung Chung slope in Hong Kong, using the Imperial College Finite Element Program (ICFEP), with the numerical predictions compared to field monitoring data of the pore water pressures / suctions from the site.

It is shown that the variation of pore pressures is very sensitive to the relationship between suction and degree of saturation, as represented by the soil water characteristic curve. Also critical are the permeability parameters of the soil, including the variation of permeability with suction (Smith, 2003).

Abdul Kareem Asmat (2002), studied the consolidation process for partially saturated soil. The method of finite elements is used to find a numerical solution to describe the behavior of soil during consolidation, also the effects of temperature differences are taken into consideration. Regarding the steady state seepage through the earth dam shown in Figure (2.4a and b), the application of the saturated-unsaturated seepage analysis reveals that there exists some flow through the unsaturated zone above the phreatic line. The main potential for this water movement is the suction potential where the air pressure is assumed atmospheric, and the water pressure is negative.



(a)



(b)

Fig. (2.4) Geometry of the steady state flows problem a) Dam with horizontal drain b) Dam with no horizontal drain.

A 10 m height of water is applied to the upstream face of the dam. The permeability function used in the analysis is shown in

Figure (2.5). The saturated coefficient of permeability, k is 1×10^{-7} m/s. The pore-air pressure is assumed to be atmospheric. Therefore, the matric suction values in Figure (2.5) are numerically equal to the pore-water pressures, and can be expressed as a pore-water pressure head, h_p . The base of the dam is chosen as the datum

The saturated-unsaturated steady state flow through an earth dam is performed on two separated examples. The first one, Figure (2.4a) represents an earth dam with a horizontal drain. The second one Figure (2.4b) represents an earth dam with no horizontal drain.

It was demonstrated that the isotropic earth dam with a horizontal drain shows the steady infiltration, shown in Figure (2.6). The 10 m height of water on the upstream face of the dam gives a 10 m hydraulic head at each node along the upstream face. A zero hydraulic head is specified at nodes along the horizontal drain. Zero nodal flow is specified at nodes along the remaining boundaries.

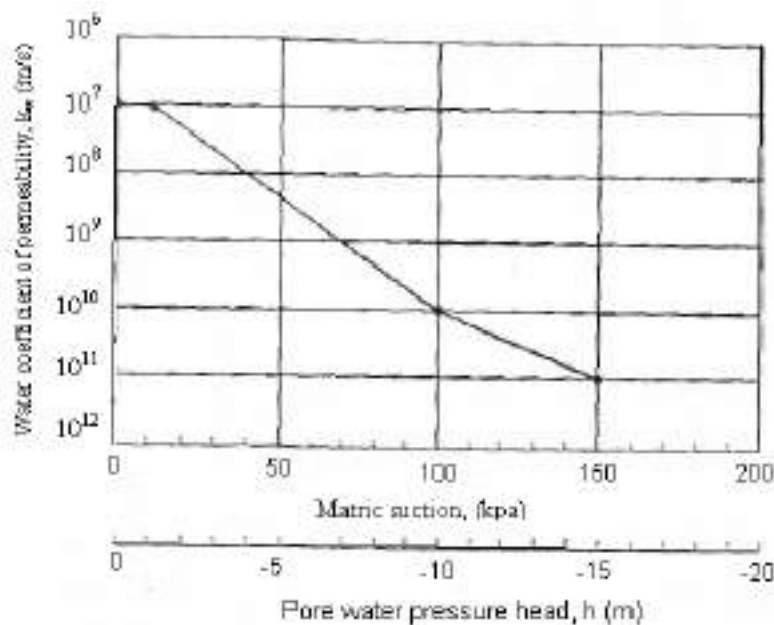


Fig. (2.5) Permeability function for analyzing steady state seepage through a dam.

The phreatic line resulting from the saturated-unsaturated flow model Figure (2.7b) is in close agreement with the empirical free surface from a conventional flow net construction Figure (2.6b). However, water can flow across the phreatic line, as indicated by the nodal flow rate vector. Water flow across the phreatic line into the unsaturated zone indicates that the phreatic line is not the uppermost flow line, as assumed in the flownet technique.

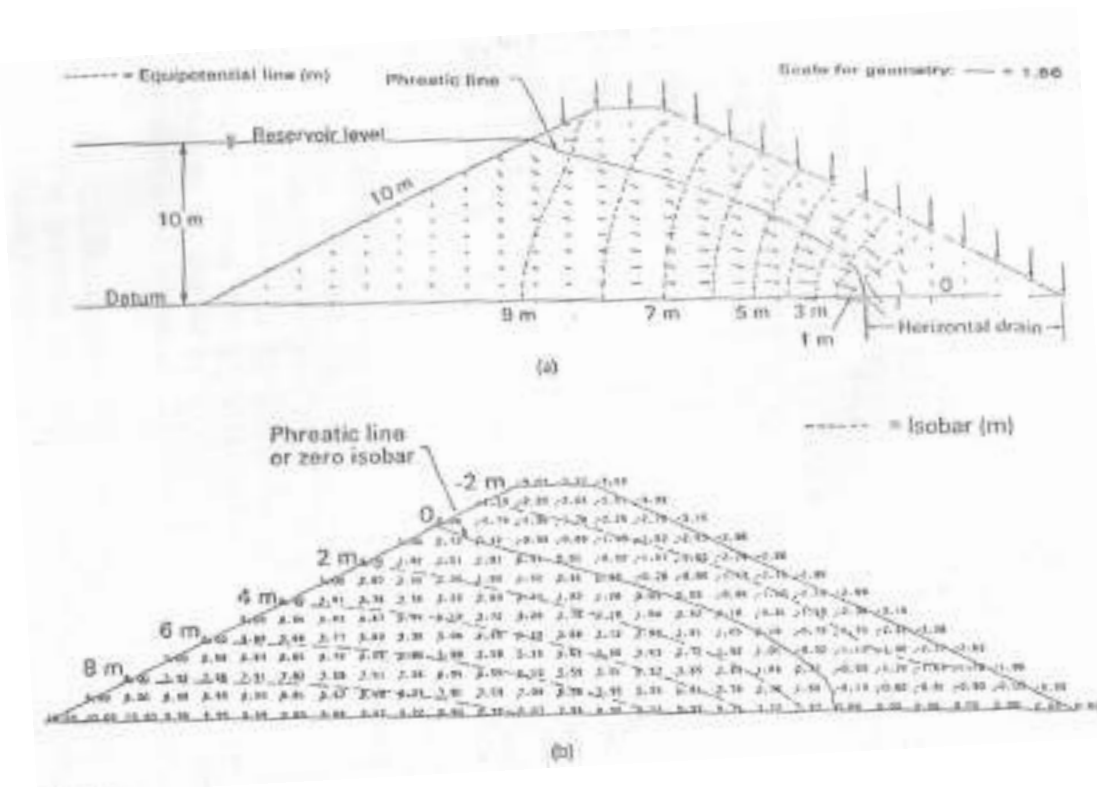


Fig. (2.6) Seepage through an isotropic earth dam with a horizontal drain under steady state infiltration (Abdul Kareem Asmat Zainai, 2002) :

- a) equipotential lines and nodal flow rate vectors throughout the dam,
- b) contours of pore-water pressure head (isobars) throughout the dam.

The difference between the phreatic line (from the finite element analysis) and the free surface (from the flow net technique) decreases as the permeability function for the unsaturated zone becomes steeper. A steep permeability function indicates a rapid reduction in the water coefficient of permeability for a small increase in matric suction. In

this case, the quantity of water flow into the unsaturated zone is considerably reduced. This condition approaches the assumption associated with the conventional flow net technique. In other words, the phreatic line approaches the empirical free surface.

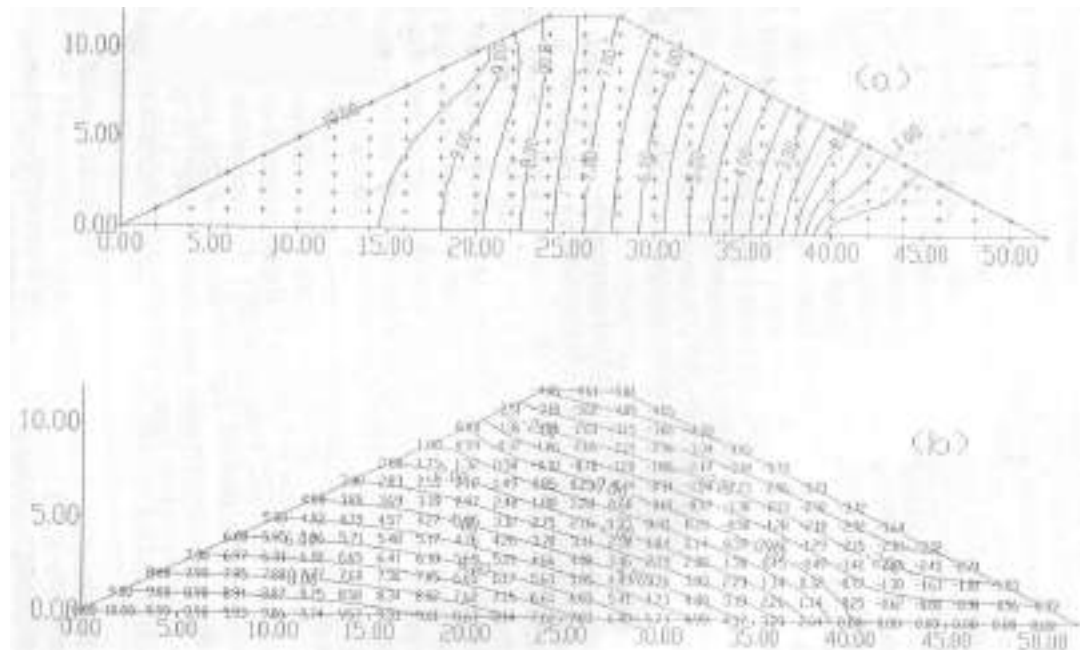


Fig. (2.7) Results obtained from the saturated/unsaturated flow regime analysis (Abdul Kareem Asmat Zainai, 2002):

- equipotential lines distribution.
- pore-water pressure heads distribution.

Equipotential lines extend from the saturated zone through the unsaturated zone, as shown in Figure (2.6a). Changes in hydraulic head between equipotential lines demonstrate that water flows in both the saturated and unsaturated zones. The amount of water flowing in the unsaturated zone depends upon the rate at which the coefficient of permeability changes with respect to matric suction. The pore-water pressure heads at all of the nodes throughout the dam are shown in Figure (2.6b). Pore-water pressure heads are computed by subtracting the elevation head from the hydraulic head. Contour lines of equal pressure heads or isobars are also shown. The pressure heads range

from positive to negative values, with the zero pressure head contour as the phreatic line. The isobars are almost parallel to the phreatic line in the central section of the dam.

The flow of water in the saturated and unsaturated zones is approximately parallel to the phreatic line, as observed from the flow rate vectors in the central section of the dam Figure (2.6a). This is not the situation for the sections close to the upstream face and the toe of the dam. Near the upstream face over the dam, water flows across the phreatic line from the saturated to the unsaturated zone and continues to flow in the unsaturated zone. The water in the saturated and unsaturated zones then flows essentially parallel to the phreatic line in the central section of the dam. The water in the saturated zone then flows across the phreatic line into the unsaturated zone at the toe of the dam.

Berney et al. (2003), worked on the thermodynamics of three-phase partially saturated soil. Their conclusion is that a theory for partially saturated materials was constructed from a saturated soil model by adding a term for the free energy of the capillary phase that included coupling between the solid and water phases. An essential idea in defining the free energy is a distinction between the water in the capillary phase and the mobile water that flows as an independent phase. This inherent relationship between the variables appearing in the free energy expression and their conjugate stress terms obviates the traditional problem of defining effective stress. The principles of the theory are illustrated by extending an existing plasticity model for saturated soils, which is based on an internal variable formulation, by adding terms that account for the free energy of the capillary phase. The model exhibits the tendency of partially saturated soil to either swell or collapse depending on the soil

state by the coupling of the volumetric water content and strain terms through the tensors of Cauchy stress and suction.

Model simulations of unconsolidated-undrained triaxial tests demonstrate the proper relationship between strength and the state as described by water content, void ratio, and total confining stress.

Defining the model in terms of its thermodynamics allows its implementation into any plasticity model whose purpose is to evaluate the intergranular stress whether it is in two phase or three phase materials Berney (2003).

Saif Jawad (2006), presented a finite element solution to the problem of consolidation and deformation of excavations, based on the theory for the transient response of saturated porous media which was developed by Biot (1941).

This procedure is ideally adapted to the situation since it can solve pore pressures and deformations while accounting for excavation rate and sequence, nonhomogeneous soil condition, nonlinear soil behavior, and the effects of essentially arbitrary types of support systems.

A simplified coupled formulation based on Biot's theory for solving problems associated with partially saturated soils, is presented. The formulation has been developed by noting that the air and water pressures in partially saturated soils are approximately equal at high degrees of saturation. In order to investigate the effect of partially saturated soils in the case of supported excavation, the results of two dimensional problems are presented and comprised with fully saturated soils. These results prove that the deformations in the state of partially saturated soil are less than fully saturated because friction between soil particles is the greater and the effect decreases with time because pore water pressure is dissipated.

The coupled field equations derived have been incorporated into a finite element program called "EXCCONPSS" written in Fortran 77. This program is a development of program "EXCCON" which was produced by Hassanein (1995).

The excavation of a three dimensional opening in a soil where pore pressure dissipation occurs is a complex problem with moving drainage boundaries and changing geometry. This situation is well suited for analysis by the developed finite element program "EXCCONPSS".

The program is employed to analyze a typical supported excavation problem. The selected excavation cross section with excavation sequence and boundary conditions is as shown in Figure (2.8). The finite element mesh is composed of 225 eight-noded isoparametric soil elements, 15 three-noded isoparametric beam elements and one three-noded isoparametric bar (truss) element (in the case of supported wall with strut). The dimensions of the problem are 17 m/ depth and 60 m width and the dimensions of the excavation zone are (6 m) depth and (11 m) width. The depth of excavation is divided into six layers and each layer is of 1 m depth and 1 m width.

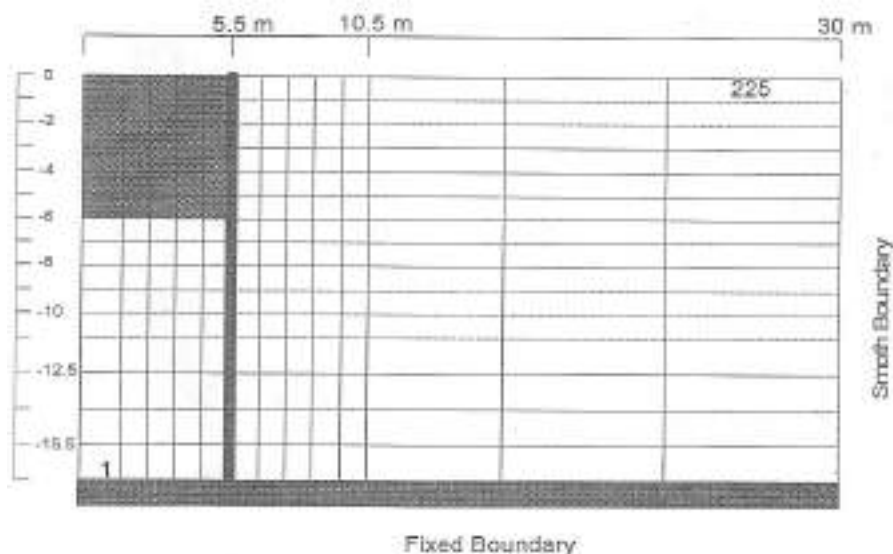


Fig. (2.8) Finite element mesh (after Saif , 2006).

Supported excavation without strut is performed. In this case of supported excavation, three states of analysis are carried out based on the degrees of saturation of the soil. All the results are taken at the end of excavation. The coefficient of permeability used in all cases is (1×10^{-4} m/day), and a rate of excavation of (0.15 m/day) is used to remove six layers of the soil.

In the first state, the soil is considered fully saturated soil ($S_r = 100\%$). In the second and third states, the soil is considered partially saturated soil which has degree of saturation equal to (90 %) in the second state and (80 %) in the third state.

From Figure (2.9), it can be seen that the state of saturated soil gives maximum wall deflection because friction in the soil is little. On the other hand, the state of partially saturated soil at degree of saturation (80 %) gives values of wall deflection less than in saturated soil especially at the surface because the degree of saturation is low and friction between the soil particles increases because the voids of the soil contain air so that the wall deflection is the smallest. It can also be seen that the wall deflection profiles are the same for all states ($S_r = 80, 90$ and 100%) in the lower part of the wall. From Figure (2.10) which represents the bending moment of the wall, it can be seen that the bending moment of the wall in the state of fully saturated soil is greater than partially saturated soil because the lateral movement of the wall is greater.

Figure (2.11) represents the surface movement behind the wall. Also, from this figure it appears that the settlement of fully saturated soil is greater than partially saturated soil because in the state of partially saturated soil friction between the wall and the soil and between the soil particles is greater and the excess pore water pressure is the smallest.

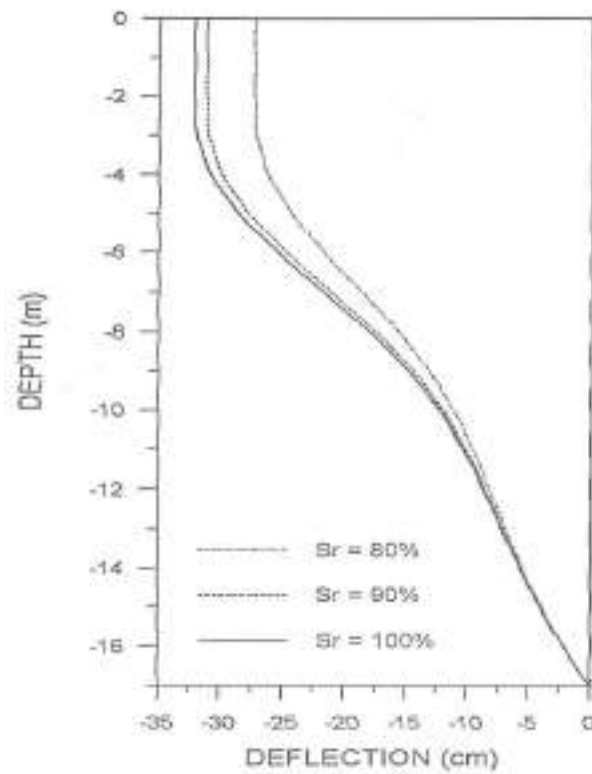


Fig. (2.9) Lateral movement predicted of the wall for different degrees of saturated (after Saif , 2006).

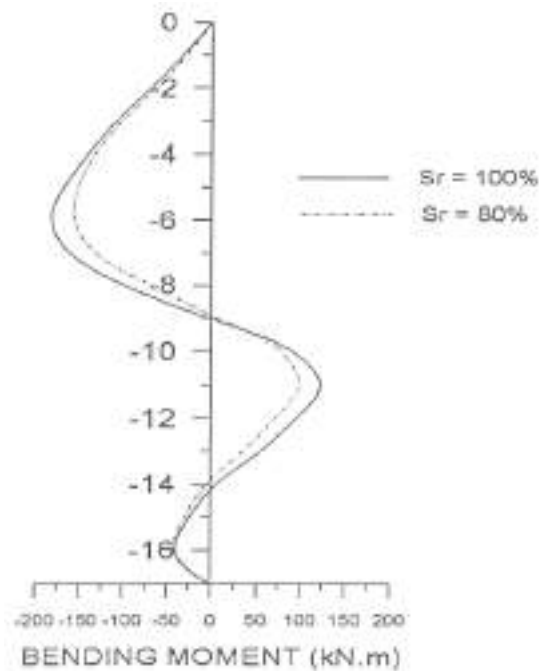


Fig. (2.10) Predicted wall bending moment for different degrees of saturation (after Saif , 2006).

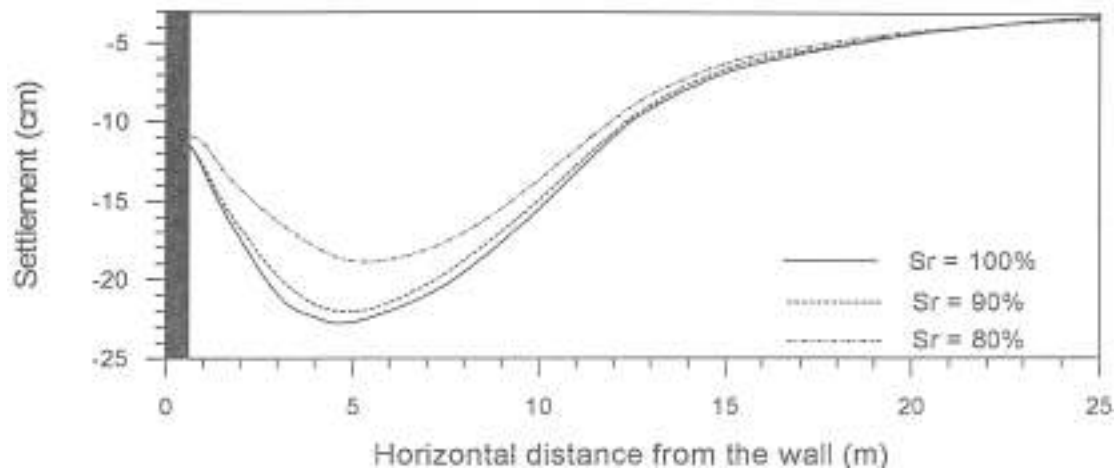


Fig. (2.11) Surface movement predicted in the soil for different degrees of saturation (after Saif , 2006).

CHAPTER THREE

FUNDAMENTAL CONSTITUTIVE RELATIONS FOR UNSATURATED SOILS

CHAPTER THREE

FUNDAMENTAL CONSTITUTIVE RELATIONS FOR UNSATURATED SOILS

3.1 Introduction

There is a wide range of unsaturated soil mechanics problems for which geotechnical engineers are asked to produce engineering designs. Most of the problems can be related to a specific constitutive relationship that must be addressed. The constitutive relationship generally has one or more soil properties that must be either measured or estimated in order to provide an adequate solution.

Classical soil mechanics has focused on three primary constitutive behaviors; namely seepage, shear strength, and volume change. Volume change constitutive behavior must be expanded to embrace all volume–mass relations when dealing with an unsaturated soil. There are also other constitutive behaviors that are of interest such as heat flow and contaminant transport. Each of the constitutive behavior areas is generally first considered as a “stand-alone” process; however, in engineering practice two or more processes may need to be simultaneously solved in a “coupled” or “uncoupled” manner (Fredlund, 2006).

In geotechnical engineering, constitutive relations have been generally proposed based on a thorough understanding of the phenomenological behavior of a representative element volume of soil. Constitutive relations describing flow take the form of a rate of movement versus the gradient of the primary potential variable producing flow. Constitutive relations describing equilibrium volume-mass conditions take the form of relationships between various state variables (e.g., stress, deformation and distortion state variables). Every constitutive relationship requires that a physical property of the soil be

defined. The soil property may be linear or nonlinear in nature. In the case where the soil property is nonlinear, it will generally be defined in terms of the state variables, thus bringing nonlinearity into subsequent formulations. The formulations generally take the form of partial differential equations that are then solved as part of a numerical model.

Constitutive relations are usually empirical or semiempirical, being based on forms that have previously been found to produce satisfactory results for similar behaviors in the past. Experimental programs are then undertaken in an attempt to verify the uniqueness of the proposed relationship. The verification process may be extremely demanding, requiring the testing of many soils. Consequently, these testing programs are rigorous, costly, and time consuming. Independent research studies may be required to propose more realistic procedures to evaluate the soil properties (or soil property functions) for the constitutive relationships. This problem is particularly relevant when dealing with unsaturated soils since behavior is highly nonlinear, difficult, and costly to measure (Fredlund, 2006).

3.2 Water Seepage Constitutive Relations

The driving potential for the flow of water under negative or positive pore–water pressure conditions (i.e., saturated or unsaturated soils), is hydraulic head gradient (Childs and Collis-George, 1950), where hydraulic head is defined as follows:

$$h = \frac{u_w}{\rho_w g} + Y \quad \dots\dots\dots(3.1)$$

where:

h = hydraulic head,

ρ_w = density of water,

g = acceleration due to gravity, and

Y = elevation head.

The velocity of flow of water through an unsaturated soil, v_w , takes the same form as flow through a saturated soil. In other words, Darcy's law applies equally to saturated and unsaturated soils. Assuming that the soil has anisotropic soil properties coinciding with the Cartesian coordinates, Darcy's flow law can be written as:

$$v_{wx} = -k_{wx} \frac{dh}{dx} \quad \dots\dots\dots(3.2a)$$

$$v_{wy} = -k_{wy} \frac{dh}{dy} \quad \dots\dots\dots(3.2b)$$

$$v_{wz} = -k_{wz} \frac{dh}{dz} \quad \dots\dots\dots(3.2c)$$

where k_{wx} , k_{wy} , and k_{wz} = coefficients of permeability for each of the Cartesian coordinate directions; and

v_{wx} , v_{wy} , and v_{wz} = velocity of water flow in the x, y, and z directions, respectively.

The coefficient of permeability is generally assumed to be a constant under all stress states for a saturated soil. However, the coefficient of permeability for an unsaturated soil can vary widely depending on the stress state and therefore takes on the form of a function or mathematical equation. Although any change in the stress state of a soil can affect the coefficient of permeability, it is mainly matric suction that influences the amount of water in the soil and therefore has the dominant influence. Figure (3.1) illustrates the nature of the permeability function for glass beads tested by Mualem (1976).

The results show that when a suction of about (3 kPa) is applied to the glass beads, the coefficient of permeability starts to decrease. A further increase in suction causes the coefficient of permeability to drop by several orders of magnitude. In addition, there are two permeability functions that can be measured, one for the drying process and the other

curve for the wetting process. In other words, the permeability function is hysteretic in the sense that it is dependent upon whether the soil is drying or wetting. Figure (3.2) shows the water content versus matric suction for the glass beads subjected to a drying and wetting process.

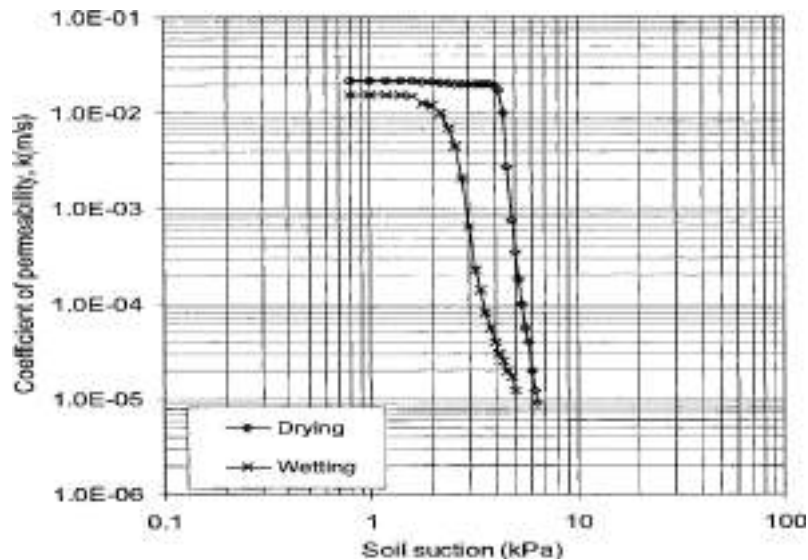


Fig. (3.1) Shape of the drying and wetting permeability function for glass beads tested by Mualem (1976).

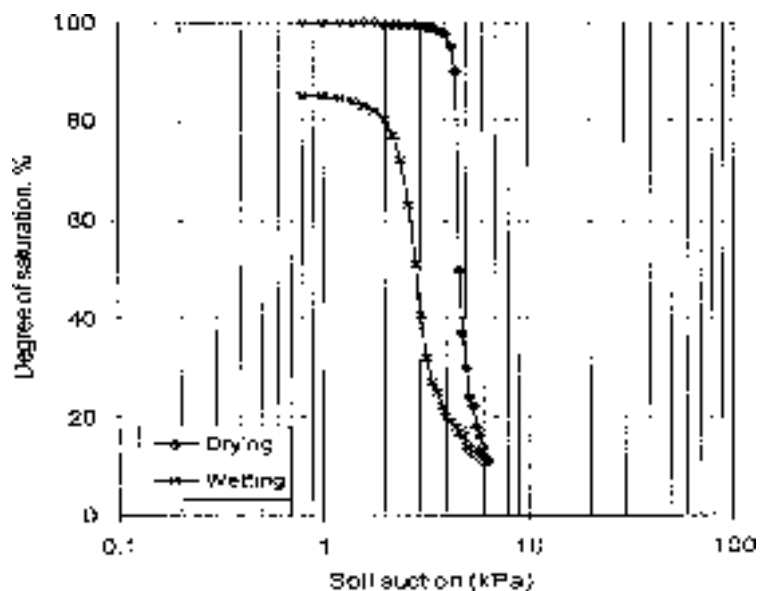


Fig. (3.2) The soil–water characteristic curve for the glass beads showing hysteresis during drying and wetting (Mualem, 1976).

The hysteresis in the water content versus matric suction relationship produces hysteresis in the permeability function. It can be observed that the decrease in coefficient of permeability commences at the air entry of the soil. It is the relationship between the permeability function and the soil–water characteristic curve (SWCC) that can subsequently be used for the estimation of the permeability function. It can be noted that the effect of hysteresis is removed when a plot is made of the water coefficient of permeability, k_w , versus volumetric water content, θ_w (Liakopoulos, 1965). However, this unique relationship provides no advantage when subsequently solving the seepage partial differential equation.

In addition to the drying and wetting curves shown, it is possible to have an infinite number of scanning curves passing from the wetting to the drying curve and vice versa. Coefficient of permeability models have been proposed for unsaturated soils that include scanning paths between the wetting and drying curves (Watson and Sardana, 1987); however, it is presently most common in geotechnical engineering for the engineer to decide whether it is a drying or wetting process that is being modeled and then select the appropriate permeability function.

The coefficient of permeability of an unsaturated soil is not routinely measured in the laboratory. Rather, the saturated coefficient of permeability and the SWCC are combined to provide an estimate of the permeability function. The drying (or desorption) branch of the SWCC is generally measured in the laboratory and consequently, the permeability function is first computed for the drying curve. The permeability function for the wetting curve is then estimated based on measured or estimated hysteresis loops associated with the SWCC (Pham et al., 2003a). Empirical estimation procedures have become quite common for the assessment of the unsaturated permeability function; however, it should be noted that these procedures may significantly underestimate the actual

unsaturated permeability function in fine-grained soils with microstructure effects associated with soil fabric (Chiu and Shackelford, 1998).

Anisotropic soil conditions add another variation to the permeability function as shown in Figure (3.3). The primary change in the permeability function is associated with the difference between the saturated maximum and minimum coefficients of permeability corresponding to the principal direct of anisotropy (Freeze and Cherry, 1979). The air entry value observed on the SWCC corresponds to the point where both the maximum and minimum coefficients of permeability start to decrease. Consequently, the mathematical form for the permeability function is similar for both the drying and wetting branches.

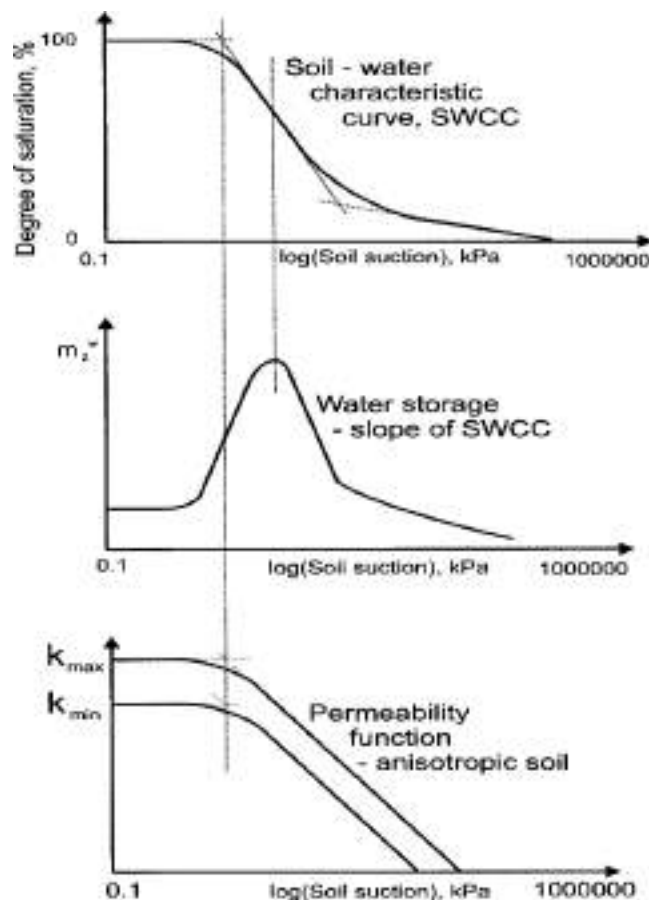


Fig. (3.3) Example of permeability and water storage functions for an anisotropic soil (Fredlund, 2006).

3.3 Ability of an Unsaturated Soil for Storage

The simulation of transient flow processes (i.e., water, air, or heat) requires a characterization of a storage property that changes with the water degree of saturation of the soil. The storage soil property is part of the partial differential equation describing a transient process.

The water storage soil property associated with water flow through an unsaturated soil, m^w_2 , is equal to the arithmetic slope of the SWCC. The differentiation of any mathematical equation proposed for the SWCC can serve as a measure of the water storage soil property. Figure (3.3) shows the form of the water storage function for a sandy soil. There is strong nonlinearity corresponding to the point of inflection along the SWCC. The nonlinearity of the water storage soil property can give rise to numerical instability and errors in computing water balances, if not properly taken into account during the solution of the seepage partial differential equation. Since there is hysteresis in the SWCC, there will also be independent water storage curves for the drying and wetting processes.

The air phase also has a storage term as well as a compressibility component in the partial differential equation. The air storage term takes the same form as the water storage function. The air compressibility and air storage terms have similar effects on a transient air flow process.

The storage term for heat flow is called specific heat, ξ . Specific heat is also controlled by the proportion of air, water, and solids comprising the soil and consequently can be written as a function of the soil–water characteristic curve (Fredlund, 2006).

3.4 Air Flow Constitutive Relations

Air has a low density and consequently, the driving potential for flow is the air pressure gradient. The mass of air flow, m_a (as opposed to

the volume of air flow), can be written using the constitutive flow relationship referred to as Fick's law (1855) :

$$m_{ax} = -D_{ax} \frac{du_a}{dx} \quad \dots\dots\dots(3.3a)$$

$$m_{ay} = -D_{ay} \frac{du_a}{dy} \quad \dots\dots\dots(3.3b)$$

$$m_{az} = -D_{az} \frac{du_a}{dz} \quad \dots\dots\dots(3.3c)$$

where m_{ax} , m_{ay} , and m_{az} = mass flow rate in the x, y, and z directions, respectively; and

D_{ax} , D_{ay} , and D_{az} = air diffusivity in the x, y, and z directions, respectively.

The assumption is generally made that changes in atmospheric air pressure are negligible. The air flow law can also be written as a velocity of flow, v_a , similar to Darcy's law (Blight, 1971), thereby taking on the following form :

$$v_{ax} = -k_{ax} \frac{du_a}{dx} \quad \dots\dots\dots(3.4a)$$

$$v_{ay} = -k_{ay} \frac{du_a}{dy} \quad \dots\dots\dots(3.4b)$$

$$v_{az} = -k_{az} \frac{du_a}{dz} \quad \dots\dots\dots(3.4c)$$

The air coefficient of permeability, k_a (and air diffusivity) is also a mathematical function in the sense that the transmission of air varies with the amount of air which, in turn, is controlled by the soil–water characteristic curve. Figure (3.4) shows a soil–water characteristic curve for sand and illustrates the form of the air permeability function (Ba-Te et al., 2005). The air permeability function takes on an inverse form to that of the water permeability function. The air coefficient of permeability tends toward the diffusion of air through water below the air entry value of the soil. Once the air entry value is exceeded, the air coefficient of

permeability increases by several orders of magnitude. The low viscosity of air indicates that air can flow through a soil with much greater ease than water.

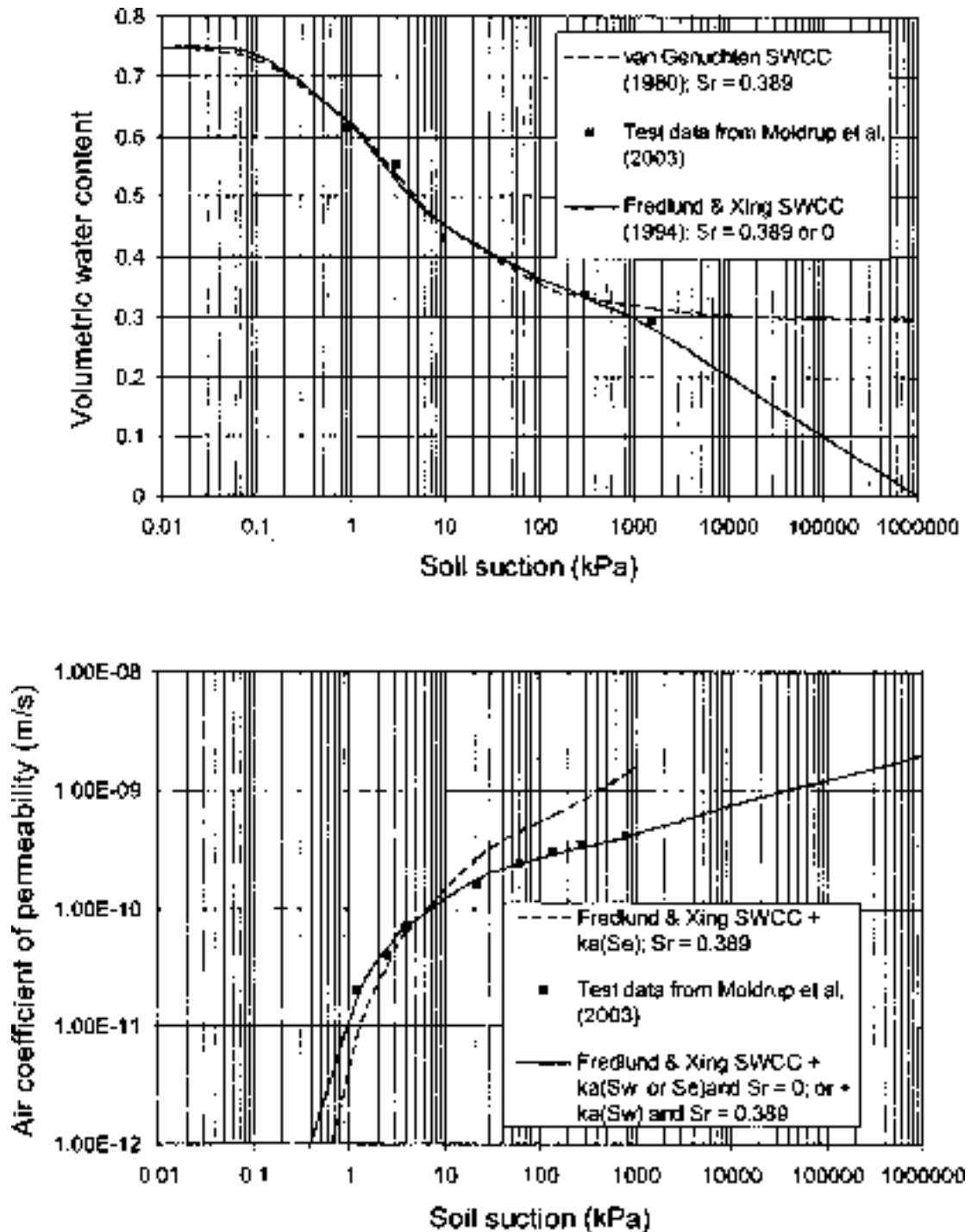


Fig. (3.4) Air permeability function estimated from the SWCC
(Ba-Te et al., 2005).

3.5 Shear Strength Constitutive Relations

The shear strength constitutive relationship provides a mathematical equation relating the normal and shear components of the stress tensor. Any one of several shear strength failure criteria could be extended from saturated soil conditions to unsaturated soil conditions. The Mohr–Coulomb failure criterion was extended to embrace unsaturated soils by Fredlund et al. (1978). In a general form, the shear strength equation can be written as follows:

$$\tau = c' + (\sigma_n - u_a)\tan\phi' + (u_a - u_w)f_1 \quad \dots\dots\dots(3.5)$$

where: τ = shear strength;

c' = effective cohesion intercept;

σ_n = total normal stress on the failure plane at failure;

ϕ' = effective angle of internal friction; and

f_1 = soil property function defining the relationship between shear strength and soil suction; the derivative of which [i.e., $df_1/d(u_a - u_w)$], gives the instantaneous rate of change in shear strength.

Figure (3.5) shows Eq. (3.5) as a three-dimensional constitutive surface with matric suction plotted perpendicular to the conventional two-dimensional Mohr–Coulomb plot. The soil properties, c' , and ϕ' , are presented as saturated soil constants but the soil property, f_1 , varies in response to the amount of water filling the voids of the soil, i.e., it is a function of matric suction (Gan et al., 1988). There is curvature to the shear strength envelope with respect to matric suction and the curvature can be related to the SWCC Figure (3.6).

The peak shear strength of an unsaturated soil bears a relationship to key points along the SWCC. Under low suction conditions (i.e., less than the air entry value of the soil), the derivative of f_1 , tends to equal the tangent of the effective angle of internal friction of the saturated soil (i.e., $\tan\phi'$). At high suction conditions (i.e., greater than residual soil suction),

the derivative of f_1 , has been shown to tend toward zero for several soils with varying silt and clay contents (Nishimura and Fredlund, 2001). Sandy soils have shown that the slope may even become negative at suctions greater than the residual value (Donald, 1956; Gan and Fredlund, 1996).

A linear form of the general shear strength equation [i.e., Eq. (3.6)] was published by Fredlund et al. (1978):

$$\tau = c' + (\sigma_n - u_a)\tan\phi' + (u_a - u_w)\tan\phi^b \quad \dots\dots\dots(3.6)$$

where ϕ^b is the angle of friction with respect to change in suction.

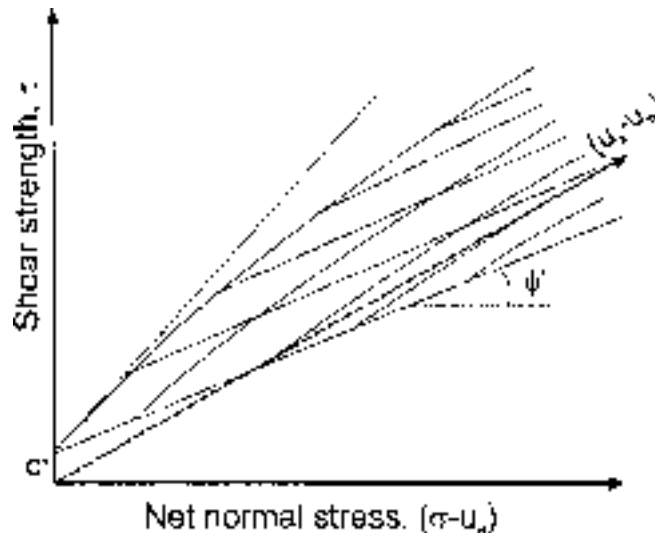
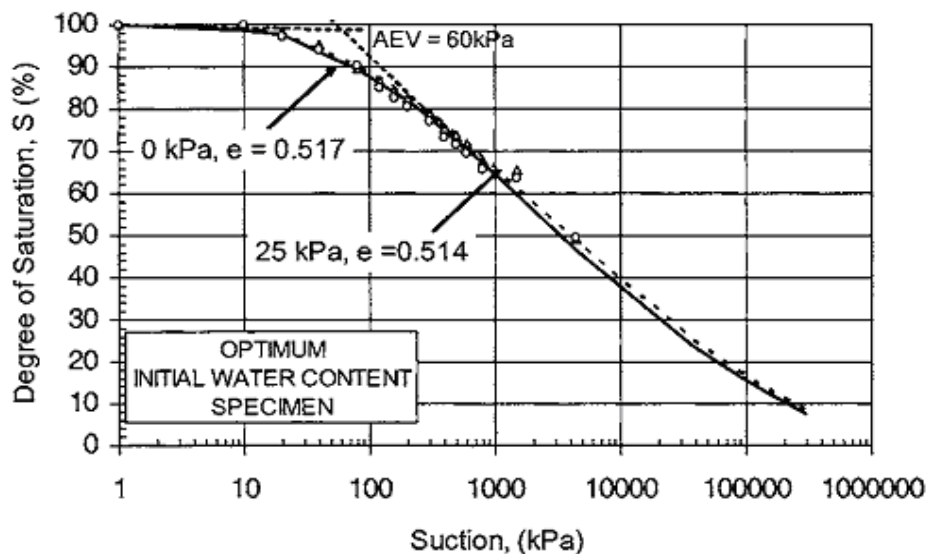
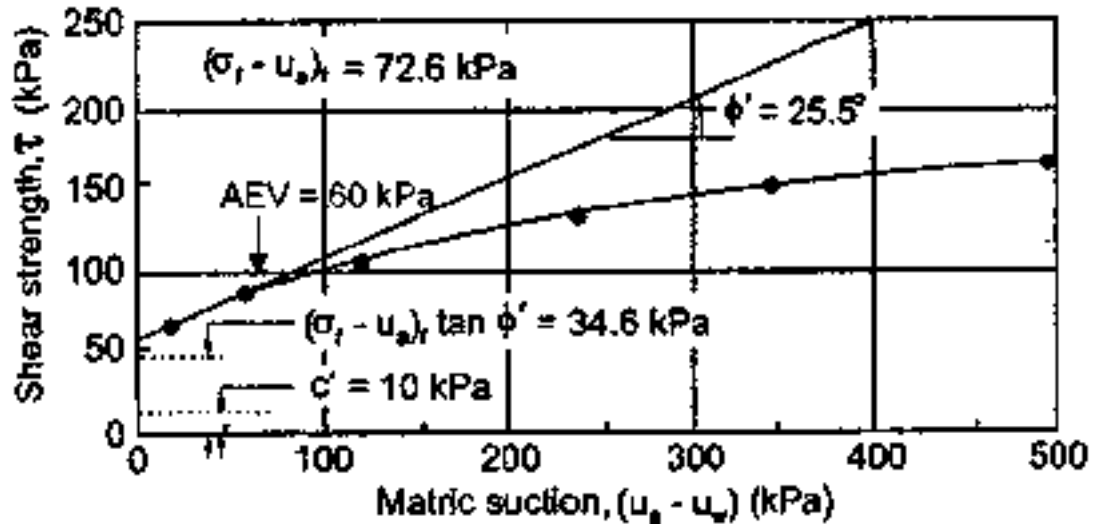


Fig. (3.5) Extended Mohr-Coulomb failure surface written as a function of the stress state (Fredlund et al., 1978).



a: Soil-water characteristic curve for glacial till



b: Multistage direct shear test results on compacted glacial till

Fig.(3.6) Curvature to the shear strength envelope with respect to matric suction:

- (a) Soil–water characteristic curve for glacial till (Vanapalli et al. (1996); and
 and
 (b) multistage direct shear test results on compacted glacial till (Gan et al., (1988).

The linear form is more appropriate for limited ranges of matric suction. Some of the earlier unsaturated soils shear strength data sets (e.g., Bishop et al., 1960) show a close fit to the linear equation (Fredlund and Rahardjo, 1993). The linear form is also more convenient to use for shear strength solutions.

Most research programs related to the shear strength of unsaturated soils appear to have been undertaken on soils that were initially compacted to an initial water content and density and then wetted such that the initial suction was allowed to come toward a zero value (Gan and Fredlund, 1996). The soil specimens are then subjected to a series of increasing matric suctions along the desorption branch of the SWCC. Since there is hysteresis between the drying and wetting curve it would be anticipated that soils may exhibit a different shear strength envelope if first subjected to high matric suction conditions and then reduced to a

series of suction values along the wetting curve. Melinda et al. (2004) reported the shear strength results on a residual soil from Singapore tested along both the drying curve and the wetting curve Figure (3.7). The results show that the measured shear strengths along the drying curve are higher than those measured along the wetting curve. These results can be explained on the basis of the hysteresis of the SWCC that shows the matric suction having a greater cross-sectional area over which to act along the drying curve, for a specific suction. The difference in shear strength between drying and wetting conditions appears to be related to the magnitude of the drying and wetting hysteresis loop.

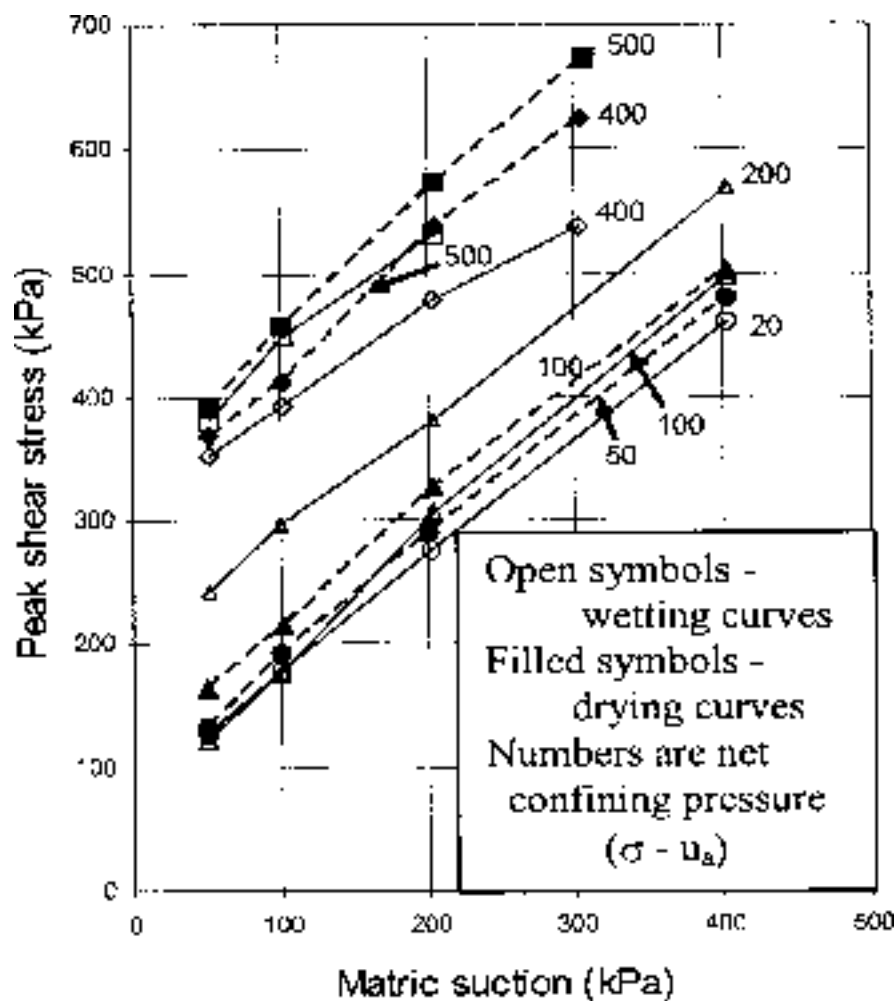


Fig.(3.7) Shear strength results showing the relationship between the SWCC and the peak shear strength of a soil (Melinda et al., 2004).

Shear strength equations formulated for saturated soils, within the context of critical state models, have also been extended to unsaturated soil conditions. Several models have been proposed (Alonso et al., 1990; Toll, 1990; Wheeler and Sivakumar, 1995; Maatouk et al., 1995; Blatz and Graham, 2003). The proposed equations attempt to describe the shear strength of an unsaturated soil under critical state condition, in terms of q - p - s space. A set of shear strength results for compacted kaolin is shown in Figure (3.8) (Wheeler and Sivakumar, 1995).

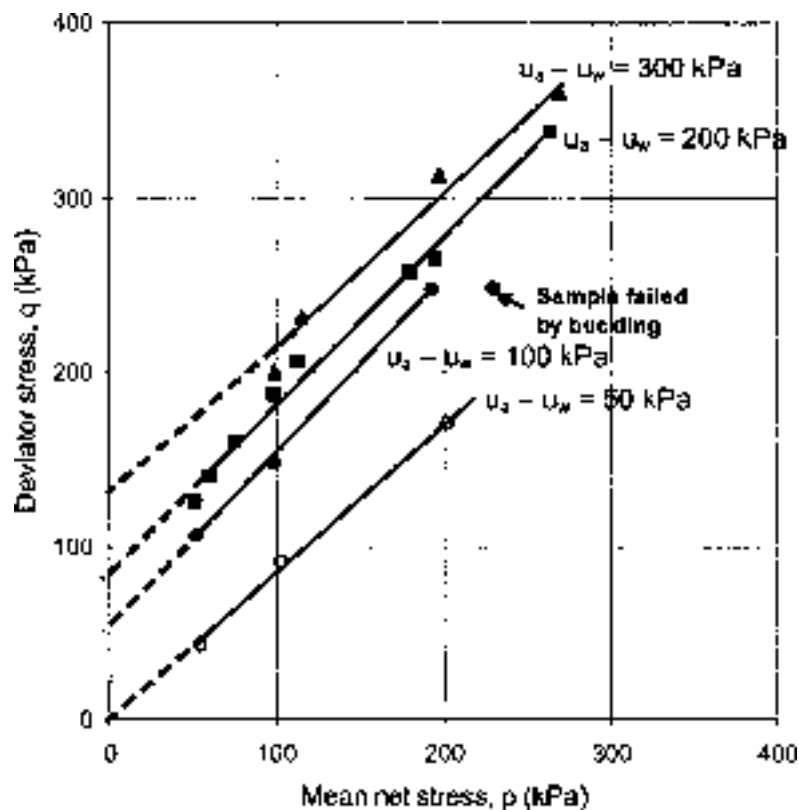


Fig.(3.8) Critical state shear strength results on compacted kaolin (Wheeler and Sivakumar, 1995).

The results show an increase in shear strength as the matric suction of the soil is increased. Specific volumes corresponding to critical state conditions are also presented. The stress state variables used to present the results are as follows:

$$q = \sigma_1 - \sigma_3 \quad \dots\dots\dots(3.7)$$

$$p = \frac{(\sigma_1 + \sigma_2 + \sigma_3)}{3} \quad \dots\dots\dots(3.8)$$

$$s = (u_a - u_w) \quad \dots\dots\dots(3.9)$$

where: σ_1 , σ_2 , and σ_3 are the principal stresses,

u_w is the pore water pressure, and

u_a is the pore air pressure.

The challenge has been to find a consistent means of incorporating the effect of matric suction, $u_a - u_w$ into the shear strength equation. A general form for the shear strength equation under critical state failure conditions can be written as follows (Fredlund, 2006):

$$q = M \cdot f_1[p - u_a, u_a - u_w] \quad \dots\dots\dots(3.10)$$

where M = a material characteristic independent of stresses; and

f_1 = an independent function of $p - u_a$ and $u_a - u_w$.

The critical state shear strength model proposed by Alonso et al. (1990) has the following form:

$$q = M(p - u_a) + k(u_a - u_w) \quad \dots\dots\dots(3.11)$$

where: k = a soil constant.

Jommi (2000) combined the net mean stress and matric suction using the water degree of saturation and suggested a similar equation:

$$q = M[(p - u_a) + S_r(u_a - u_w)] \quad \dots\dots\dots(3.12)$$

Wheeler and Sivakumar (1995) suggested a critical shear strength equation where the two shear strength properties were functions of matric suction:

$$q = M_s(p - u_a) + \mu_s \quad \dots\dots\dots(3.13)$$

where: M_s and μ_s are functions of matric suction.

3.5.1 State surfaces

The volume change characteristics of an unsaturated soil can be expressed as the variation of the void ratio, e , and the variation of the

degree of saturation, S_r . The relationships between these variations and the stress parameters $(\sigma - u_a)$ and $(u_a - u_w)$ can be shown by "state surfaces" obtained from three-dimensional plots of e and the stress parameters and of S_r and the stress parameters.

Several authors have adopted this approach. Matyas and Radhakrishna (1968) presented experimental data to prepare the state surface plots shown in Figure (3.9)

It is seen that the state surface for the void ratio (e) is warped and is therefore able to account for the swelling (volume increase) that the soil will experience if it is flooded at a low value of net stress and its collapse (its volume decrease) when it is flooded at a high value of net stress.

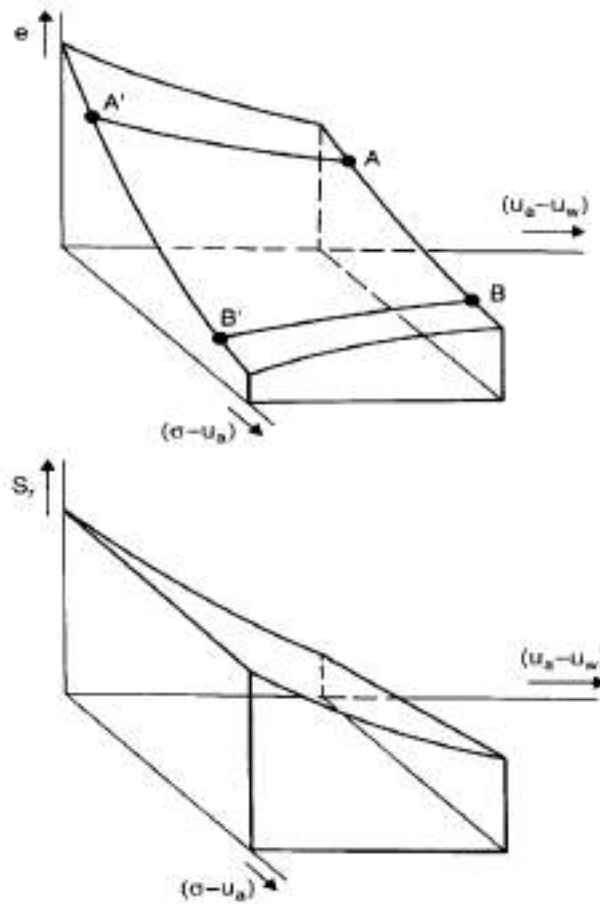


Fig. (3.9) State surface plots (based on Matyas and Radhakrishna, 1968).

3.6 Volume–Mass Constitutive Relations

Two volume–mass constitutive relations are required in order to relate all volume–mass soil properties to the stress state (Fredlund and Morgenstern, 1976). The most common volume–mass properties used in geotechnical engineering to define volume–mass relations are: void ratio, e ; water content, w ; and water degree of saturation, S_w .

The volume–mass constitutive relationships for an unsaturated soil use the saturated soil conditions as a reference or starting point in a manner similar to that shown for seepage and shear strength. The overall volume change has historically been defined in terms of void ratio change, de , and related to effective stresses. More recently, critical state models have used changes in specific volume, $d(1+e)$, as the reference deformation state variable.

Figure (3.10) shows the reference compression curve relationship for a saturated soil under K_o loading (plotted to the base 10 logarithm) and isotropic loading conditions (plotted to a natural logarithm). Loading along the virgin compression line, as well as the unloading and reloading lines, are commonly approximated as straight lines on the semilogarithm plot. Isotropic loading conditions have formed the reference relationship for elastoplastic models and provide a separation from the application of deviator stresses (or shear stresses). However, K_o loading is easier to perform with equipment commonly available in soil mechanics laboratories. The equation representing the reference stress deformation line for the saturated soil, as defined by the virgin compression line, is written as follows (Fredlund, 2006):

$$e = e_o - C_c \log(p - u_w) / (p_o - u_w) \quad \dots\dots\dots(3.14)$$

where e_o = initial void ratio at $(p_o - u_w)$;

p_o = initial total stress (i.e., vertical stress for K_o loading);

p = any total stress state under consideration; and

C_c = compressive index (i.e., slope of the virgin compression branch).

One-dimensional oedometer results have conventionally been plotted as void ratio versus logarithm of vertical stress (base 10). Within the elastoplastic framework, the specific volume, $(1+e)$, is generally plotted versus the logarithm of the mean applied stress (natural log base). The mathematical relationship between K_o loading and isotropic loading conventions can be expressed as

$$\lambda = C_c / \ln(10) \approx 0.434C_c \quad \dots\dots\dots(3.15)$$

$$\kappa = C_s / \ln(10) \approx 0.434C_s \quad \dots\dots\dots(3.16)$$

where λ is slope of the virgin compression line on a plot of specific volume and the natural logarithm of effective stress and κ is slope of the rebound or reloading compression line on a plot of specific volume and the natural logarithm of effective stress.

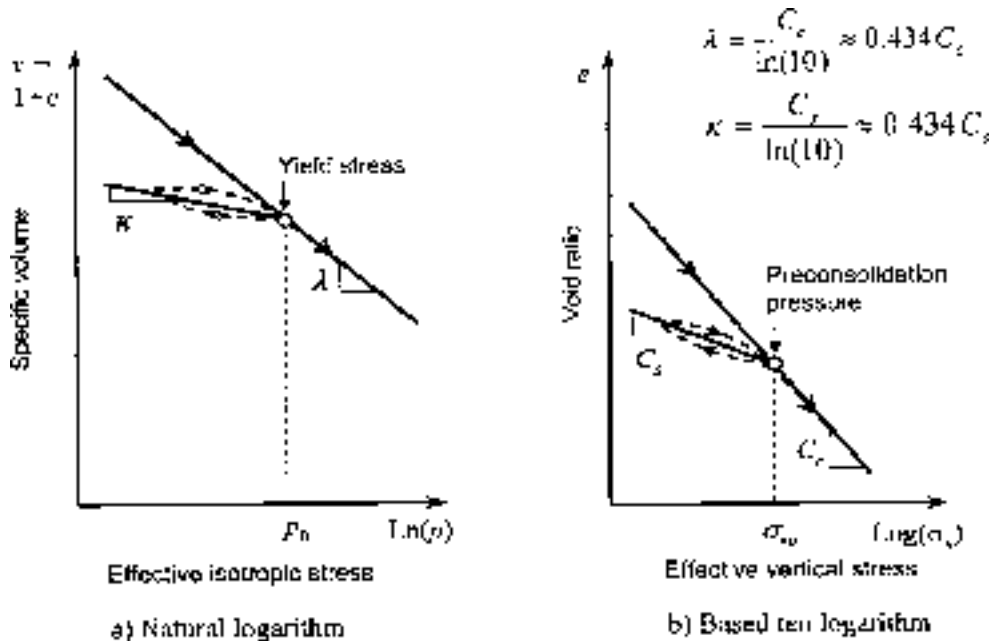


Fig. (3.10) Reference compression curves for a saturated soil (Fredlund, 2006).

The volume change versus effective stress equations for the saturated soil can be converted to an incremental elasticity form with respect to the stress state. Consequently, the volume change soil property changes with stress state and the solution becomes nonlinear. Stress reversals and complex loading paths can be better accommodated through use of more rigorous elastoplastic models.

The constitutive relations for an unsaturated soil require an extension of the nonlinear models for the saturated soil. The extended models must include the effect of changes in matric suction which results in further nonlinearities. Fredlund and Morgenstern (1976) used three-dimensional surfaces to represent the void ratio change, de , and water content, w , constitutive relations for an unsaturated soil. Figure (3.11) illustrates the limiting or bounding relationships associated with a typical clayey silt soil.

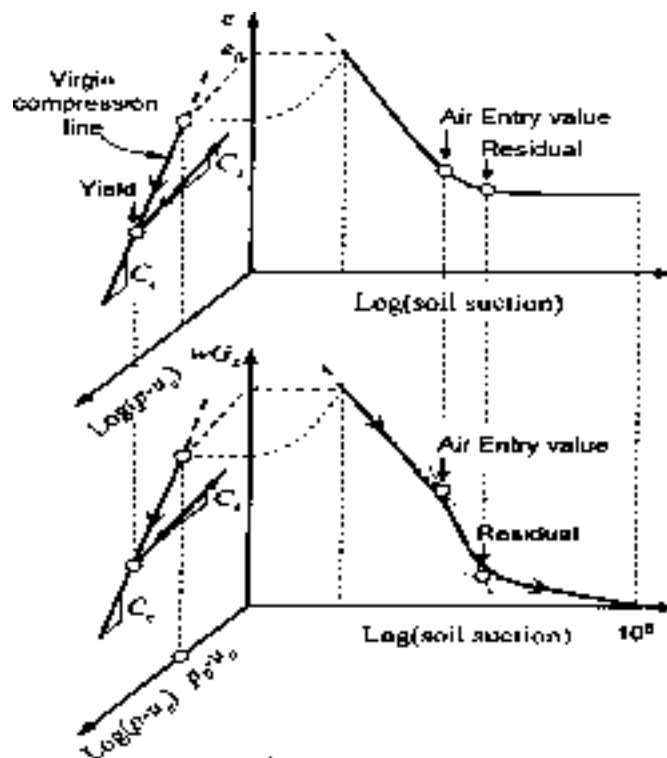


Fig. (3.11) Illustration of the limiting or bounding relationships for a typical clayey silt soil (Fredlund, 2006).

A general differential equation can be such written that it is applicable at any stress point on the void ratio and water content constitutive surfaces (Fredlund, 2006):

$$de = \frac{\partial e}{\partial(\sigma_m - u_a)} d(\sigma_m - u_a) + \frac{\partial e}{\partial(u_a - u_w)} d(u_a - u_w) \dots\dots\dots(3.17)$$

$$dw = \frac{\partial w}{\partial(\sigma_m - u_a)} d(\sigma_m - u_a) + \frac{\partial w}{\partial(u_a - u_w)} d(u_a - u_w) \dots\dots\dots(3.18)$$

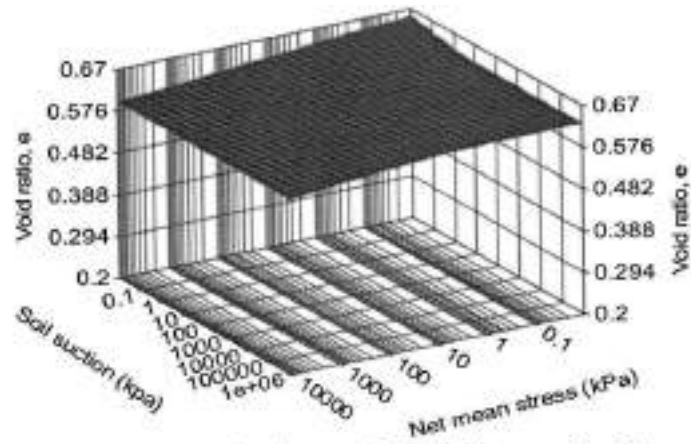
where $\sigma_m = (\sigma_1 + \sigma_2 + \sigma_3) / 3$ and

$\sigma_m - u_a =$ mean net stress.

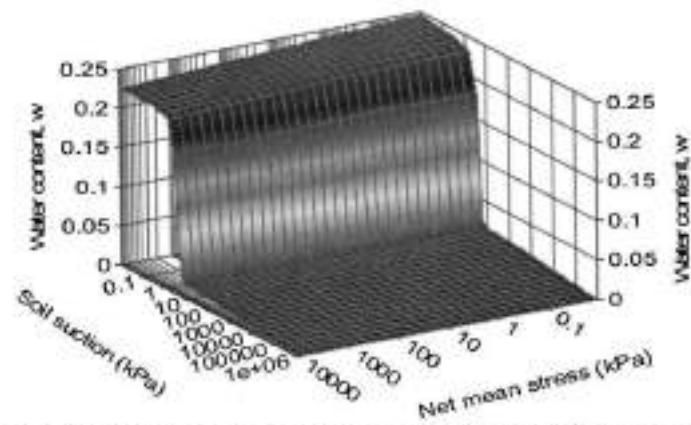
The differential equation has one part that designates the stress point under consideration (i.e., $\sigma_m - u_a$ and $u_a - u_w$) and another part that provides a general representation of the associated soil properties [e.g., $\delta_e / \delta(\sigma_m - u_a)$ and $\delta_e / \delta(u_a - u_w)$]. The soil properties at a point on the constitutive surface can be approximated as a linear compressibility modulus provided the stress increments are relatively small. The compressibility modulus can also be written as a function of the stress state. There is need for an equation that can represent the entire constitutive surface. Once such an equation is available it will be possible to differentiate the equation to obtain the soil properties necessary for nonlinear numerical modeling.

The volume–mass constitutive surfaces have distinct characteristics for sands, silts and clays. All unsaturated soils have features such as the air entry value and the residual suction. The following figures (i.e., Figures 3.12 and 3.13) show typical volume–mass constitutive surfaces (i.e., void ratio, gravimetric water content, and water degree of saturation) generated from measured data on Beaver Creek sand, and Regina clay (Pham, 2005). Each of the constitutive surfaces is uniquely influenced by the yield stress (or preconsolidation pressure), the air entry value, and the

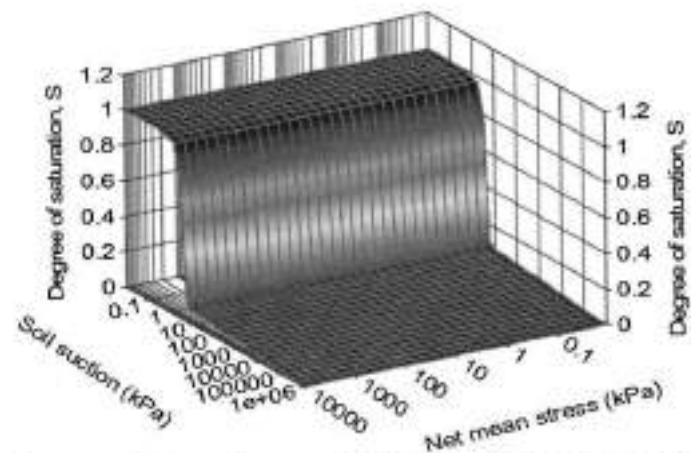
residual suction of the soil. Each of these terms is a function of the stress state.



a: Void ratio constitutive surface of Beaver Creek sand

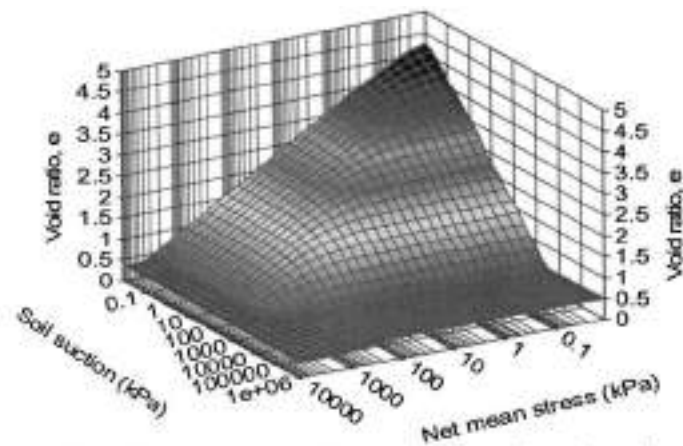


b: Gravimetric water content constitutive surface of Beaver Creek sand

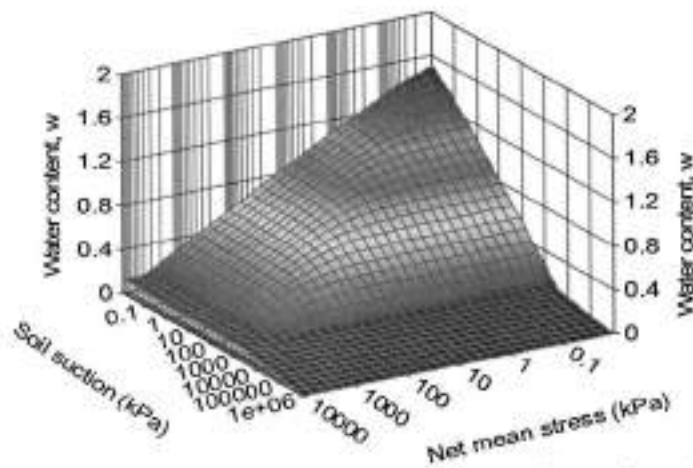


c: Water degree of saturation constitutive surface of Beaver Creek sand

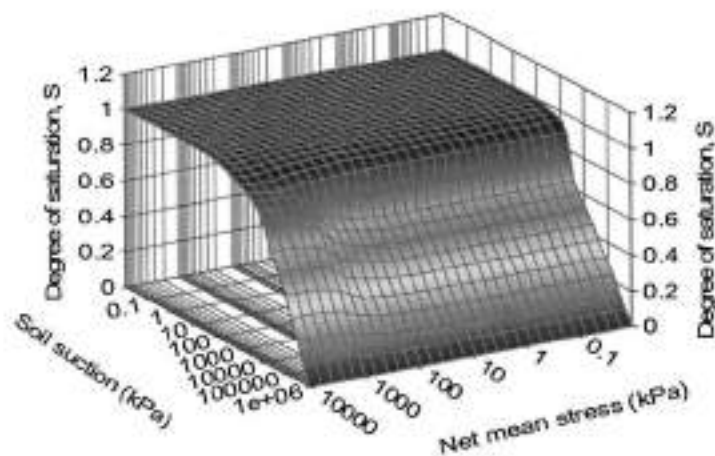
Fig. (3.12) Volume–mass constitutive surfaces for Beaver Creek sand (Pham, 2005).



a: Void ratio constitutive surface of Regina clay



b: Gravimetric water content constitutive surface of Regina clay



c: Water degree of saturation constitutive surface of Regina clay

Fig. (3.13) Volume–mass constitutive surfaces for Regina clay (Pham, 2005).

3.7 Definition of Unsaturated Soil in the Present Work

In this thesis, a relation similar to the shear strength constitutive relation is adopted for describing the pore water pressure change with the soil stiffness.

In unsaturated soil, the soil stiffness increases with increasing suction. This behavior can be described by an H-modulus function as illustrated in Figure (3.14). The unsaturated soil modulus (H) is only used in the unsaturated zone (pore water pressure (0)).

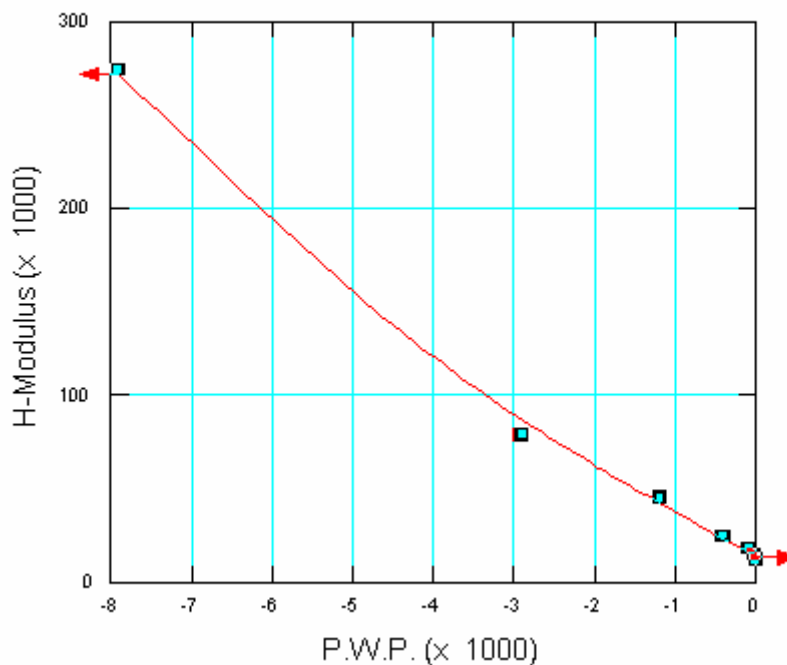


Fig. (3.14) A Typical H-modulus function (Manual user's guide of SIGMA/W, 2002).

CHAPTER FOUR

FINITE ELEMENT FORMULATION FOR CONSOLIDATION PROBLEMS

CHAPTER FOUR

FINITE ELEMENT FORMULATION FOR CONSOLIDATION PROBLEMS

4.1 Introduction

A finite element analysis consists of two steps. The first step is to model the problem, while the second step is to formulate and solve the associated finite element equations. Modeling involves designing the mesh, defining the material properties, choosing the appropriate constitutive soil model, and defining the boundary conditions. The modeling, however, must be done first; that is, the user must design an acceptable mesh, select the applicable soil properties, and control the boundary conditions. Good modeling techniques require practice and experience.

4.2 Element Shape

The accuracy and performance of an element is affected to some extent by its shape. For quadrilateral elements, the best performance is achieved when the interior angles are 90 degrees (a rectangle); for triangular elements, the best performance is achieved when one interior angle is 90 degrees and the other two angles are 45 degrees. Acceptable performance can be obtained for elements with interior angles that deviate from 45 and 90 degrees; however, the performance of the elements deteriorates rapidly if any interior angle approaches zero or 180 degrees. In the case of quadrilateral elements, interior angles equal to or greater than 180 degrees are unacceptable. Figure (4.1) shows the shape and performance rating of elements.


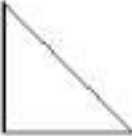


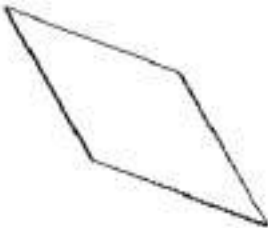

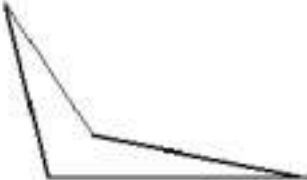

Quadrilateral	Triangular	Performance
		Best
		Acceptable
		Poor
		Unacceptable

Fig. (4.1) Element slopes and performance.

The aspect ratio (length to height) of elements can also affect the performance. As the aspect ratio increases, the element performance deteriorates. The best performance of long, thin elements is achieved by quadrilateral elements with eight nodes and nine point integration. The poorest performance comes from three-noded long, thin elements with one point integration. Generally, the higher order elements should be used when the aspect ratio is high.

Difficulties with aspect ratios can easily arise when you are working with an unevenly scaled problem, i.e. one uses a scale in the x -direction different from that in the y -direction.

4.3 Higher Order Elements

When an element has secondary nodes at the mid-points between the corner nodes, the element is known as a "higher order" element, since the equations describing the deformation within the element are of a higher order than when there are no secondary nodes.

As a general rule, ordinary elements are adequate for the linear-elastic model. While the ordinary elements result in a poor stress distribution within a single element, the stress distribution is reasonable when averaged to the nodes for contouring. Also, for a linear-elastic model, the material property is not a function of the computed stress; consequently, the poor stress distribution has little effect on the computed deformations. If linear-elastic deformation is the primary objective of the analysis, then ordinary 4-noded or 3-noded elements are usually adequate.

For the nonlinear constitutive soil models, the material properties are a function of the computed stresses. Therefore, a reasonable stress distribution within the element is essential, and higher order elements should be used. This is particularly true for elements which are subject to bending, such as elements located at the edge of a footing or in a retaining wall.

In summary, higher order elements are essential for the nonlinear soil models, particularly in regions where the stress and strain changes are high. In regions where the stress and strains changes are small or the material is assigned a linear-elastic model, the ordinary 4-noded and 3 noded elements may be adequate (SIGMA/W User's Guide, 2002).

4.4 Consolidation Analysis

Consolidation analysis can be done by coupling displacements and pore water pressures. In a consolidation analysis, we are interested in how displacement and pore-water pressure change simultaneously.

When coupled, the analysis contributes to forming a common global characteristic (stiffness) matrix. Three equations are created for each node in the finite element mesh. Two are equilibrium (displacement) equations and the third is a continuity (flow) equation. Solving all three equations simultaneously gives both displacement and pore-water pressure changes.

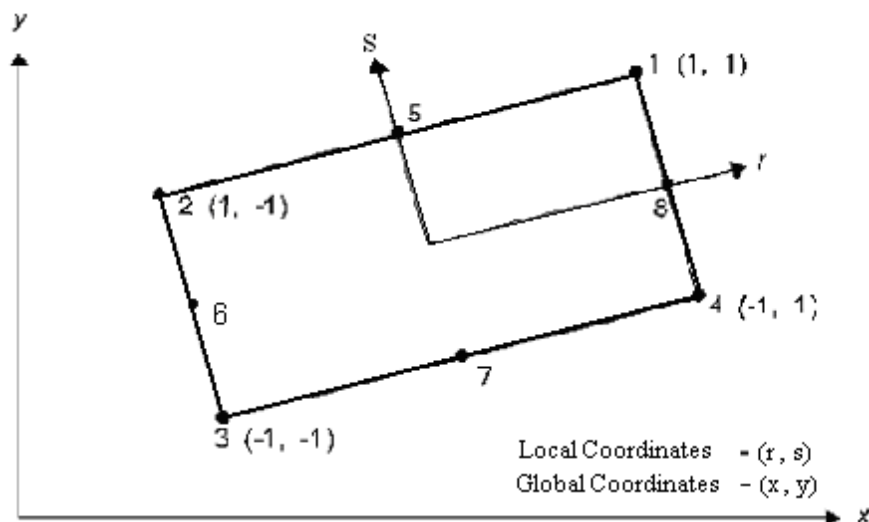
4.4.1 Coordinate Systems

The global coordinate system used in the formulation is the conventional Cartesian $x y$ system. The finite element grid lies in the first quadrant, with the positive y axis coinciding with the vertically upward direction. In an axisymmetric analysis, the x -axis is used to represent the radial distance and the y -axis is the axis of symmetry.

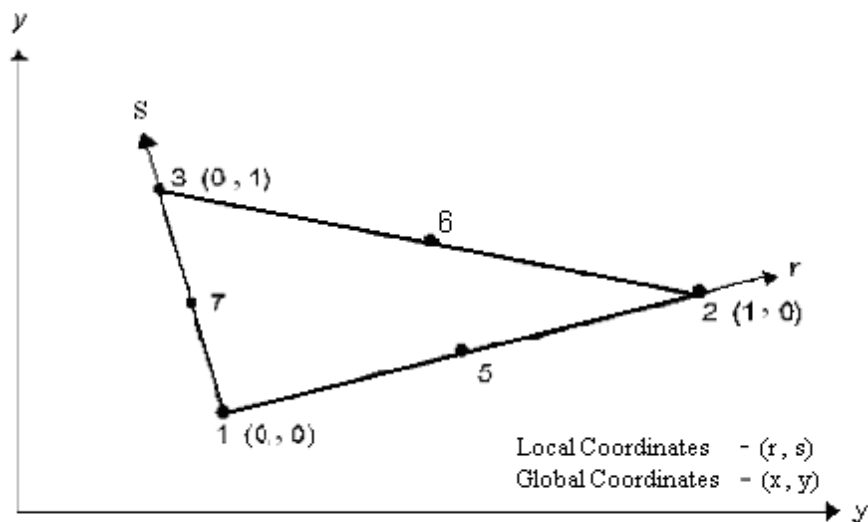
The local coordinate system used in the formulation of element matrices is presented in Figure (4.2). Presented as well in Figure (4.1) is the local element node numbering system. The local coordinates for each of the nodes are given in Table (4.1).

Table (4.1) Local element node numbering system.

Element Type	Node	r	x
Quadrilateral	1	+1	-1
	2	-1	-1
	3	-1	-1
	4	+1	-1
	5	0	-1
	6	-1	0
	7	0	-1
	8	1	0
Triangular	1	0	0
	2	1	0
	3	1	1
	4	-	-
	5	1/2	0
	6	1/2	1/2
	7	0	1/2
	8	-	-



(a) Quadrilateral Element



(b) Triangular Element

Fig. (4.2) Global and local coordinate systems.

The local and global coordinate systems are related to each other by a set of interpolation functions for both types of elements.

SIGMA/W applies the same set of interpolating functions to a finite element when modeling the geometry (relating local to global coordinates) as when describing the variation in the field variable (displacement). In an infinite element, a different set of interpolating functions, called mapping functions, is used to model the geometry.

The x and y coordinates within a finite element are related to the coordinates of its nodes through the following equations:

$$x = \langle N \rangle \{ X \} \quad \dots\dots\dots$$

(4.1)

$$y = \langle N \rangle \{ Y \}$$

\dots\dots\dots(4.2)

where $\langle N \rangle = \langle N1 \ N2 \ N3 \ N4 \ N5 \ N6 \ N7 \ N8 \rangle$ is a vector of interpolating functions, and $\{ X \}$ and $\{ Y \}$ are the global x y coordinates of the element nodes. These interpolating functions are expressed in terms of local coordinates as shown in the Interpolating Functions section of this chapter. Once a set of local coordinates (r, s) has been specified, the corresponding global coordinates can be determined by using the above equations. In an infinite element, global and local coordinates are related in a similar manner using the mapping functions $\langle M \rangle$.

4.4.2 Field Variable Model

To formulate a finite element analysis, it is necessary to adopt a model for the distribution of the field variable within each finite element. The field variable in a stress/deformation analysis is nodal displacement. The displacement distribution model at any given location inside a finite element is given by the following set of equations:

$$u = \langle N \rangle \{ U \} \quad \dots\dots\dots(4.3)$$

$$v = \langle N \rangle \{ V \} \quad \dots\dots\dots(4.4)$$

where:

u = x-displacement at the given location,

v = y-displacement at the given location,

$\{ U \}$ = x-displacement at the nodes of the element,

$\{ V \}$ = y-displacement at the nodes of the element, and

$\langle N \rangle$ = interpolation functions evaluated at the given point.

4.4.3 Derivatives of Interpolating Functions

The fundamental constitutive relationship used in the formulation relates stress, σ , to strain, ε , using the stiffness, E , of the material. In equation form:

$$\sigma = E\varepsilon \quad \dots\dots\dots(4.5)$$

In a two-dimensional plane strain problem, there are three basic strain components: longitudinal strain in the x-direction, ε_x , longitudinal strain in the y-direction, ε_y , and shear strain in the x-y plane, γ_{xy} . For small displacement, and small strain problems, the strain components are related to x- and y displacements, u and v , as follows:

$$\varepsilon_x = \frac{\partial u}{\partial x} \quad \dots\dots\dots(4.6)$$

$$\varepsilon_y = \frac{\partial v}{\partial y} \quad \dots\dots\dots(4.7)$$

$$\gamma_{xy} = \frac{\partial u}{\partial y} + \frac{\partial v}{\partial x} \quad \dots\dots\dots(4.8)$$

At any point within a finite element, displacements u and v are related to the nodal displacement vectors $\{U\}$ and $\{V\}$ by:

$$u = \langle N \rangle \{U\} \quad \dots\dots\dots(4.9)$$

$$v = \langle N \rangle \{V\} \quad \dots\dots\dots(4.10)$$

Strains, when expressed in terms of nodal displacements, can be written as follows:

$$\varepsilon_x = \frac{\partial u}{\partial x} = \left\langle \frac{\partial N}{\partial x} \right\rangle \{U\} \quad \dots\dots\dots(4.11)$$

$$\varepsilon_y = \frac{\partial v}{\partial y} = \left\langle \frac{\partial N}{\partial y} \right\rangle \{V\} \quad \dots\dots\dots(4.12)$$

$$\gamma_{xy} = \frac{\partial u}{\partial y} + \frac{\partial v}{\partial x} = \left\langle \frac{\partial N}{\partial y} \right\rangle \{U\} + \left\langle \frac{\partial N}{\partial x} \right\rangle \{V\} \quad \dots\dots\dots(4.13)$$

The above equations show that, in order to calculate strains, it is necessary to differentiate the interpolating functions with respect to x and y . The derivatives of the interpolating functions in the local and global coordinate systems are given by the chain rule:

$$\begin{Bmatrix} \left\langle \frac{\partial N}{\partial r} \right\rangle \\ \left\langle \frac{\partial N}{\partial s} \right\rangle \end{Bmatrix} = \begin{bmatrix} \frac{\partial x}{\partial r} & \frac{\partial y}{\partial r} \\ \frac{\partial x}{\partial s} & \frac{\partial y}{\partial s} \end{bmatrix} \begin{Bmatrix} \left\langle \frac{\partial N}{\partial x} \right\rangle \\ \left\langle \frac{\partial N}{\partial y} \right\rangle \end{Bmatrix} \quad \dots\dots\dots(4.14)$$

in which :

$$\begin{bmatrix} \frac{\partial x}{\partial r} & \frac{\partial y}{\partial r} \\ \frac{\partial x}{\partial s} & \frac{\partial y}{\partial s} \end{bmatrix} = [J], \text{ the Jacobian matrix} \quad \dots\dots\dots(4.15)$$

Thus, the derivative of the interpolation functions with respect to x and y can be determined by inverting Equation (4.14):

$$\begin{Bmatrix} \left\langle \frac{\partial N}{\partial x} \right\rangle \\ \left\langle \frac{\partial N}{\partial y} \right\rangle \end{Bmatrix} = [J]^{-1} \begin{Bmatrix} \left\langle \frac{\partial N}{\partial r} \right\rangle \\ \left\langle \frac{\partial N}{\partial s} \right\rangle \end{Bmatrix} \quad \dots\dots\dots(4.16)$$

where $[J]^{-1}$ is the inverse of the Jacobian.

The Jacobian matrix can be obtained by substituting Equations (4.1) and (4.2) into Equation (4.15), (Zienkiewicz and Taylor, 2000):

$$[J] = \begin{bmatrix} \frac{\partial N_1}{\partial r} & \frac{\partial N_2}{\partial r} & \dots & \frac{\partial N_8}{\partial r} \\ \frac{\partial N_1}{\partial s} & \frac{\partial N_2}{\partial s} & \dots & \frac{\partial N_8}{\partial s} \end{bmatrix} \begin{bmatrix} X_1 & Y_1 \\ X_2 & Y_2 \\ \vdots & \vdots \\ X_8 & Y_8 \end{bmatrix} \quad \dots\dots\dots(4.17)$$

4.4.4 Finite Element Equations

The finite element equation for a given time increment is (Zienkiewicz and Taylor, 2000):

$$\int_v [B]^T [D] [B] dv \{a\} = b \int_v \langle N \rangle^T dv + p \int_A \langle N \rangle^T dA + \{Fn\} \quad \dots\dots\dots(4.18)$$

where:

[B] = strain-displacement matrix,

[D] = constitutive matrix,

{a} = column vector of nodal incremental x- and y-displacements,

A = area along the boundary of an element,

v = volume of an element,

b = unit body force intensity,

<N> = row vector of interpolating functions,

p = incremental surface pressure, and

{Fn} = concentrated nodal incremental loads.

Summation of this equation over all elements is implied. For each time step, incremental displacements are calculated for the incremental applied load. These incremental values are then added to the values from the previous time step. The accumulated values are reported in the output files. Using this incremental approach, the unit body force is only applied when an element is included for the first time during an analysis.

For a two-dimensional plane strain analysis, all elements are considered to be of unit thickness. For constant element thickness, t, Equation (4.18) can be written as:

$$t \int_A [B]^T [D] [B] da \{a\} = bt \int_A \langle N \rangle^T dA + pt \int_L \langle N \rangle^T dL \quad \dots\dots\dots(4.19)$$

However, in an axisymmetric analysis, the equivalent element thickness is the circumferential distance about the axis of symmetry. Although the complete circumferential distance is 2π radians times the radial distance, R, formulation is made for one radian (unity). Consequently, the equivalent thickness is R and the finite element equation for the axisymmetric case becomes:

$$\int_A \left[[B]^T [D] [B] R \right] dA = b \int_A (R \langle N \rangle^T) dA + p \int_L (R \langle N \rangle^T) dL + \{F_n\} \quad \dots\dots\dots(4.20)$$

Unlike the thickness, t , in a two-dimensional analysis, this radial distance, R , is not a constant within an element. Consequently, R needs to be evaluated inside the integral.

In an abbreviated form, the finite element equation is,

$$[K] \{a\} = \{F\} = \{F_b\} + \{F_s\} + \{F_n\} \quad \dots\dots\dots(4.21)$$

where:

$[K]$ = element characteristic (or stiffness) matrix

$$= t \int_A \left([B]^T [D] [B] \right) dA \quad \text{(for plane strain), or} \quad \dots\dots\dots(4.22)$$

$$= \int_A \left([B]^T [D] [B] R \right) dA \quad \text{(for axi-symmetric)} \quad \dots\dots\dots(4.23)$$

$\{a\}$ = nodal incremental displacements,

$\{F\}$ = applied nodal incremental force which is made up of the following:

$\{F_b\}$ = incremental body forces,

$\{F_s\}$ = force due to surface boundary incremental pressures,

$$= p t \int_L (\langle N \rangle^T) dL \quad \text{for two-dimensional analysis, or}$$

$$= p \int_L (R \langle N \rangle^T) dL \quad \text{for axi-symmetric analysis}$$

$\{F_n\}$ = concentrated nodal incremental forces.

4.4.5 Strain-Displacement Matrix

Engineering shear strain is used in defining the strain vector:

$$\{\mathcal{E}\} = \left\{ \begin{array}{c} \mathcal{E}_x \\ \mathcal{E}_y \\ \mathcal{E}_z \\ \gamma_{xy} \end{array} \right\} \quad \dots\dots\dots(4.24)$$

The field variable of a stress/deformation problem is displacement which is related to the strain vector through:

$$\{\varepsilon\} = [B] \begin{Bmatrix} u \\ v \end{Bmatrix} \quad \dots\dots\dots(4.25)$$

where:

[B] = strain - displacement matrix, and

u, v = nodal displacement in x- and y-directions, respectively.

For a two-dimensional plane strain problem, ε_z is zero and the strain - displacement matrix is defined as (Zienkiewicz and Taylor, 2000):

$$[B] = \begin{bmatrix} \frac{\partial N_1}{\partial x} & 0 & \dots & 0 \\ 0 & \frac{\partial N_1}{\partial y} & \dots & \frac{\partial N_8}{\partial y} \\ 0 & 0 & \dots & 0 \\ \frac{\partial N_1}{\partial x} & \frac{\partial N_1}{\partial y} & \dots & \frac{\partial N_8}{\partial y} \end{bmatrix} \quad \dots\dots\dots(4.26)$$

For an axisymmetric problem, the strain matrix can be written as:

$$\{\varepsilon\} = \begin{Bmatrix} \varepsilon_x \\ \varepsilon_y \\ \varepsilon_z \\ \gamma_{xy} \end{Bmatrix} = \begin{Bmatrix} \frac{\partial u}{\partial x} \\ \frac{\partial v}{\partial y} \\ \frac{u}{r} \\ \frac{\partial u}{\partial y} + \frac{\partial v}{\partial x} \end{Bmatrix} \quad \dots\dots\dots(4.27)$$

The associated strain - displacement matrix [B] is then:

$$[B] = \begin{bmatrix} \frac{\partial N_1}{\partial x} & 0 & \dots & \frac{\partial N_1}{\partial x} & 0 \\ 0 & \frac{\partial N_1}{\partial y} & \dots & 0 & \frac{\partial N_8}{\partial y} \\ \frac{N_1}{R} & 0 & \dots & \frac{N_8}{R} & 0 \\ \frac{\partial N_1}{\partial x} & \frac{\partial N_1}{\partial y} & \dots & \frac{\partial N_8}{\partial x} & \frac{\partial N_8}{\partial y} \end{bmatrix} \quad \dots\dots\dots(4.28)$$

4.4.6 Elastic Constitutive Relationship

Stresses are related to strains as follows, within the theory of elasticity,

$$\{\sigma\}=[D]\{\varepsilon\} \quad \dots\dots\dots(4.29)$$

where [D] is the constitutive (element property) matrix and is given by:

$$[D]=\frac{E}{(1+\nu)(1-2\nu)}\begin{bmatrix} 1-\nu & \nu & \nu & 0 \\ \nu & 1-\nu & \nu & 0 \\ \nu & \nu & 1-\nu & 0 \\ 0 & 0 & 0 & \frac{1-2\nu}{2} \end{bmatrix} \quad \dots\dots\dots(4.30)$$

where:

E = Young's modulus, and

ν = Poisson's ratio.

4.4.7 Body Forces

Body forces applied in both the vertical and the horizontal directions can be modeled. These forces are applied to all elements when they first become active. The body force in the vertical direction, b_v , is due to gravity acting on an element. For a given material, the unit body force intensity in the vertical direction is given by its unit weight, γ_s , which is in turn related to its mass density, ρ :

$$\gamma_s = \rho \cdot g \quad \dots\dots\dots(4.31)$$

where g is the gravitational constant. When the unit weight γ_s is non-zero, the integral $\gamma_s \int_v \langle N \rangle^T dv$ is evaluated by numerical integration and a vertically downward (negative) force is applied at each node of the element.

4.5 Soil-Pore Fluid Interaction (The Problem and the Governing Equations)

It is well known that the behavior of soils (and indeed other geomaterials) is strongly influenced by the pressures of the fluid present in the pores of the material. Indeed, the concept of effective stress is here of

paramount importance. Thus if σ describes the total stress (positive in tension) acting on the total area of the soil and the pores, and p is the pressure of the fluid (positive in compression) in the pores (generally of water), the effective stress is defined as (Zienkiewicz and Bettess, 1982):

$$\sigma' = \sigma + mp \quad \dots\dots\dots(4.32)$$

Here $m^T = [1, 1, 1, 0, 0, 0]$.

Now it is well known that it is only the effective stress σ' which is responsible for the deformations (or failure) of the solid skeleton of the soil (excluding here a very small volumetric grain compression which has to be included in some cases). Assuming for the development given here that the soil can be represented by a linear elastic model we have:

$$\sigma' = D.\varepsilon \quad \dots\dots\dots(4.33)$$

Immediately the total discrete equilibrium equations for the soil-fluid mixture can be written in exactly the same form as is done for all problems of solid mechanics:

$$\mathbf{M}\ddot{\mathbf{u}} + \mathbf{C}\dot{\mathbf{u}} + \int_{\Omega} \mathbf{B}^T \sigma \, d\Omega + \mathbf{f} = \mathbf{0} \quad \dots\dots\dots(4.34)$$

where $\tilde{\mathbf{u}}$ are the displacement discretization parameters , i.e.

$$\mathbf{u} \approx \hat{\mathbf{u}} = \mathbf{N}\tilde{\mathbf{u}} \quad \dots\dots\dots(4.35)$$

\mathbf{B} is the strain-displacement matrix and \mathbf{M} , \mathbf{C} , \mathbf{f} have the usual meaning of mass, damping and force matrices, respectively.

Now, however, the term involving the stress must be split as follows:

$$\int_{\Omega} \mathbf{B}^T \sigma \, d\Omega = \int_{\Omega} \mathbf{B}^T \sigma' \, d\Omega - \int_{\Omega} \mathbf{B}^T m p \, d\Omega \quad \dots\dots\dots(4.36)$$

to allow the direct relationship between effective stresses and strains (and hence displacements) to be incorporated. For a linear elastic soil skeleton we immediately have:

$$\mathbf{M}\ddot{\mathbf{u}} + \mathbf{C}\dot{\mathbf{u}} + \mathbf{K}\tilde{\mathbf{u}} - \mathbf{Q}\dot{p} + \mathbf{f} = \mathbf{0} \quad \dots\dots\dots(4.37)$$

where \mathbf{K} is the standard stiffness matrix written as:

$$\int_{\Omega} \mathbf{B}^T \boldsymbol{\sigma}' d\Omega = \left(\int_{\Omega} \mathbf{B}^T \mathbf{D} \mathbf{B} d\Omega \right) \bar{\mathbf{u}} = \mathbf{K} \bar{\mathbf{u}} \quad \dots\dots\dots(4.38)$$

and \mathbf{Q} couples the field of pressures in the equilibrium equations assuming these are discretized as :

$$p \approx \hat{p} = N_p \tilde{\mathbf{p}} \quad \dots\dots\dots(4.39)$$

Thus :

$$\mathbf{Q} = \int_{\Omega} \mathbf{B}^T \mathbf{m} N_p d\Omega \quad \dots\dots\dots(4.40)$$

In the above discretization, conventionally the same element shapes are used for the $\tilde{\mathbf{u}}$ and $\tilde{\mathbf{p}}$ variables, though not necessarily identical interpolations. With the dynamic equations coupled to the pressure field an additional equation is clearly needed from which the pressure field can be derived. This is provided by the transient seepage equation of the form:

$$-\nabla^T (k \nabla p) + \frac{1}{Q} \dot{p} + \dot{\varepsilon}_v = 0 \quad \dots\dots\dots(4.41)$$

where: Q is related to the compressibility of the fluid,

k is the permeability, and

ε_v , is the volumetric strain in the soil skeleton, which on discretization of displacements is given by :

$$\varepsilon_v = \mathbf{m}^T \boldsymbol{\varepsilon} = \mathbf{m}^T \mathbf{B} \tilde{\mathbf{u}} \quad \dots\dots\dots(4.42)$$

The equation of seepage can now be discretized in the standard Galerkin manner as :

$$\mathbf{Q}^T \dot{\bar{\mathbf{u}}} + \mathbf{S} \dot{\bar{\mathbf{p}}} + \mathbf{H} \bar{\mathbf{p}} + \mathbf{q} = 0 \quad \dots\dots\dots(4.43)$$

where Q is precisely that of Equation (4.40), and

$$\mathbf{S} = \int_{\Omega} \mathbf{N}_p^T \frac{1}{Q} \mathbf{N}_p d\Omega \quad \mathbf{H} = \int_{\Omega} (\nabla \mathbf{N}_p)^T k \nabla \mathbf{N}_p d\Omega \quad \dots\dots\dots(4.44)$$

with Q containing the forcing and boundary terms.

4.6 Additional Material Properties for Unsaturated Coupled Analysis

For a coupled analysis involving unsaturated soils, two additional material properties H and R need to be defined. H is a modulus relating to the change of volumetric strain in the soil structure to a change in suction. R is another modulus relating the change in volumetric water content to suction; therefore, it is given by the inverse of the slope of the soil water characteristic curve.

In this section, a procedure to obtain the H modulus parameter from the slope of a void ratio (e) versus matric suction ($u_a - u_w$) curve is described. For a soil element, a change in its volume can be decomposed into two parts:

$$dV = dV_s + dV_v \quad \dots\dots\dots(4.45)$$

where:

dV_s = the change in volume of the soil particles

dV_v = the change in the volume of voids.

If the volume change in the soil particles, dV_s , is small and thus neglected, the volumetric strain can be approximated as follows:

$$dV = dV_v \quad \dots\dots\dots(4.46)$$

From the definition of void ratio, e, a change in void ratio, de, is given by:

$$de = d \left[\frac{V_v}{V_s} \right] = \frac{dV_v}{V_s} = \frac{dV_v}{(1-n)V} = \frac{d\varepsilon_v}{(1-n)} \quad \dots\dots\dots(4.47)$$

where:

n = the porosity of the soil.

The slope of a void ratio versus matrix suction curve can be written as:

$$\frac{de}{d(u_a - u_w)} = \frac{d\varepsilon_v}{(1-n)d(u_a - u_w)} \quad \dots\dots\dots(4.48)$$

In an unsaturated soil element, when only a change in matric suction occurs, the incremental volumetric strain, $d\varepsilon_v$, can be written as:

$$d\varepsilon_v = d\varepsilon_x + d\varepsilon_y + d\varepsilon_z = \frac{3d(u_a - u_w)}{H} \quad \dots\dots\dots(4.49)$$

or

$$\frac{d\varepsilon_v}{d(u_a - u_w)} = \frac{3}{H} \quad \dots\dots\dots(4.50)$$

After substituting Equation (4.50) into Equation (4.48), it can be seen that the slope of a void ratio versus matric suction curve is $\frac{3}{(1-n)H}$.

CHAPTER FIVE

TECHNICAL OVERVIEW ON THE COMPUTER PROGRAM AND VERIFICATIONS

CHAPTER FIVE

TECHNICAL OVERVIEW ON THE COMPUTER PROGRAM AND VERIFICATIONS

5.1 Introduction

This chapter explains the program SIGMA/W. It is divided into four parts. The first part defines the program SIGMA/W. The second part discusses the applications of the program for stress and deformation analysis of geotechnical engineering problems. The third part describes load and deformation analysis (constitutive models, total and effective stresses, boundary conditions, finite element implementation). In the fourth part, some problems are reanalyzed using the program SIGMA/W and the results are compared with previous analysis results.

5.2 The Program SIGMA/W

SIGMA/W is a finite element software product that can be used to perform stress and deformation analyses of earth structures. Its comprehensive formulation makes it possible to analyze both simple and highly complex problems. For example, one can perform a simple linear elastic deformation analysis or a highly sophisticated nonlinear elastic-plastic effective stress analysis. When coupled with SEEP/W, (another GEO-SLOPE software product), it can also model the pore-water pressure generation and dissipation in a soil structure in response to external loads.

5.3 The Program Applications

SIGMA/W is a general finite element software product for stress and deformation analyses of geotechnical engineering structures. A variety of

different stress-strain constitutive relationships can be used, these range from simple linear-elastic, to non-linear elasto-plastic models. Loads can be applied and removed in stages, and SIGMA/W can be used to compute the changes in pore-water pressures that arise from stress state changes. The following are some typical cases that can be analyzed using SIGMA/W.

5.3.1 Deformation Analysis

The most common application of SIGMA/W is to compute deformations caused by earthworks such as foundations, embankments, excavations and tunnels.

5.3.2 Embankment/Excavation Construction

Finite elements can be added or removed from the finite element mesh to simulate the construction of fill placement or excavation. Elements can be identified to be activated or deactivated at various stages, making it possible to simulate the process over time.

5.3.3 Excess Pore-Water Pressures

The effect of excess pore-water pressures generated during fill placement is often a major consideration in slope stability during construction. SIGMA/W can be used to estimate these types of pore-water pressures.

5.3.4 Soil-Structure Interactions

SIGMA/W can accommodate soil-structure interaction problems by including structural elements in two-dimensional plane strain analyses. These elements can be beam elements which have flexural stiffness, and bar elements which have only axial stiffness with no flexural stiffness.

These structural elements are particularly useful when analyzing cases such as sheetpile walls.

5.3.5 Consolidation Analyses

SIGMA/W can be used together with SEEP/W to perform a fully-coupled consolidation analysis. When these two integrated products are run simultaneously, SIGMA/W calculates the deformations resulting from pore-water pressure changes while SEEP/W calculates transient pore-water pressure changes. This procedure is used to simulate the consolidation process in both saturated and unsaturated soils. A fully-coupled analysis is required to correctly model the pore-water pressure response to an applied load. In certain cases, the pore-water pressure increase under an applied load can be greater than the applied load. This phenomenon is known as the Mendel-Cryer effect.

5.4 Load and Deformation Analysis

5.4.1 Constitutive Models:

SIGMA/W is formulated for several elastic and elasto-plastic constitutive soil models. All models may be applied to two-dimensional plane strain and axisymmetric problems. The following models are supported:

- Linear Elastic (Figure 5.1).
- Nonlinear Elastic (Hyperbolic) (Figure 5.2).
- Anisotropic Linear Elastic (Figure 5.3).
- Strain-Softening (Figure 5.4).
- Elastic Plastic (Mohr-Coulomb or Tresca) (Figure 5.5).
- Cam-Clay (Critical state) (Figure 5.6).
- Modified Cam-clay (Critical State) (Figure 5.7).

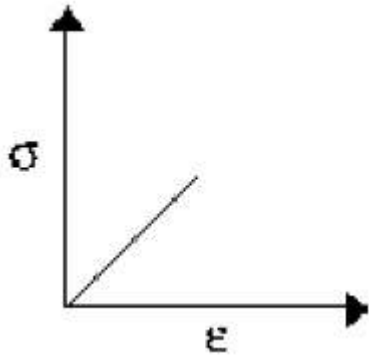


Fig.(5.1) Linear Elastic.

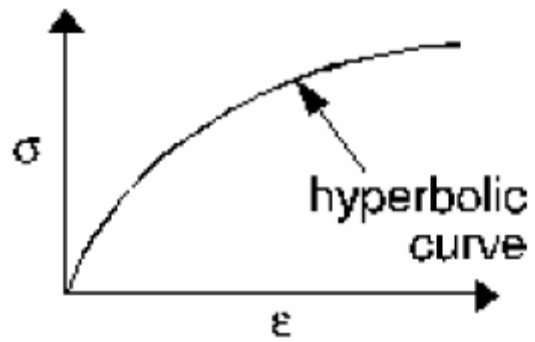


Fig.(5.2) Nonlinear Elastic (Hyperbolic).

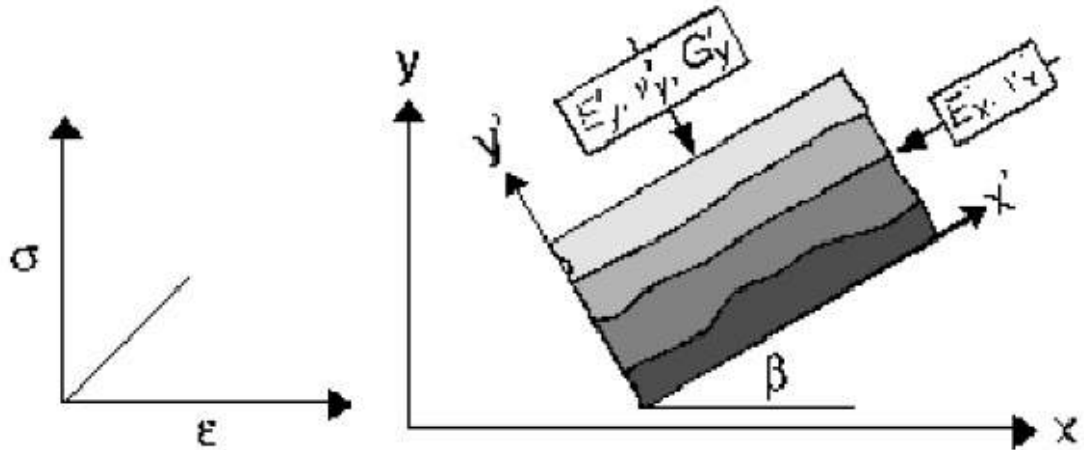


Fig.(5.3) Anisotropic Linear Elastic.

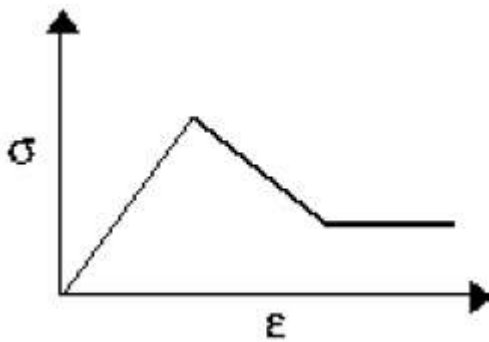


Fig.(5.4) Strain-Softening.

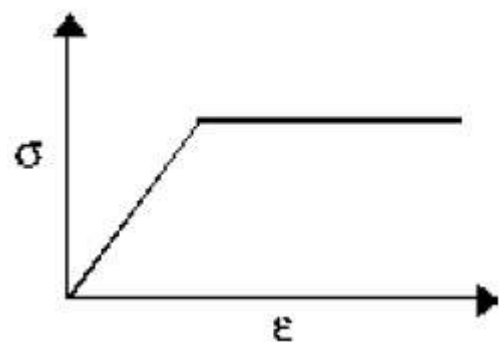


Fig.(5.5) Elastic Plastic (Mohr-Coulomb or Tresca).

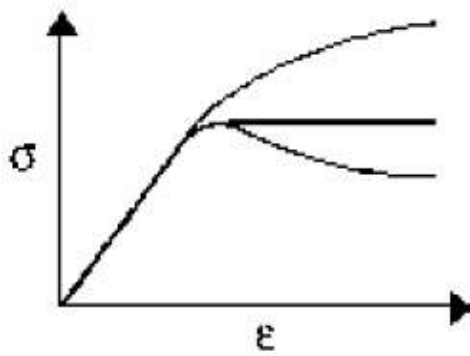


Fig.(5.6) Cam-Clay model (Critical state).

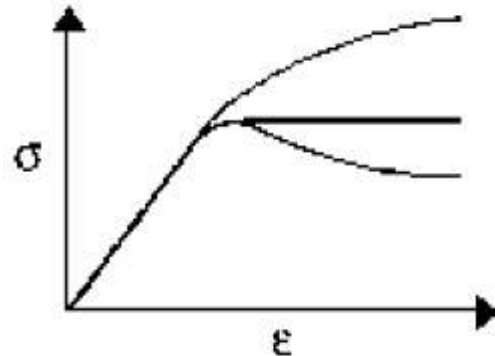


Fig.(5.7) Modified Cam-clay model (Critical State).

5.4.2 Material Models in an Unsaturated Consolidation Analysis

Only linear elastic and nonlinear elastic (Hyperbolic) material models can be used in an unsaturated consolidation analysis. The elastic plastic and Cam-clay material models are not formulated in SIGMA/W for use in unsaturated soil consolidation.

5.4.3 H-Modulus Function in a Consolidation Analysis

H is the unsaturated modulus that relates the volumetric strain of the soil to a change in negative pore water pressure or change in suction. The H modulus may be defined as a function of negative pore-water pressure. At saturation, H is related to the elastic constants E and ν by the equation:

$$H = \left(\frac{E}{1-2\nu} \right) \quad \dots(5.1)$$

Therefore, H must be set to $E/(1-2\nu)$ at zero pore-water pressure when defining an H-Modulus vs. pore-water pressure function. As a soil dries and the pore-water pressure becomes highly negative, the soil becomes very stiff. This increase in stiffness can be represented by an increase in H. Figure (5.8) illustrates a potential increase in H as a function of the negative pore water pressure.

The H Modulus cannot be specified less than $E/(1-2\nu)$. If an H Modulus function is defined with an H value less than $E/(1-2\nu)$, SIGMA/W will automatically set H to $E/(1-2\nu)$ during the analysis. Consequently, when an H Modulus function is defined, the lowest H value should be $E/(1-2\nu)$ at the point where the pore-water pressure is zero.

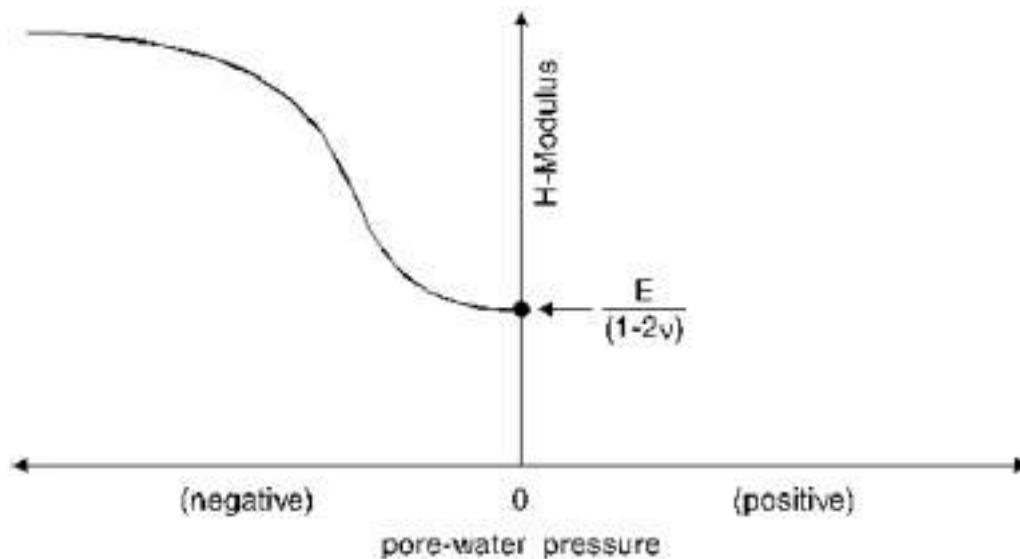


Fig. (5.8) H-Modulus as a function of pore-water pressure (Manual user's guide of SIGMA/W, 2002).

5.4.4 Total and Effective Stresses

Following common geotechnical practice, material properties can be specified in SIGMA/W using either effective stress parameters for analyses of drained soils, or total stress parameters for undrained soils. In materials specified using total stress parameters, undrained pore-water pressure changes can be computed from total stress changes using pore-pressure parameters **A** and **B**.

The pore-pressure parameters **A** and **B** are defined using functions. **B** is defined as a function of the pore-water pressure and **A** is defined as a function of the deviatoric stress. The **B** function can be defined for both

positive and negative pore-water pressures, which makes it possible to analyze both saturated and unsaturated soil conditions. Examples of functions of these parameters are shown in Figures (5.9) and (5.10).

In a load-deformation analysis, materials with properties specified using effective stress parameters and materials specified using total stress properties can be intermixed. However, in a fully coupled consolidation analysis using SEEP/W only materials with effective stress parameters are allowed.

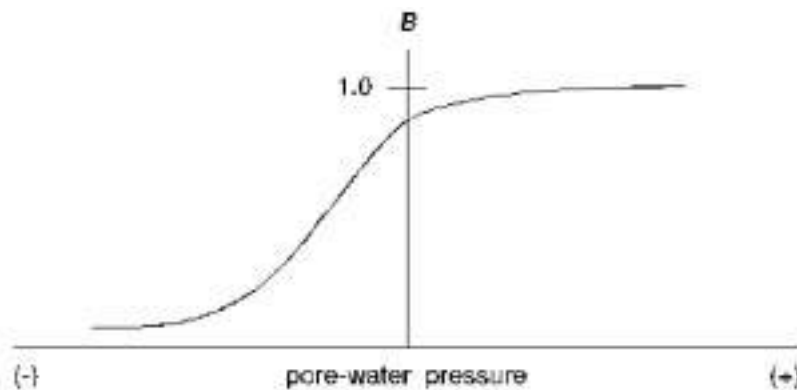


Fig.(5.9) Example of pore pressure B function (Manual user's guide of SIGMA/W, 2002).

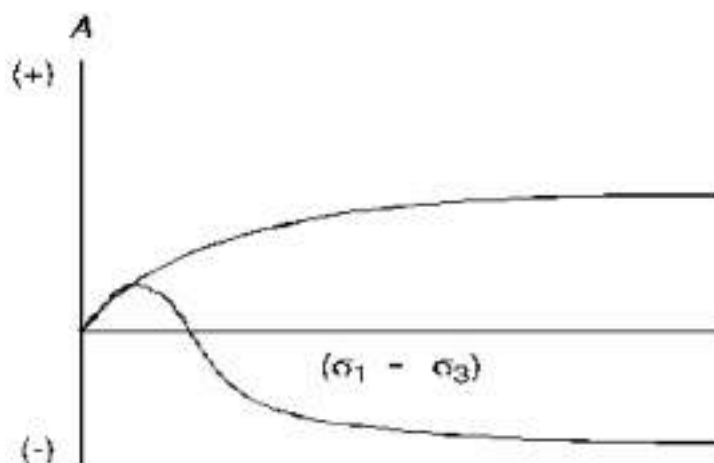


Fig.(5.10) Examples of pore pressure A function (Manual user's guide of SIGMA/W, 2002).

5.4.5 Boundary Conditions

- Multiple boundary condition types.

Multiple boundary condition types are implemented to support virtually all load deformation modeling scenarios. In SIGMA/W, displacement, force or spring boundary conditions may be applied to nodes, and stress and fluid pressure boundary conditions may be applied to edges. Stress boundary conditions can be applied to external element edges and may be specified as a normal and tangential stress pair, or as an x-stress and y-stress pair.

The broad range of boundary condition types means that SIGMA/W can model many problems. For example, struts used in a braced excavation can be modelled by using a spring boundary condition at the location of the struts as shown in Figure (5.11).

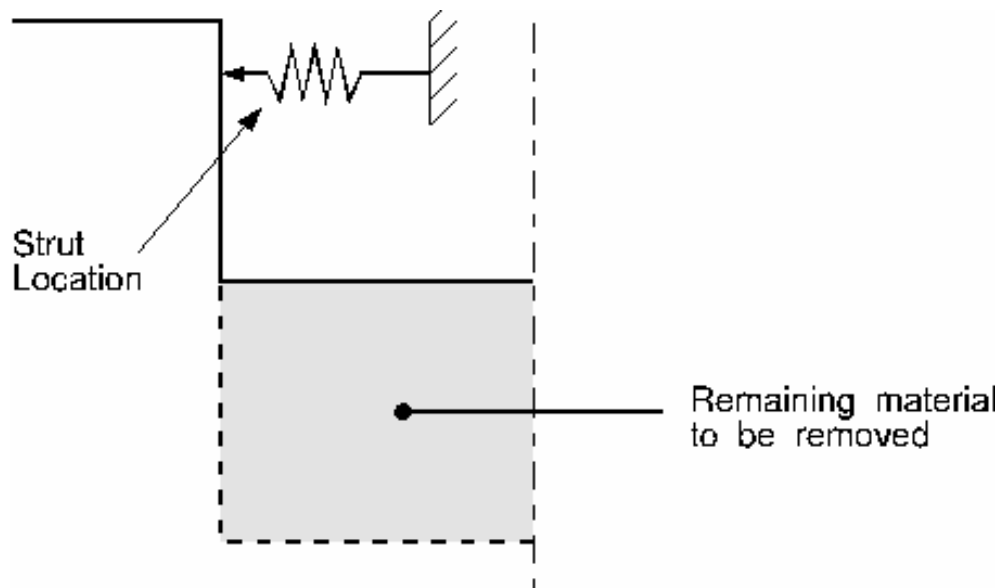


Fig. (5.11) Sample of boundary conditions (Manual user's guide of SIGMA/W, 2002).

- Transient boundary conditions.

A boundary condition function may be associated with each boundary condition. This feature is useful for specifying boundary

conditions that vary with time or load step. In addition, transient boundary conditions may be cycled, allowing specification of transient boundary conditions that repeat themselves with some frequency.

5.4.6 Finite Element Implementation

- Isoparametric quadrilateral and triangular finite elements.

Isoparametric quadrilateral and triangular finite elements are implemented and each may have various numbers of optional secondary nodes to provide higher order interpolation of nodal values within the element. In this thesis eight node isoparametric quadrilateral finite elements are used.

- Staged addition and removal of elements.

Elements can be added or removed in stages. This feature makes it possible to simulate the construction of embankments and excavations.

- No specific limits on problem size.

SIGMA/W has been implemented using dynamic memory allocation, so there are no specific limits on problem size in terms of number of nodes, element or material types. Therefore the maximum size of the problem is a function of the amount of available computer memory.

5.5 KeyIn Initial Water Table

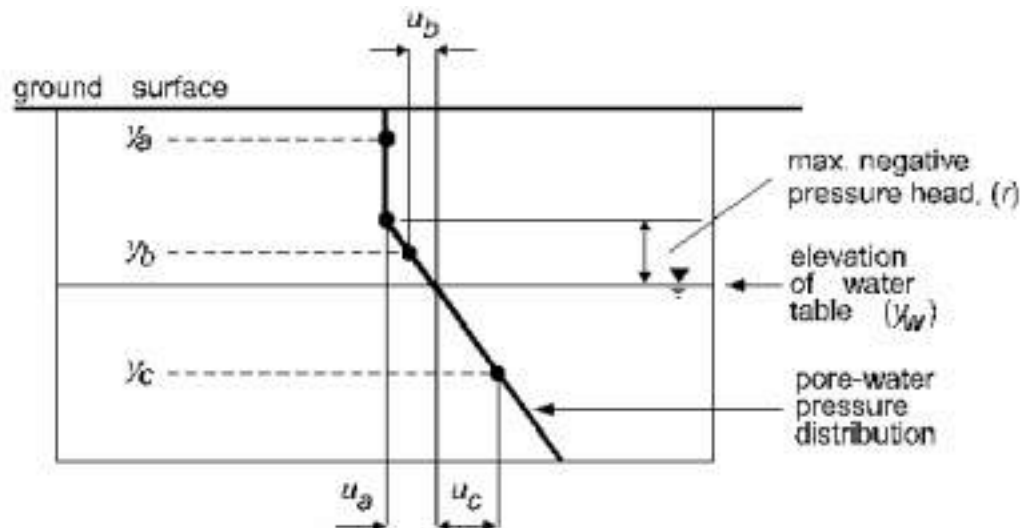
It defines the position of an initial water table to be used in estimating the initial pore-water pressure conditions.

An initial water table consists of a series of points. At each point, its x coordinate and the elevation (y-coordinate) of the water table are defined. The primary method of defining an initial water table is by drawing it on

the screen with "Draw Initial Water Table". The main purpose of KeyIn Initial Water Table is to:

- View the coordinates of each point numerically.
- Insert or delete points in the defined initial water table.

This feature is available for all analysis types in SIGMA/W. When defining an initial water table, the initial pore-water pressure at each node is computed proportionally to the vertical distance between the node and the defined water table. The effect is that the pore-water pressure varies hydrostatically with distance above and below the water table. Above the water table, the negative pore-water pressure can be set to a limit to produce a pressure distribution such as shown in Figure (5.12).



$$U_a = (y_w - y_r) \gamma_w, \quad r = \text{max. negative pressure head}$$

$$U_b = (y_w - y_b) \gamma_w$$

$$U_c = (y_w - y_c) \gamma_w$$

Fig (5.12) Calculation of initial pore-water pressure(Manual user's guide of SIGMA/W, 2002).

5.6 Keyin Functions Conductivity

A conductivity function defines the relationship between pore-water pressure and hydraulic conductivity. Figure (5.13) shows a typical conductivity function.

A soil desaturates and the water content decreases when the pore-water pressure becomes negative; the ability of the soil to conduct water decreases as the water content decreases. The soil hydraulic conductivity consequently decreases as the pore-water pressure becomes increasingly negative.

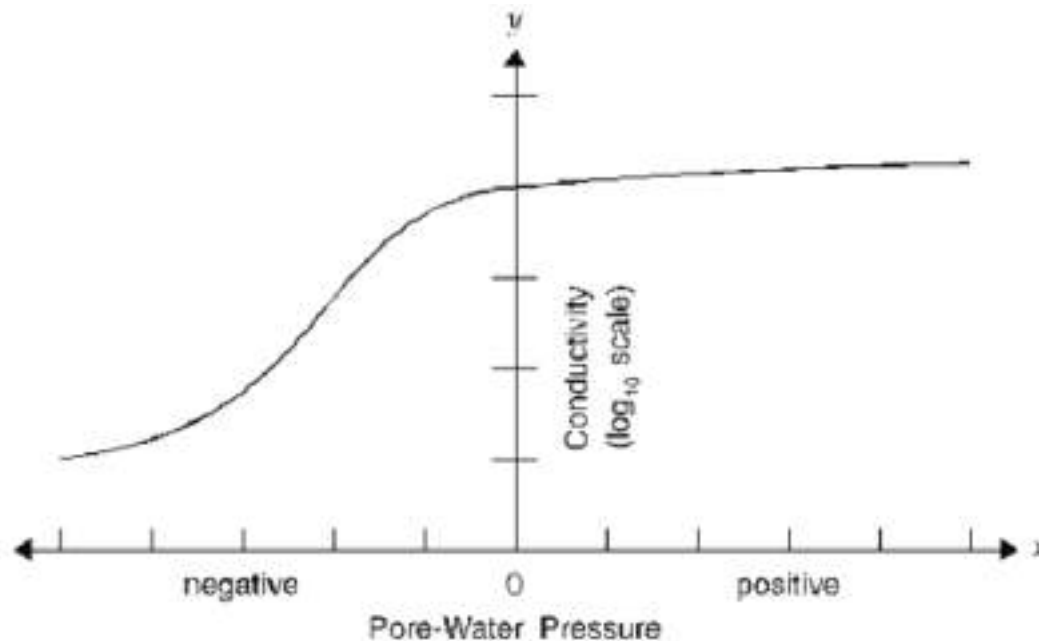


Fig (5.13) A Conductivity function (Manual user's guide of SEEP/W, 2002).

A conductivity function is defined by specifying a series of discrete data points and fitting a weighted spline curve to the data points in order to create a continuous function.

Conductivity functions can be defined in SEEP/W in any of the following ways:

- Specifying each data point in the function by typing the coordinates or by clicking on the function graph.
- Estimating the function from an existing volumetric water content function.
- Importing an existing conductivity function from the SEEP/W function database or from another SEEP/W problem and modify it.

5.7 Negative Pore-Water Pressure

The cohesive component of a soil can consist of two components; namely, effective cohesion and cohesion due to matric suction (Fredlund and Rahardjo, 1993):

$$c = c' + (u_a - u_w) \tan \phi^b \quad \dots\dots\dots(5.2)$$

where:

c = total cohesion intercept on the Mohr-Coulomb failure envelope
 $(u_a - u_w)$ = matric suction (i.e., negative pore-water pressure referenced to the pore-air pressure)

ϕ^b = an angle relating the increase in shear strength of a soil to an increase in matric suction

5.8 Verification

In order to assess the program capability in dealing with coupled problems, a verification problem is needed. An example from the soil mechanics textbook of (Lambe and Whitman, 1979) is chosen. Figure (5.14) shows the problem geometry. The problem consists of a circular footing (3 m diameter) resting on a saturated soil layer.

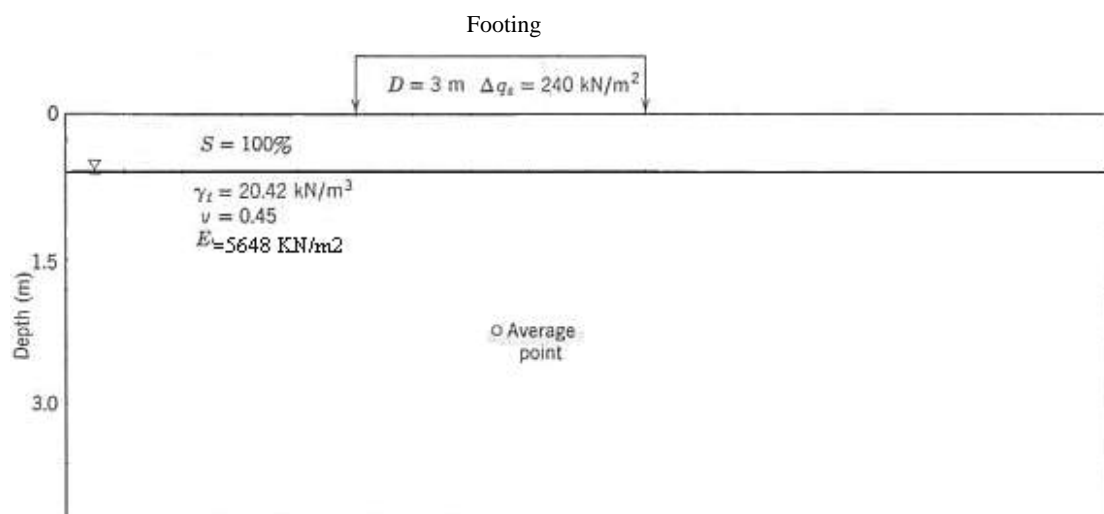


Fig. (5.14) Problem geometry (Lambe and Whitman, 1979).

The soil has properties are shown in table (5.1).

Table (5.1) Soil properties for the verification problem.

Parameter	Value	Units
Modulus of elasticity (E)	5648	kN/m ²
Poisson's ratio (ν)	0.45	—
Total unit weight (γ_t)	20.42	kN/m ³
Hydraulic conductivity (k)	1×10^{-4}	cm/sec
Degree of Saturation (S_r)	100 %	—

The programs SIGMA/W and SEEP/W are used to analyze the problem. The finite element mesh is shown in Figure (5.15) which consists of 400 eight-noded isoparametric soil elements with two way drainage condition. The right and left hands edges of the mesh were restricted to move horizontally and the bottom of the mesh was restricted in both horizontal and vertical directions. The top edge is free in both directions.

The dimensions of the problem are (5 m) depth and (3 m) diameter of footing with water table level at (0.6 m) under the ground surface. The soil is fully saturated. Only one-half of the axi-symmetric problem is modeled.

Figure (5.16) illustrates the relationship between the pore water pressure and depth, while Figure (5.17) illustrates the relationship between the total stress and depth.

Figures (5.18, 5.19, 5.20) illustrates the contour lines of vertical settlement, vertical stress and volumetric strain respectively.

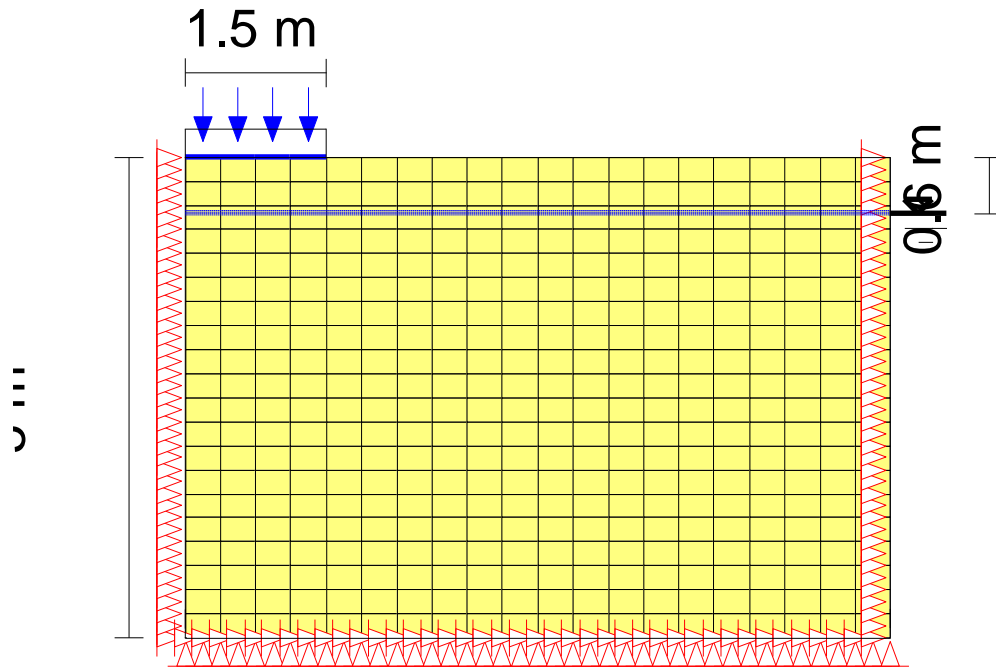


Fig. (5.15) Finite element mesh of the problem.

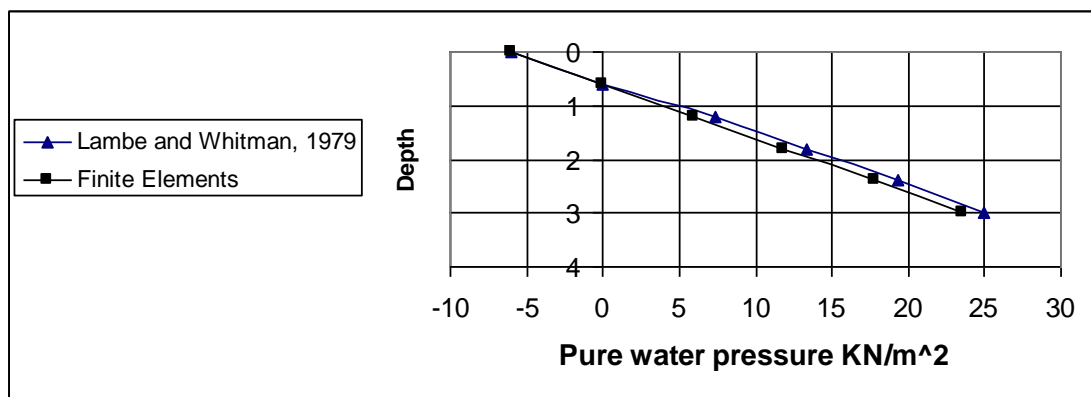


Fig. (5.16) The relationship between the pore water pressure and depth.

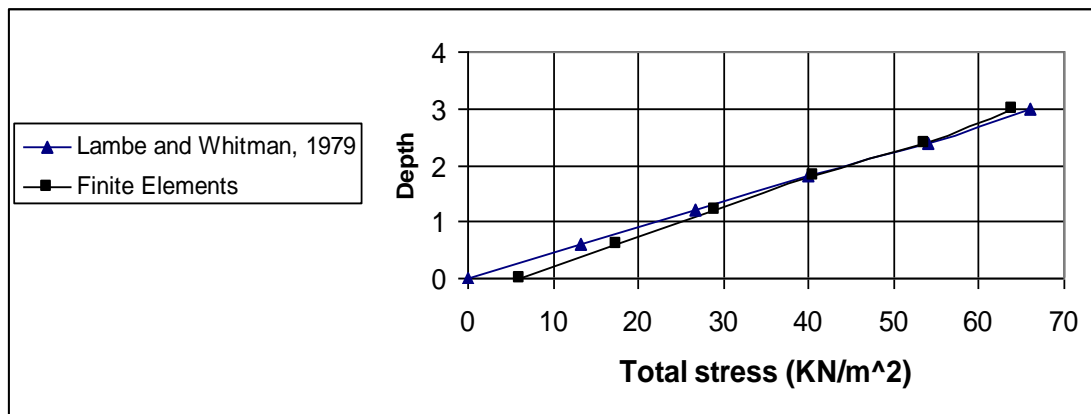


Fig. (5.17) The relationship between the total stress and depth.

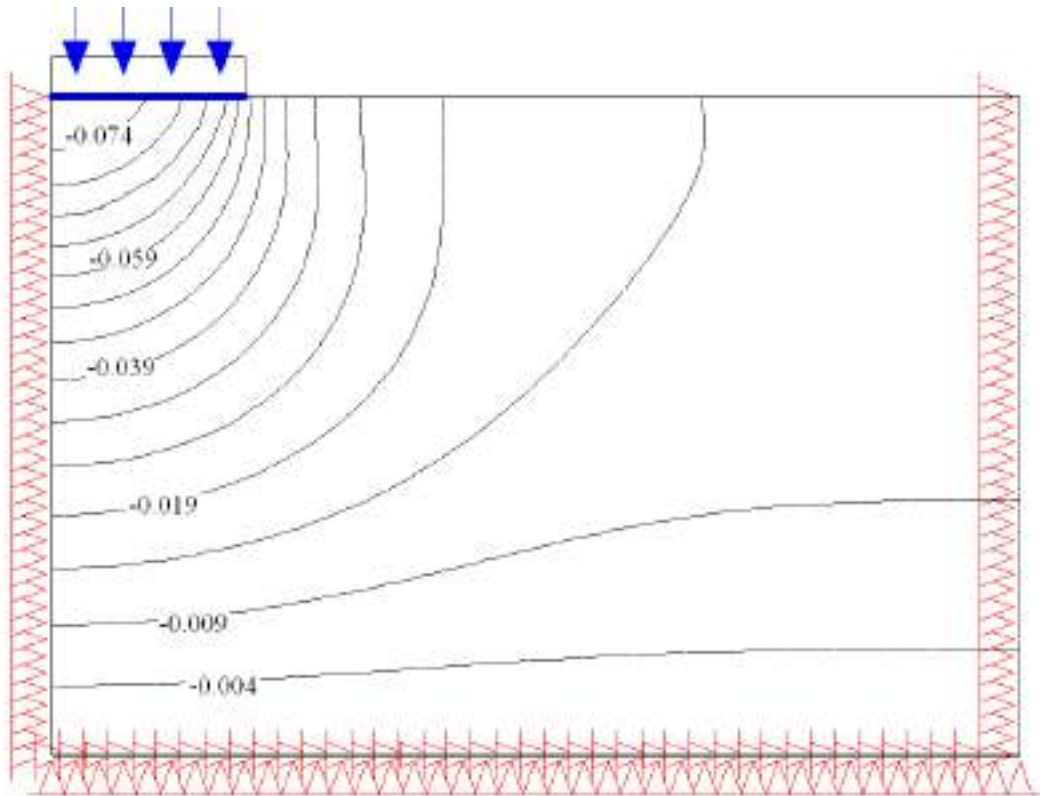


Fig. (5.18) Contour lines of vertical settlement

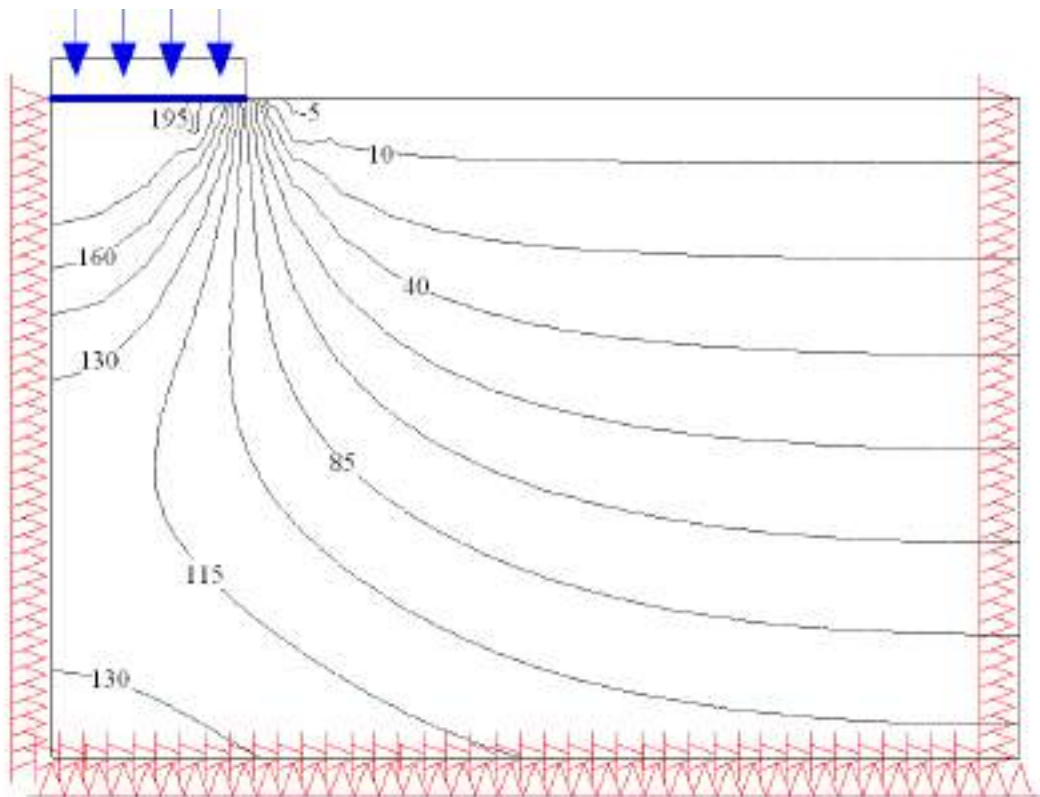


Fig. (5.19) Contour lines of vertical stress

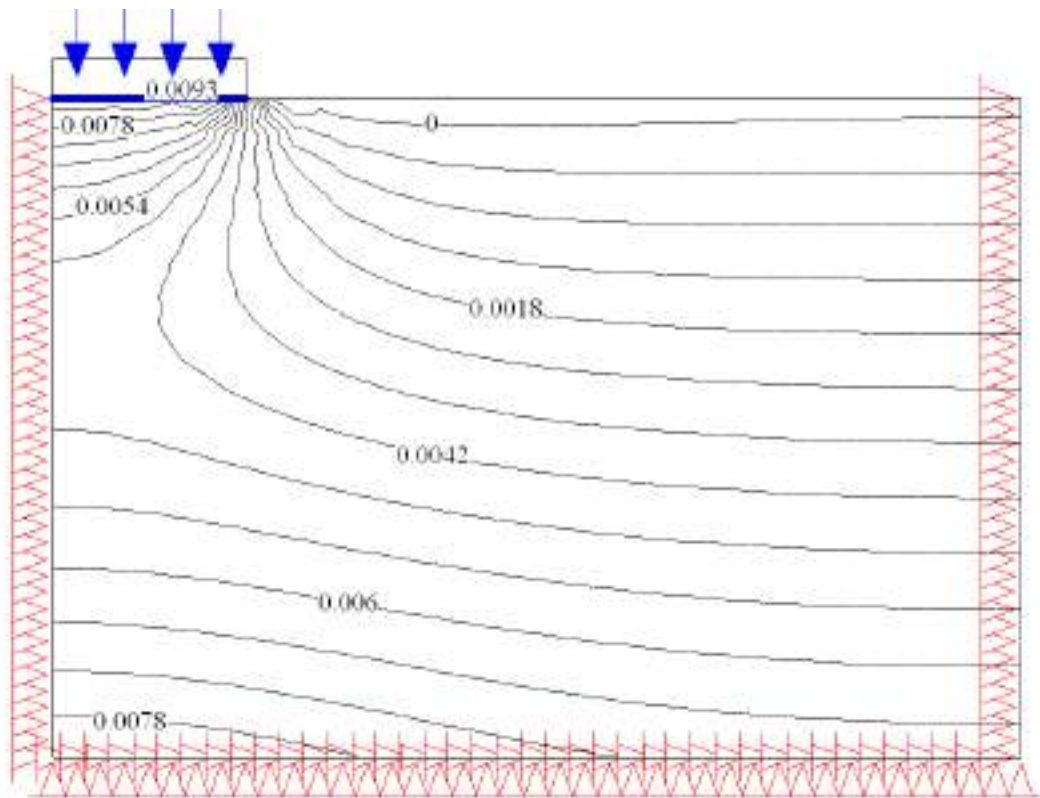


Fig. (5.20) Contour lines of volumetric strain

CHAPTER SIX

RESULTS AND DISCUSSION

CHAPTER SIX

RESULTS AND DISCUSSION

6.1 Introduction

In chapters three and four, the fundamental constitutive relations for unsaturated soils, and finite element formulation for consolidation are described. In this chapter, these relations are applied to problems related to geotechnical engineering, by using the programs SIGMA/W and SEEP/W that are described in chapter Five. The aim of this chapter is to make a comparison between the results of fully saturated soil behaviour and unsaturated condition behaviour through carrying out consolidation problem.

6.2 Problem Description

Al-Mdaina trial embankment was constructed in the southern part of Iraq alongside of the road between Talha and Al-Mdaina (near Al-Qurna in Al-Basrah province) in 1979. The height of the embankment is (5 meters), the width at the top is (12 meters), and the width at the bottom is (37 meters) with side slopes of (2.5:1).

6.3 Problem Profile

The site investigation of the foundation zone of the Mdaina trial embankment revealed that: the first (6 m) is a brown clayey silt with organic material. From (6-12 m) under the ground surface the soil is a gray silty clay, and (12-18 m) from the ground surface the soil is brown to gray silty clay (Al-Hamrany, 1980).

Below (18 m) there is a layer of dense sand, Figure (6.1) shows the cross-section of Al-Mdaina trial embankment.

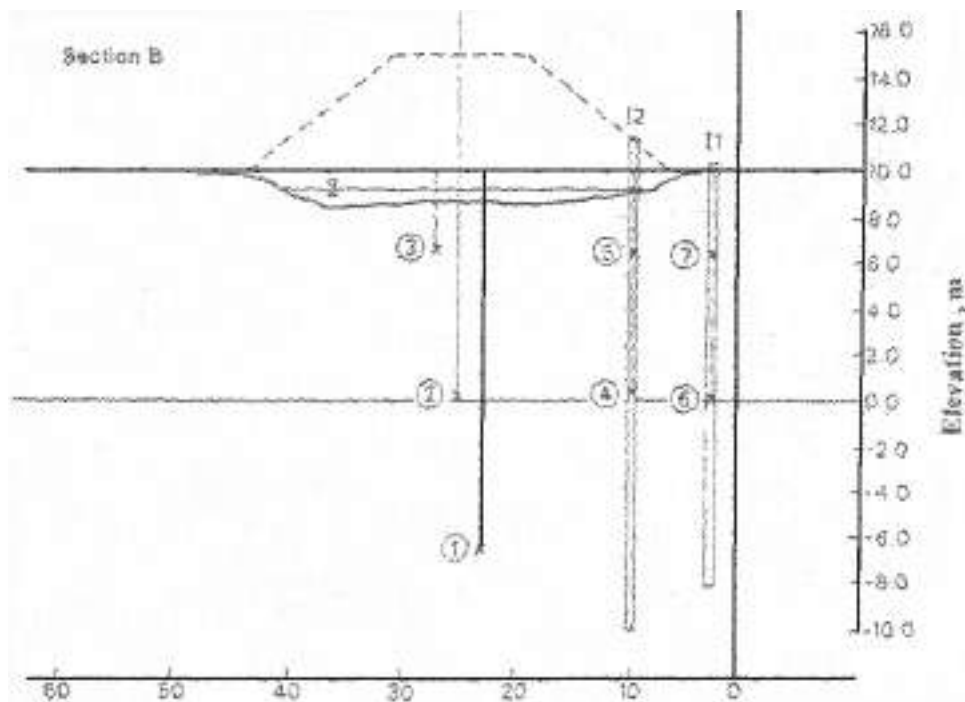


Fig. (6.1) Cross-section of Al-Mdaina trial embankment.

6.4 Modelling and Material Properties

The soil of Al-Mdaina embankment and the soil beneath it have properties as shown in Table (6.1).

In this work, the foundation soil is considered to be homogeneous, the properties of one layer (the first layer) is considered for all the depths of the soil.

The finite element mesh is illustrated in Figure (6.2). Due to symmetry, (210) elements are used for modelling half of the soil and embankment geometry. Eight noded isoparametric quadrilateral elements are used for modelling both the soil skeleton and pore water pressure.

The right and left hand edges of the mesh were restricted to move horizontally and the bottom of the mesh was restricted in both horizontal

and vertical directions. The top edge is free in both directions. In addition, the side boundaries are assumed to be impermeable, i.e. no flow is allowed through these sides.

The soil is assumed to follow **elastic-plastic** behaviour in which Mohr-Columb criterion is adopted.

Table (6.1) Material properties for the Mdaina trial embankment (after Al-Hamrany, 1980).

Position	Parameter	Value	Units
Embankment	Modulus of elasticity (E)	5000	kN/m ²
	Poisson's ratio (ν)	0.45	—
	Total unit weight (γ_t)	16	kN/m ³
Foundation Soil	Modulus of elasticity (E)	2870	kN/m ²
	Poisson's ratio (ν)	0.4	—
	Total unit weight (γ_t) (calculated)	18.66	kN/m ³
	Hydraulic conductivity (k)	5.76×10^{-8}	cm/sec
	Cohesion (c)	17.6	kN/m ²
	Angle of internal friction (ϕ)	30	degrees

6.5 Analysis and Results

For analysis, different cases are considered. At first, different water table levels are tried while the same modulus of elasticity of the problem (2870 kN/m²) is used. The water table levels were selected to be at the ground level (fully saturated), and (2 m, 4 m, 6 m and 8 m) below the ground level. The problem was solved under two way drainage condition by defining the drainage conditions in the program SEEP/W.

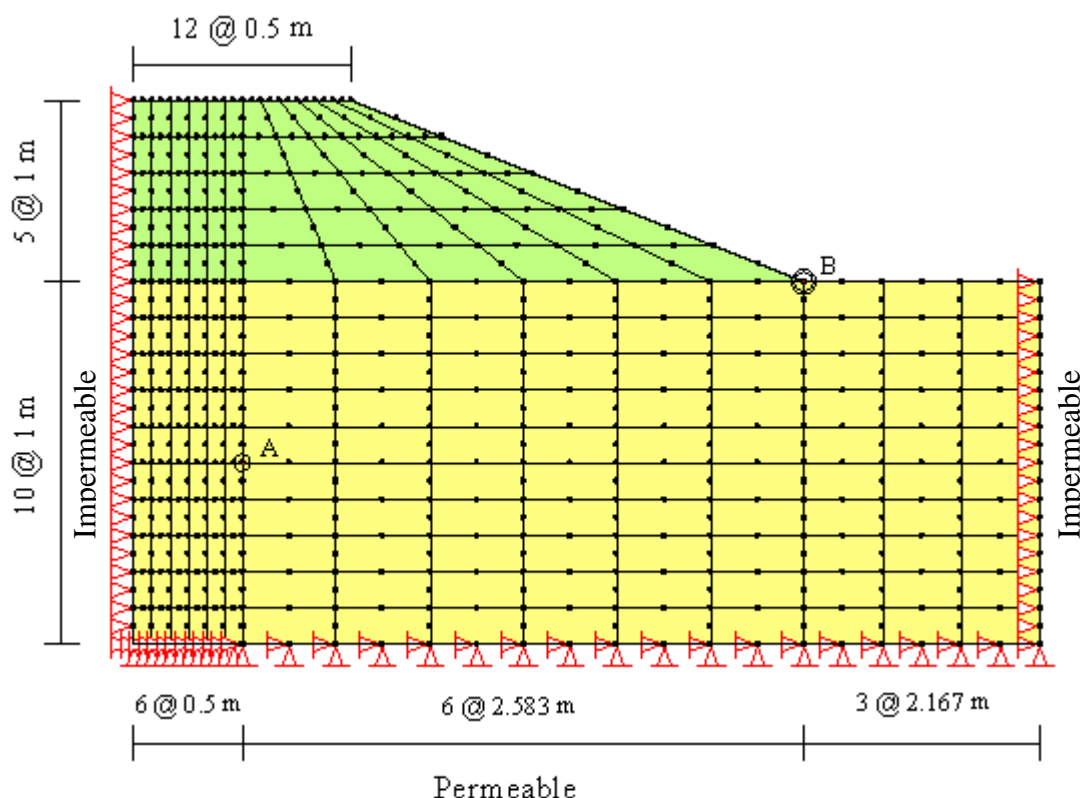


Fig. (6.2) Finite element mesh of Al-Mdaina trial embankment.

Then, the modulus of elasticity is changed from (2870 kN/m^2) to (10000 kN/m^2) and (20000 kN/m^2), and for each modulus of elasticity, the problem was re-solved with the same water table levels.

Later, the hydraulic conductivity (k) was changed from ($5.76 \times 10^{-8} \text{ cm/sec}$) to ($3 \times 10^{-9} \text{ cm/sec}$) and ($3 \times 10^{-6} \text{ cm/sec}$), and for each hydraulic conductivity, the problem was re-solved with the same water table levels.

Then, for modulus of elasticity of (2870 kN/m^2) and hydraulic conductivity of ($5.76 \times 10^{-8} \text{ cm/sec}$), the unsaturated soil modulus (H) was changed. The H -modulus values were either assumed or taken from the program SIGMA/W library for typical soils.

6.5.1 Pore Water Pressure

Figures (6.3), (6.4), (6.5), and (6.6) show the relationship between the pore water pressure and modulus of elasticity at point A (in Figure

6.2) at different elevations of water table.

Figures (6.7), (6.8), (6.9), and (6.10) show the relationship between the pore water pressure and modulus of elasticity at point B (in Figure 6.2) at different elevations for water table.

In these figures, u_p refers to pore water pressure for the case of partially saturated soil while u_f refers to pore water pressure in the case of fully saturated soil.

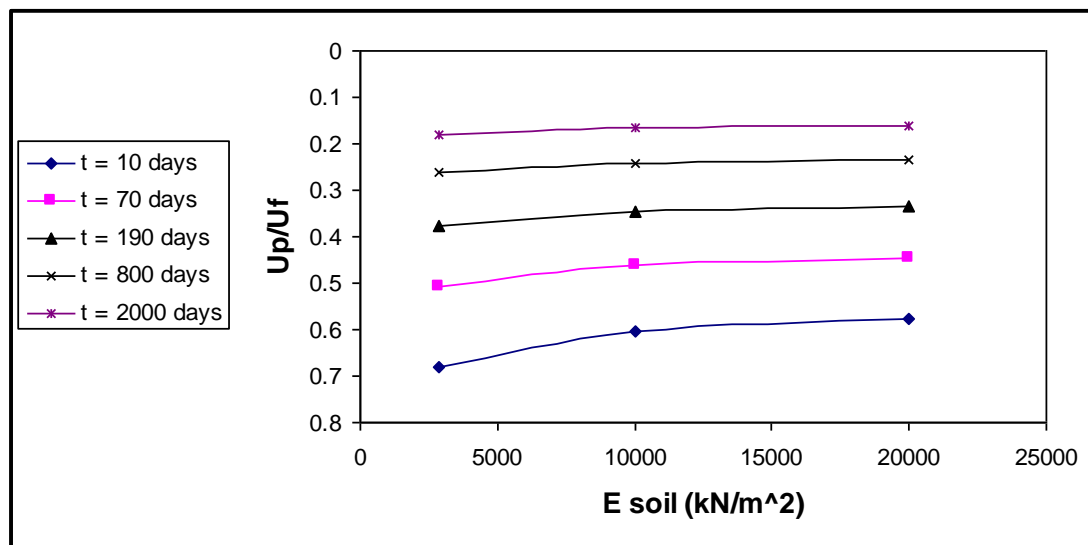


Fig. (6.3) The relation between (u_p/u_f) and soil modulus of elasticity at point (A) with water table at (2 m) from the ground level.

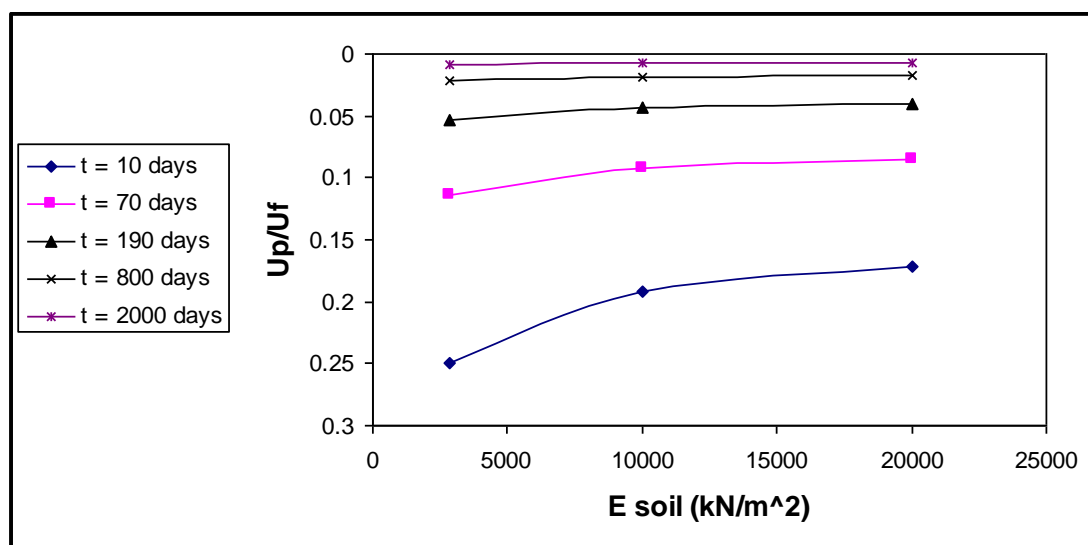


Fig. (6.4) The relation between (u_p/u_f) and soil modulus of elasticity at point (A) with water table at (4 m) from the ground level.

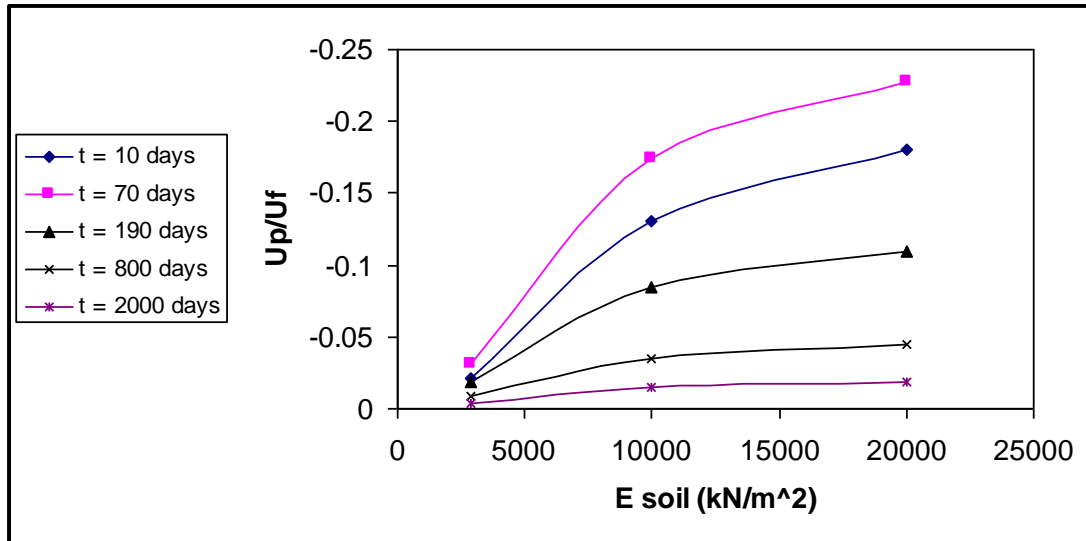


Fig. (6.5) The relation between (u_p/u_f) and soil modulus of elasticity at point (A) with water table at (6 m) from the ground level.

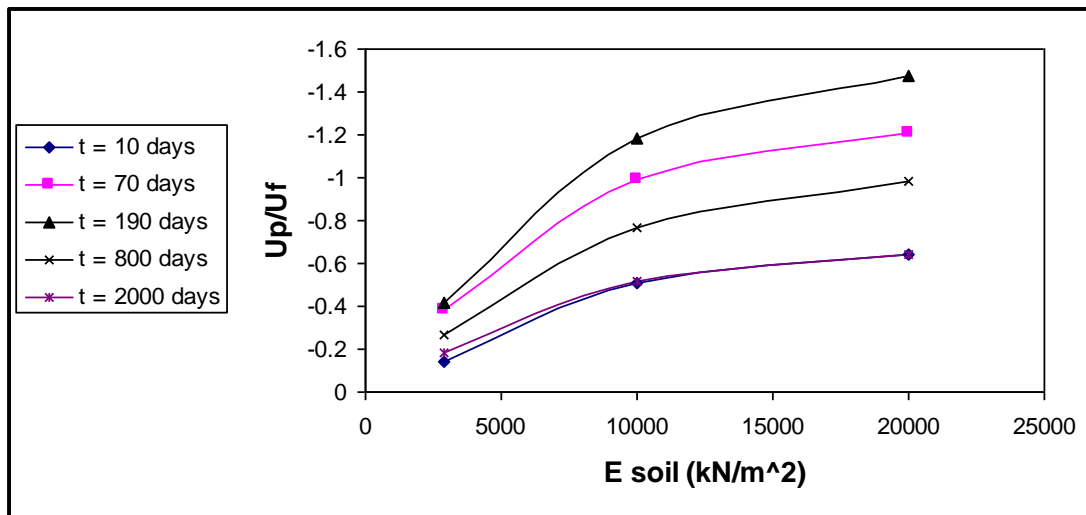


Fig. (6.6) The relation between (u_p/u_f) and soil modulus of elasticity at point (A) with water table at (8 m) from the ground level.

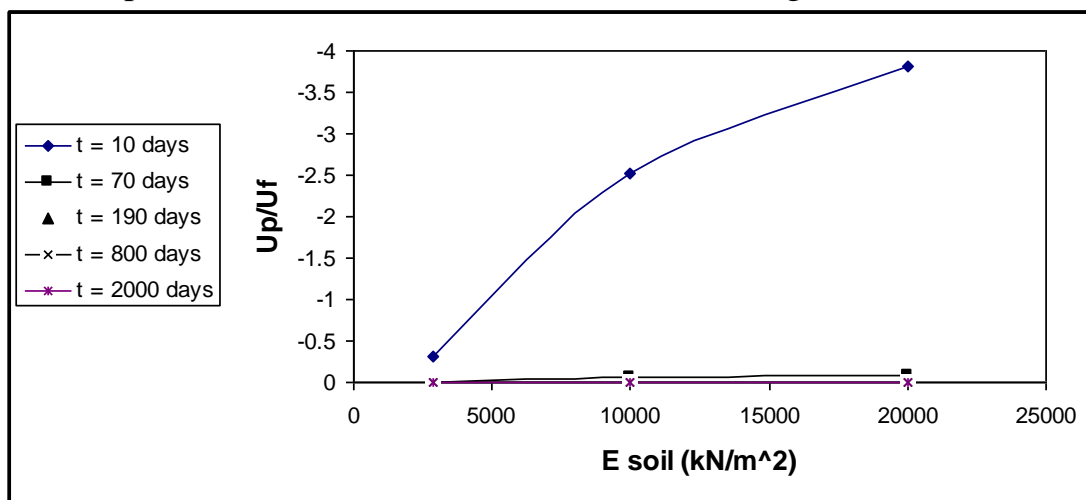


Fig. (6.7) The relation between (u_p/u_f) and soil modulus of elasticity at point (B) with water table at (2 m) from the ground level.

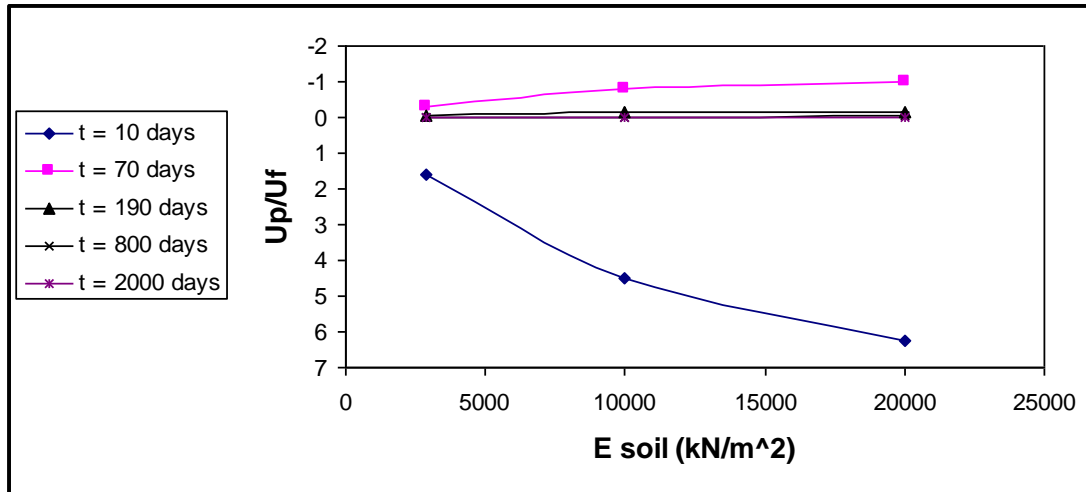


Fig. (6.8) The relation between (u_p/u_f) and soil modulus of elasticity at point (B) with water table at (4 m) from the ground level.

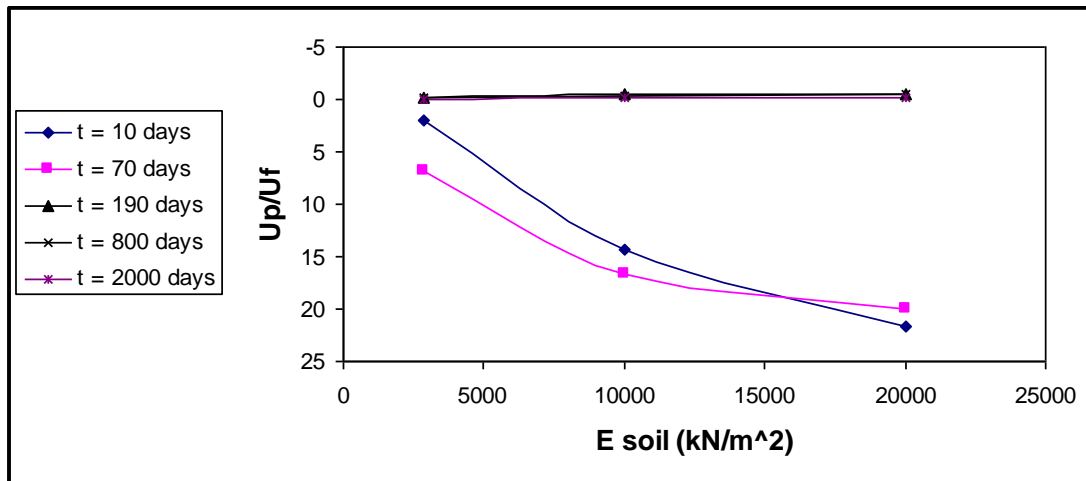


Fig. (6.9) The relation between (u_p/u_f) and soil modulus of elasticity at point (B) with water table at (6 m) from the ground level.

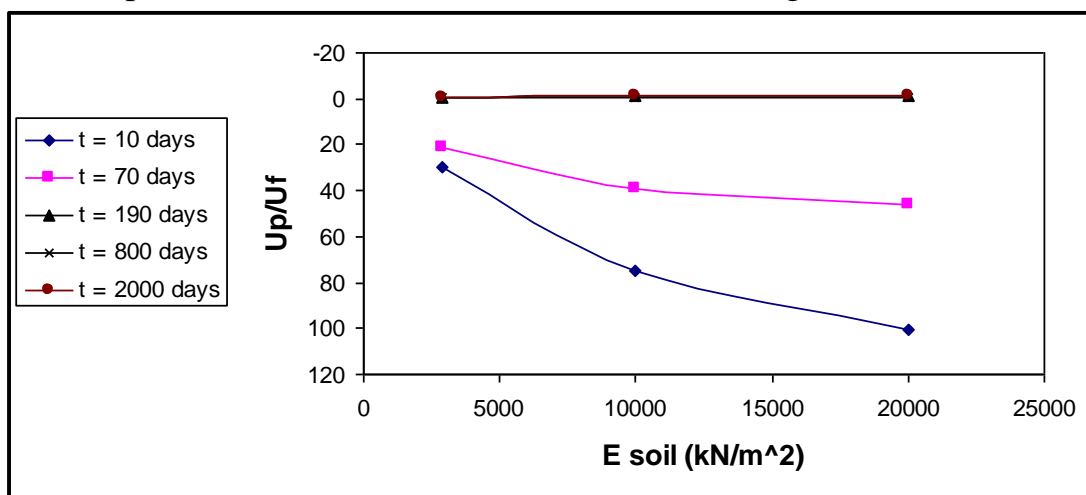


Fig. (6.10) The relation between (u_p/u_f) and soil modulus of elasticity at point (B) with water table at (8 m) from the ground level.

From Figure (6.3) it can be noticed that the difference between the pore water pressure in the case of partially saturated soil and fully saturated soil decreases with passage of time. The percentage of pore water pressure (u_p) to (u_f) is about (0.68) at a time of (10 days), this percent is reduced to about (0.18) at the time of (2000 days). This is also the case in Figure (6.4).

It can be concluded that the effect of unsaturated soil on consolidation characteristics appears at early stages of consolidation. In addition, when the clay layer consists of soft clay ($E_{soil} < 10000 \text{ kN/m}^2$), the effect of unsaturated soil is apparent, while effect of the modulus of elasticity diminishes when the soil is stiff.

It was also noticed that, with increase in the modulus of elasticity, the difference between pore water pressure of partially saturated soil and pore water pressure of fully saturated soil is decreased clearly. For instance, in Figure (6.3), at time (10 days) the percentage of (u_p/u_f) when the modulus of elasticity value is (2870 kN/m^2) is equal to (0.68), while this percentage becomes (0.6) when the modulus of elasticity is (10000 kN/m^2) and reaches about (0.58) when the modulus of elasticity becomes (20000 kN/m^2). Moreover, it is noticed that the effect of modulus of elasticity on pore water pressure decreases with passage of time. It was concluded that, the difference between the values of (u_p/u_f) at the time (10 days) reaches (0.1) for the case of modulus of elasticity of (2870 kN/m^2) and (20000 kN/m^2). This difference decreases up to (0.02) at time (2000 days). This is also clear in Figure (6.4).

For clayey soil, with a relatively high degree of saturation, from about (90 %) (the case of W.T. at 2 m from the ground surface), the air in the soil is occluded and can often be assumed to have little effect on the pore water pressure. In such a case, the unsaturated soil will tend to behave as if it were saturated and the effective stress can be assumed to

be equal to $(\sigma - u_w)$. the exception is a fine grained soil near to but on the dry side of optimum where the air may not be occluded. In this case, the effective stress will not even be approximately equal to $(\sigma - u_w)$ (Smith and Smith, 1998).

Figure (6.6) illustrates different behaviours of the soil, the percentage (u_p/u_f) increases with passage of time until reaching (190 days) after that, the percentage returns to decrease again until it becomes compatible with the previous cases at time of (2000 days). This means that the effect of modulus of elasticity on the behaviour of unsaturated soil is apparent in early stages of consolidation and diminishes when the time proceeds. It is also noticed that, the percentage of (u_p/u_f) increases at the same time with the increasing of the value of modulus of elasticity. For example, at the time (190 days) the difference reaches about (1.1) when the modulus of elasticity was changed from (2870 kN/m^2) to (20000 kN/m^2) , but however, this difference decreases after (190 days).

In Figure (6.5), the soil behaves as in Figure (6.6), with exception that, the increase of the percentage (u_p/u_f) was continued until the time of (70 days) and after that returned to decrease. In all cases, the effect of partial saturation of the soil diminishes at the end of consolidation, i.e. at time of about 2000 days. Due to what was mentioned above, it can be concluded that the behaviour of the soil, when the depth of water is (6 m) and below, is different from that when the depth of water is less. When negative value of pore water pressure is generated, the behaviour can be explained by that the value of negative pressure after (4 m) was overriding the phenomenon of Mendel-Cryer which leads to increase in the value of initial pore water pressure and this will eliminate the negative value of water pressure up to a depth of (4 m).

Figure (6.7) represents the pore water pressure at a point on the embankment toe, at the time (10 days). It is noticed clearly that the

percentage (u_p/u_f) increases with increasing the value of modulus of elasticity. At the time (70 days) and afterward, it was noticed that the unsaturation has no effect on changing the pore water pressure.

Figure (6.8) reveals that the percentage (u_p/u_f) is increasing toward the positive values at the time (10 days) with increase in modulus of elasticity. This increase is reflected negatively toward the time (70 days) with a few differences in this percentage of increase in modulus of elasticity. After (70 days) the percentage (u_p/u_f) reaches zero, and therefore, the effect of increasing of modulus of elasticity will decrease.

In Figure (6.9) ,the percentage (u_p/u_f) increases at time (10 days) with increasing of modulus of elasticity and. At time (70 days), the percentage (u_p/u_f) becomes greater in comparison with the value at time (10 days) at the same modulus of elasticity, and this attitude continues until reaching a value of (16000 kN/m²), where after this value, a conversion will occur and the percentage (u_p/u_f) becomes greater at time (10 days) in comparison with (70 days). At time (190 days) and after, the curves were compacted on each other at a value approaches zero, nearly with modulus of elasticity of (2870 kN/m²) and with a slight increase in the percentage toward the negative with a slight increase in modulus of elasticity.

Figure (6.10) reveals that at time (10 days), the value of the percentage (u_p/u_f) increases with increasing values of modulus of elasticity, and the value is changed from (30) at modulus of elasticity of (2870 kN/m²) to (100) at modulus of elasticity value of (20000 kN/m²). However, this increase becomes lower at time (70 days) as it will range between (20) at modulus of elasticity of (2870 kN/m²) and (45) at modulus of elasticity of (20000 kN/m²). At time (190 days) and afterward, the curves will be compacted again on each other with reducing of the difference of the percentage (u_p/u_f) with increasing of

modulus of elasticity, and the value of (u_p/u_f) is between $(- 2.5)$ at the modulus of elasticity of (2870 kN/m^2) and $(- 4)$ at modulus of elasticity of (20000 kN/m^2) .

This behaviour can be explained by the fact that voids of unsaturated soil are filled either with water, a water and air mixture or simple air. With air and water filled voids, small lenses of water from menisci around the particle contacts. With clays, there will also be absorbed water, so strongly attached to the soil particles that it can be regarded as being part of the soil skeleton.

Although the volume of meniscus water in an unsaturated soil may be very small, it can have a dramatic effect on the mechanical behaviour of the soil, an effect that can not be estimated.

6.5.2 Vertical displacement

Figures (6.11), (6.12), (6.13) and (6.14), present the relationship between the vertical displacement and modulus of elasticity at point (A) (shown in Figure 6.2) at different elevations of water table.

Figures (6.15), (6.16), (6.17), (6.18), show the relationship between the vertical displacement and modulus of elasticity at point (B) (shown in Figure 6.2) at different elevations of water table.

In these figures, δ_{vp} and δ_{vf} refer to vertical displacement in the case of partially and fully saturated soil, respectively.

Figures (6.11) to (6.14) generally illustrate a similar behaviour, when the modulus of elasticity is (2870 kN/m^2) , the percentage of vertical displacement of partially saturated soil to vertical displacement of fully saturated soil $(\delta_{vp}/\delta_{vf})$ decreases with passage of time. This is also the case when the modulus of elasticity varies between $(10000 - 20000 \text{ kN/m}^2)$. It is noticed that at a certain time, the percentage $(\delta_{vp}/\delta_{vf})$ was decreased with increasing the value of modulus of elasticity. It is noticed

also that with increasing the depth of water, the percentage (δ_{vp}/δ_{vf}) at a certain time and at a certain value of modulus of elasticity is decreased. For example, in Figure (6.11), the value of (δ_{vp}/δ_{vf}) at time (10 days) and when the modulus of elasticity is (10000 kN/m^2) is (0.967) while the value was (0.86) in Figure (6.14) where the water table is at depth (8 m).

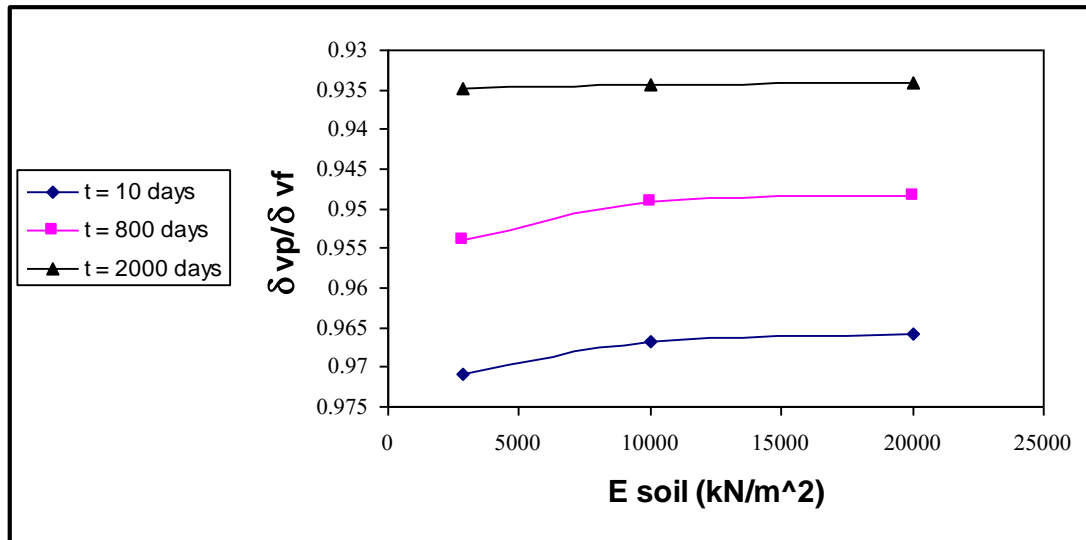


Fig. (6.11) The relation between (δ_{vp}/δ_{vf}) and soil modulus of elasticity at point (A) with water table at (2 m) from the ground level.

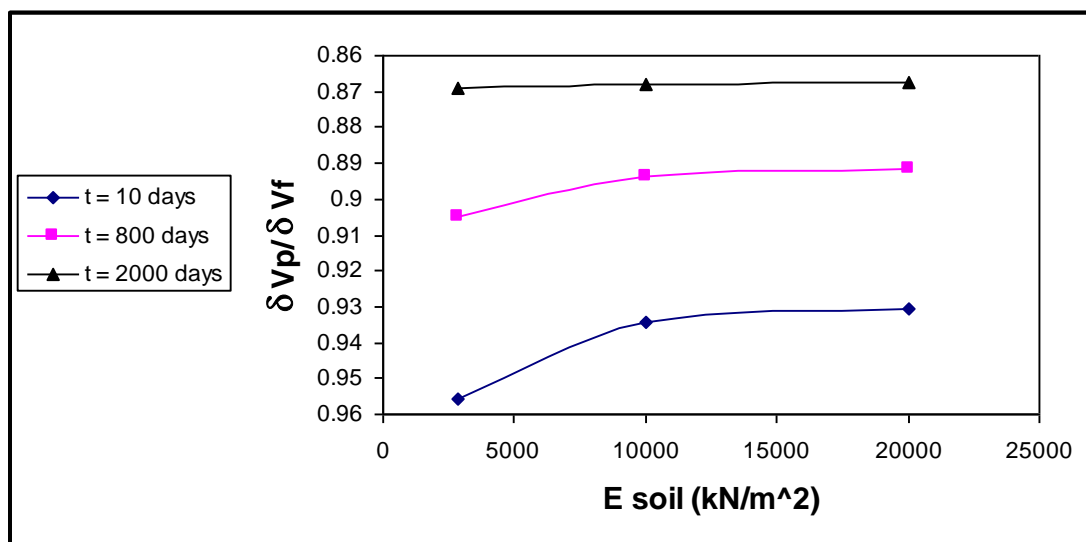


Fig. (6.12) The relation between (δ_{vp}/δ_{vf}) and soil modulus of elasticity at point (A) with water table at (4 m) from the ground level.

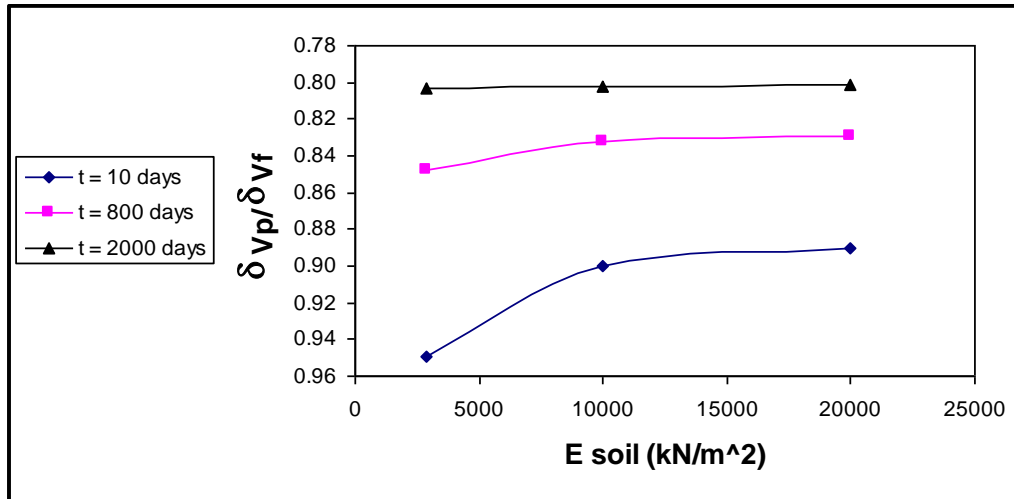


Fig. (6.13) The relation between $(\delta_{vp}/\delta_{vf})$ and soil modulus of elasticity at point (A) with water table at (6 m) from the ground level.

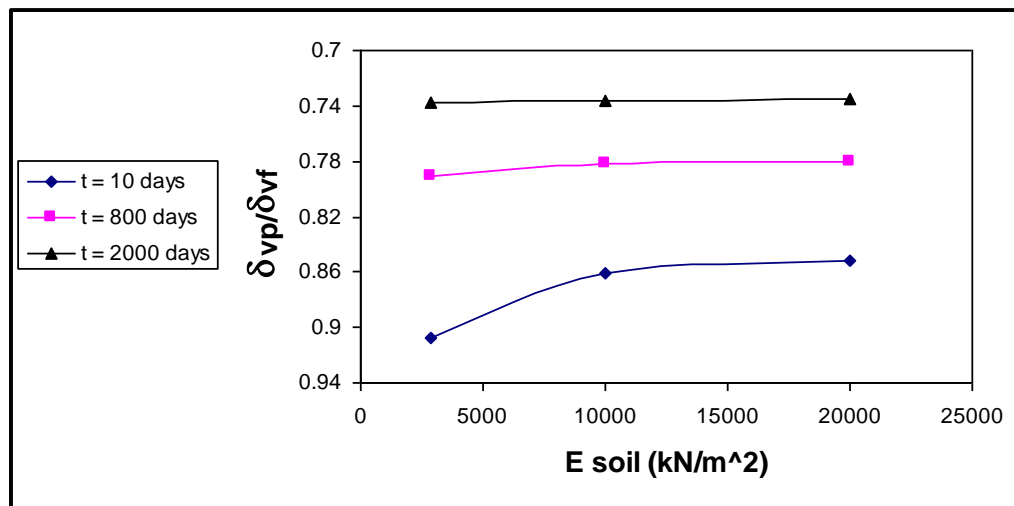


Fig. (6.14) The relation between $(\delta_{vp}/\delta_{vf})$ and soil modulus of elasticity at point (A) with water table at (8 m) from the ground level.

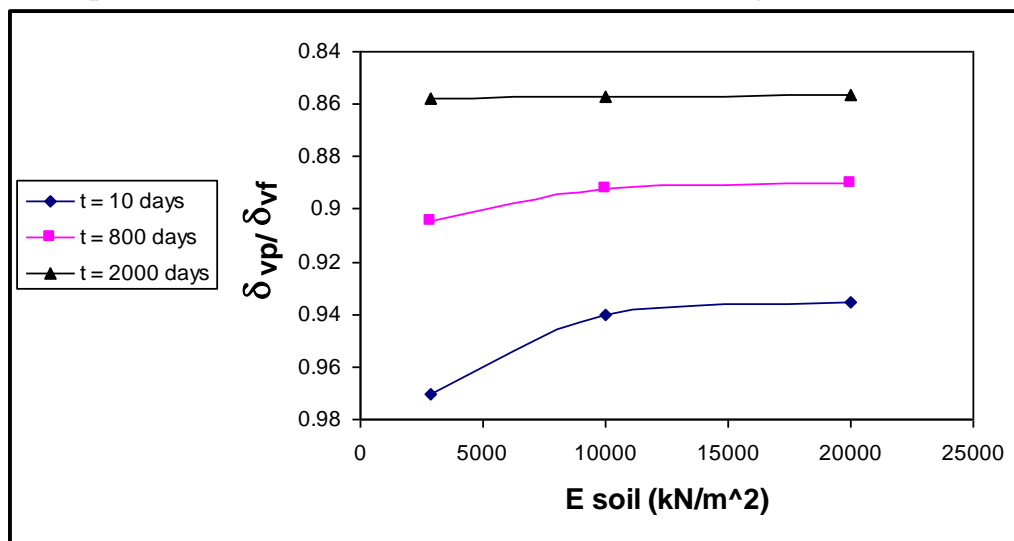


Fig. (6.15) The relation between $(\delta_{vp}/\delta_{vf})$ and soil modulus of elasticity at point (B) with water table at (2 m) from the ground level.

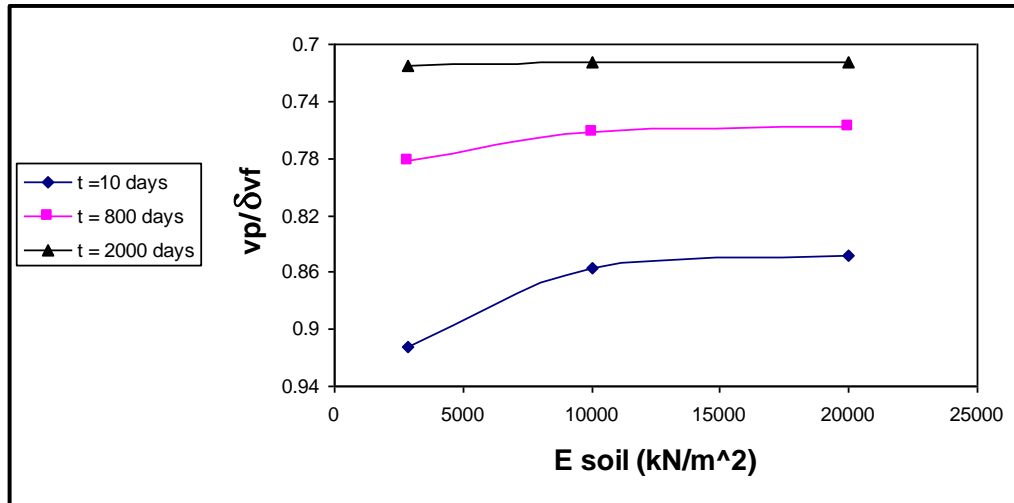


Fig. (6.16) The relation between $(\delta_{vp}/\delta_{vf})$ and soil modulus of elasticity at point (B) with water table at (4 m) from the ground level.

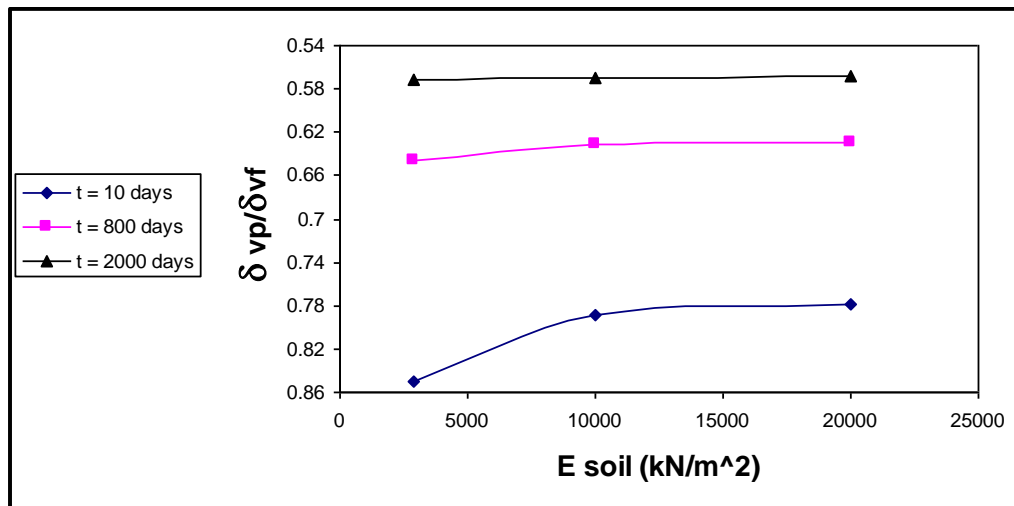


Fig. (6.17) The relation between $(\delta_{vp}/\delta_{vf})$ and soil modulus of elasticity at point (B) with water table at (6 m) from the ground level.

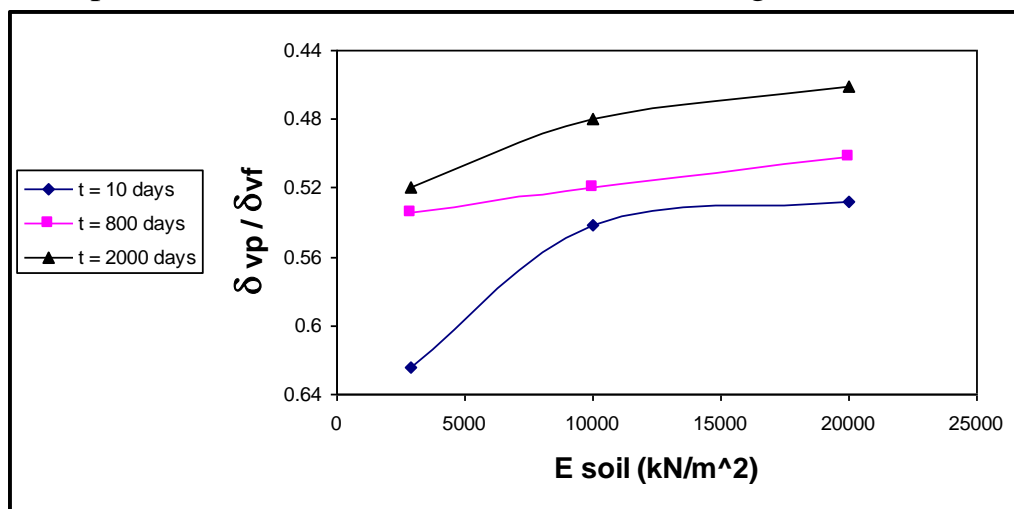


Fig. (6.18) The relation between $(\delta_{vp}/\delta_{vf})$ and soil modulus of elasticity at point (B) with water table at (8 m) from the ground level.

Figures (6.15) to (6.18) reveal the same previous behaviour of the soil but with a less percentage of $(\delta_{vp}/\delta_{vf})$ for a certain depth. For example, in Figure (6.17) at time (800 days) and when the modulus of elasticity is (20000 kN/m^2) , the value of $(\delta_{vp}/\delta_{vf})$ is (0.63) while it becomes (0.83) in Figure (6.13) for the same time and modulus of elasticity value.

This means that the effect of unsaturation becomes greater at the middle of the clay layer and near the center line of the embankment where the load concentrates more than at its toe.

Generally the settlement of fully saturated soil is greater than partially saturated soil because in the state of partially saturated soil friction between the soil particles is greater and the excess pore water pressure is the smallest. These results are compatible with those found by (saif jawad).

6.5.3 Horizontal displacement

Figures (6.19), (6.20), (6.21) and (6.22), show the relationship between the horizontal displacement and modulus of elasticity at point (A) (shown in Figure 6.2) at different elevations of water table.

Figures (6.23), (6.24), (6.25) and (6.26), show the relationship between the horizontal displacement and modulus of elasticity at point (B) (shown in Figure 6.2) at different elevations of water table.

In these figures, δ_{hp} and δ_{hf} refer to horizontal displacement in case of partially saturated and fully saturated, respectively.

In Figures (6.19),(6.20),(6.21),(6.23),(6.24) and (6.25), the soil shows similar behaviour, the percentage of $(\delta_{hp}/\delta_{hf})$ increases with increase in time, and this percentage is decreased when compared at a certain time with increase in the depth of water.

It was noticed that with the increase of the modulus of elasticity, the value of $(\delta_{hp}/\delta_{hf})$ was increased, but the increase in values of $(\delta_{hp}/\delta_{hf})$ will be maximum at time (10 days), then the difference starts to decrease with passage of time. It is clear that the difference in values of $(\delta_{hp}/\delta_{hf})$ will be very great when the modulus of elasticity is small, i.e. (2870 kN/m²) and (10000 kN/m²) and the difference becomes less when the modulus of elasticity is greater than (10000 kN/m²).

This means that the effect of partial saturation is greater on soft soils than other types.

It is also noticed that, at a certain depth of water and in case that all other parameters were fixed, the percentage of $(\delta_{hp}/\delta_{hf})$ would be maximum at the embankment toe rather than at point (A) at the middle of clay layer.

In Figures (6.22) and (6.26), the soil behaviour at time (10 days) is similar to that mentioned above, but however, at time (800 days) and (2000 days) different behaviour is obtained, as the difference in the value of $(\delta_{hp}/\delta_{hf})$ becomes less at the modulus of elasticity of (2870 kN/m²) and this difference was abolished at the modulus of elasticity equal to or greater than (10000 kN/m²), and at that time the curves become compacted on each other. It is also noticed that the value of $(\delta_{hp}/\delta_{hf})$ would be greater at point (B) in comparison with point (A) in case that all parameters are fixed because point (B) lies above water table always at partial saturated case. This result is compatible with that **Saif Jawad** found it.

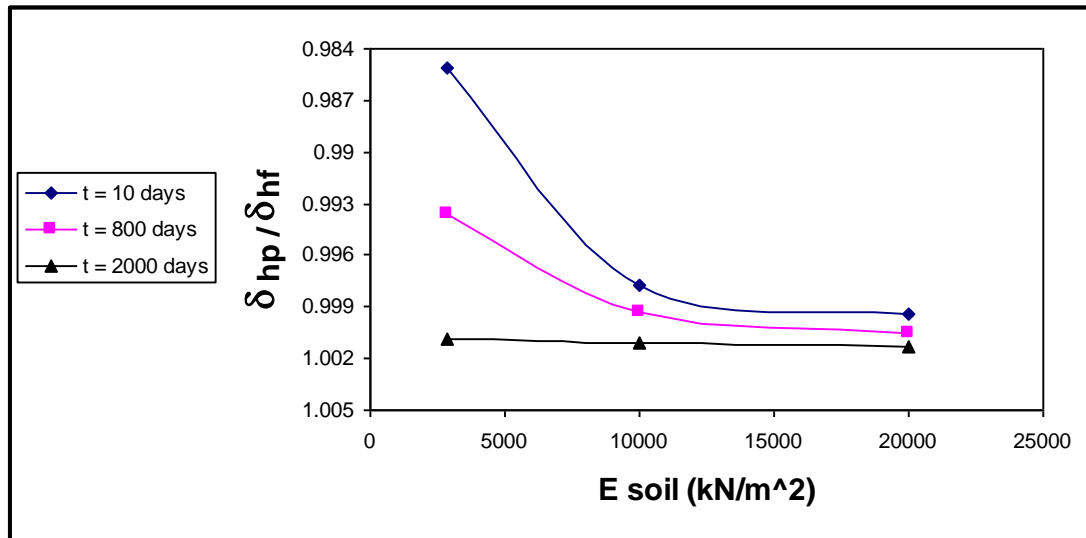


Fig. (6.19) The relation between $(\delta_{hp}/\delta_{hf})$ and soil modulus of elasticity at point (A) with water table at (2 m) from the ground level.

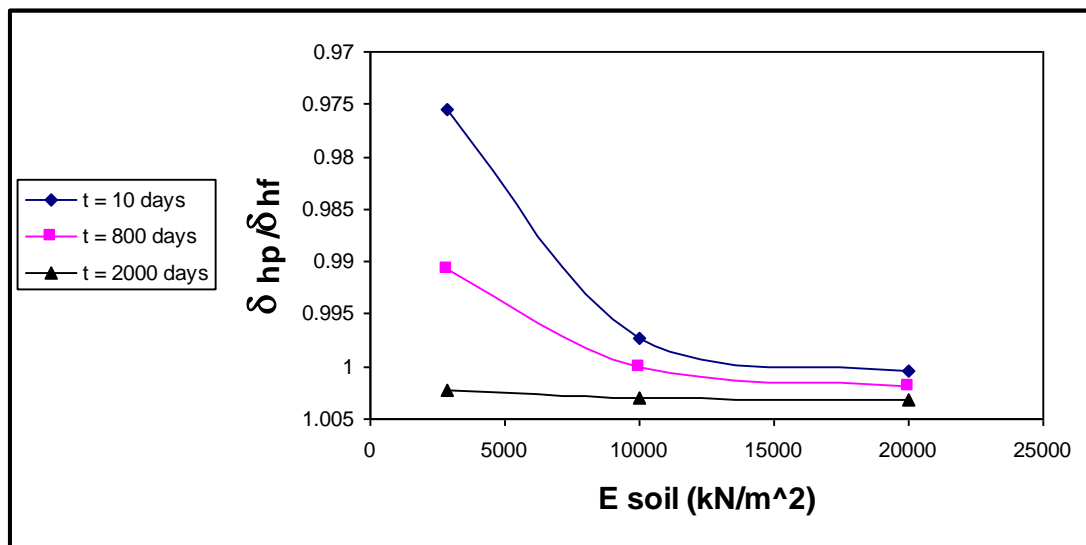


Fig. (6.20) The relation between $(\delta_{hp}/\delta_{hf})$ and soil modulus of elasticity at point (A) with water table at (4 m) from the ground level.

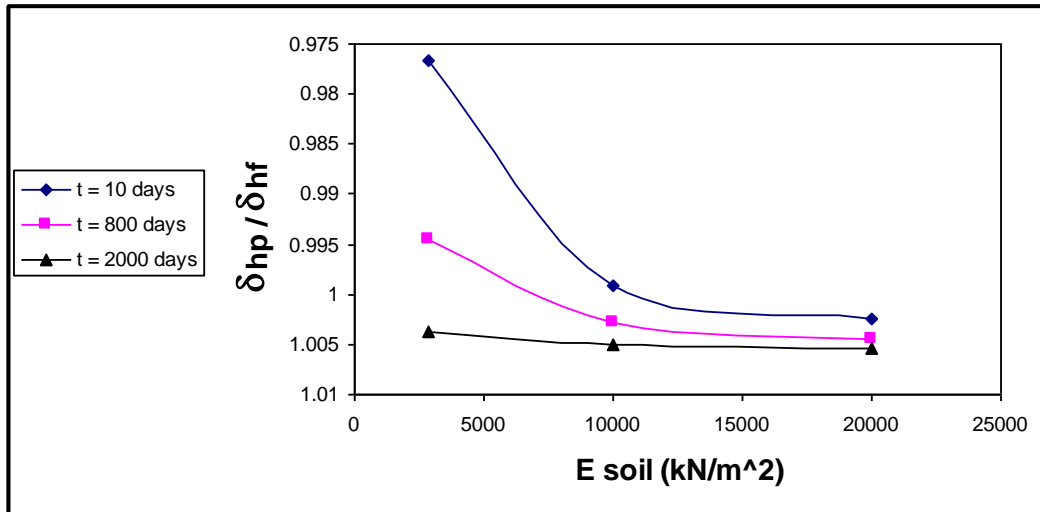


Fig. (6.21) The relation between $(\delta_{hp}/\delta_{hf})$ and soil modulus of elasticity at point (A) with water table at (6 m) from the ground level.

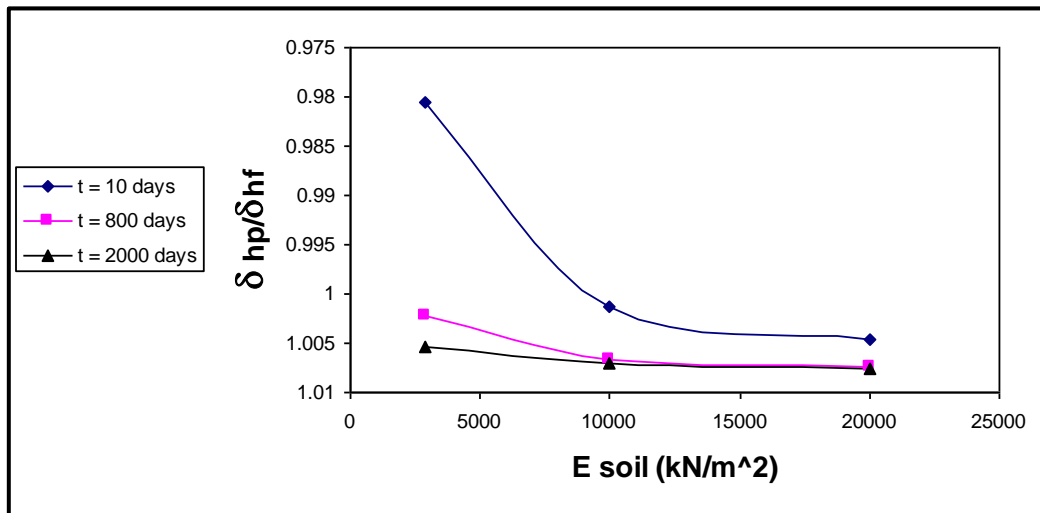


Fig. (6.22) The relation between $(\delta_{hp}/\delta_{hf})$ and soil modulus of elasticity at point (A) with water table at (8 m) from the ground level.

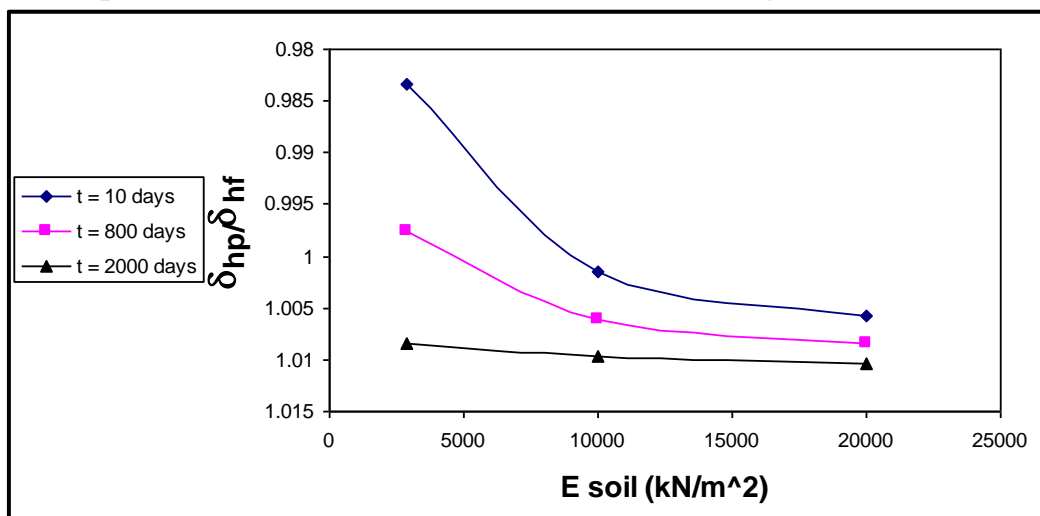


Fig. (6.23) The relation between $(\delta_{hp}/\delta_{hf})$ and soil modulus of elasticity at point (B) with water table at (2 m) from the ground level.

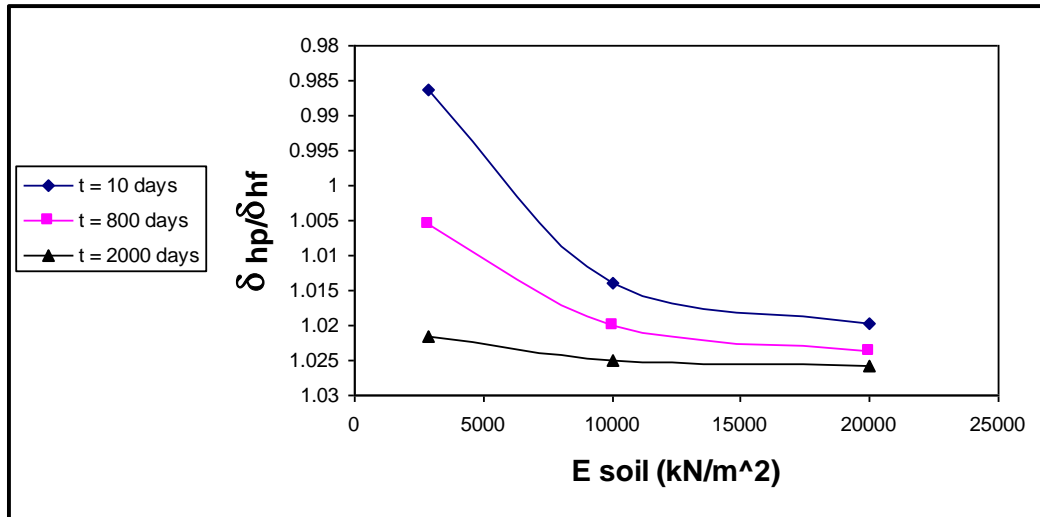


Fig. (6.24) The relation between $(\delta_{hp}/\delta_{hf})$ and soil modulus of elasticity at point (B) with water table at (4 m) from the ground level.

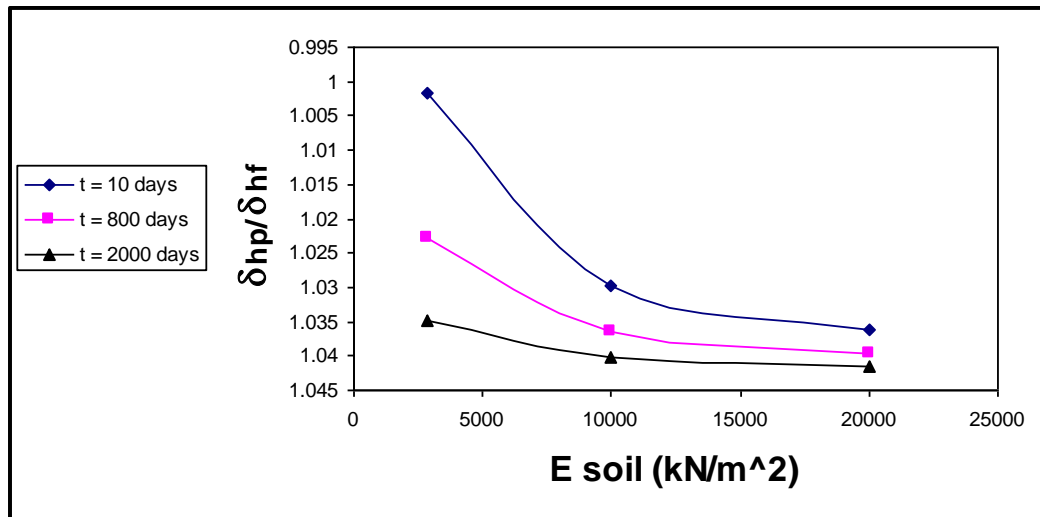


Fig. (6.25) The relation between $(\delta_{hp}/\delta_{hf})$ and soil modulus of elasticity at point (B) with water table at (6 m) from the ground level.

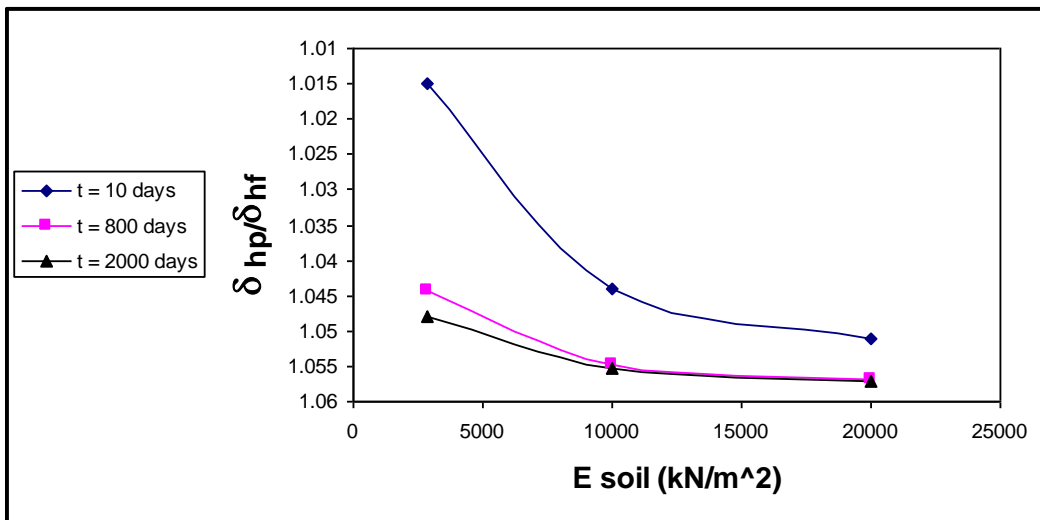


Fig. (6.26) The relation between $(\delta_{hp}/\delta_{hf})$ and soil modulus of elasticity at point (B) with water table at (8 m) from the ground level.

6.5.4 Contour Lines of Pore Water Pressure

Figures (6.27) to (6.35), show the contour lines of pore water pressure through the soil at different conditions of water table and different times.

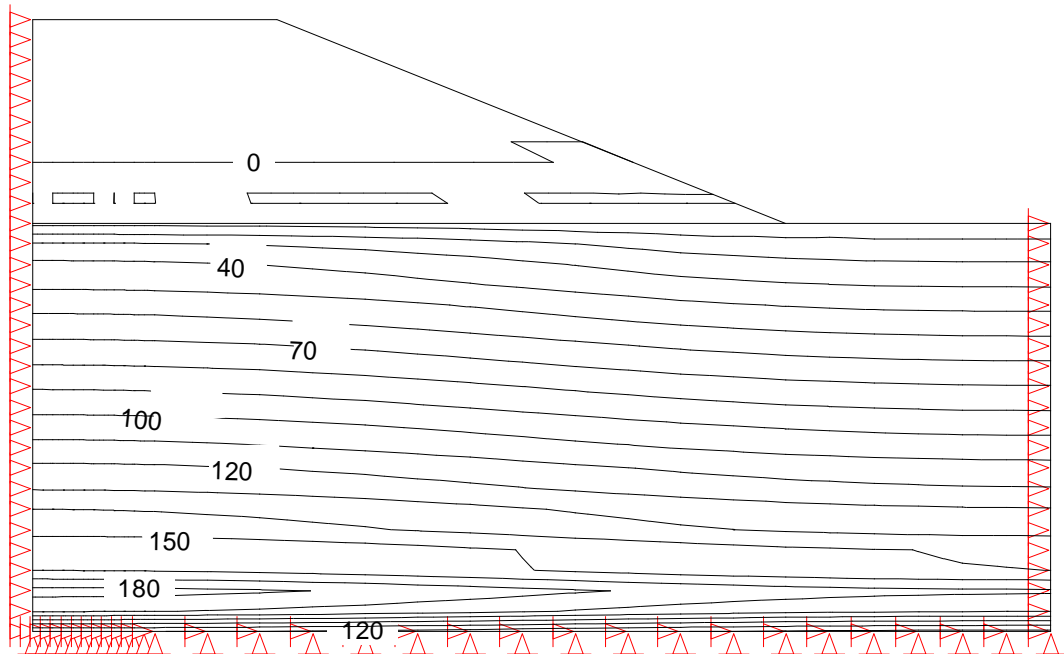


Fig. (6.27) Contour lines of pore water pressure (kPa) of fully saturated soil after 1 day.

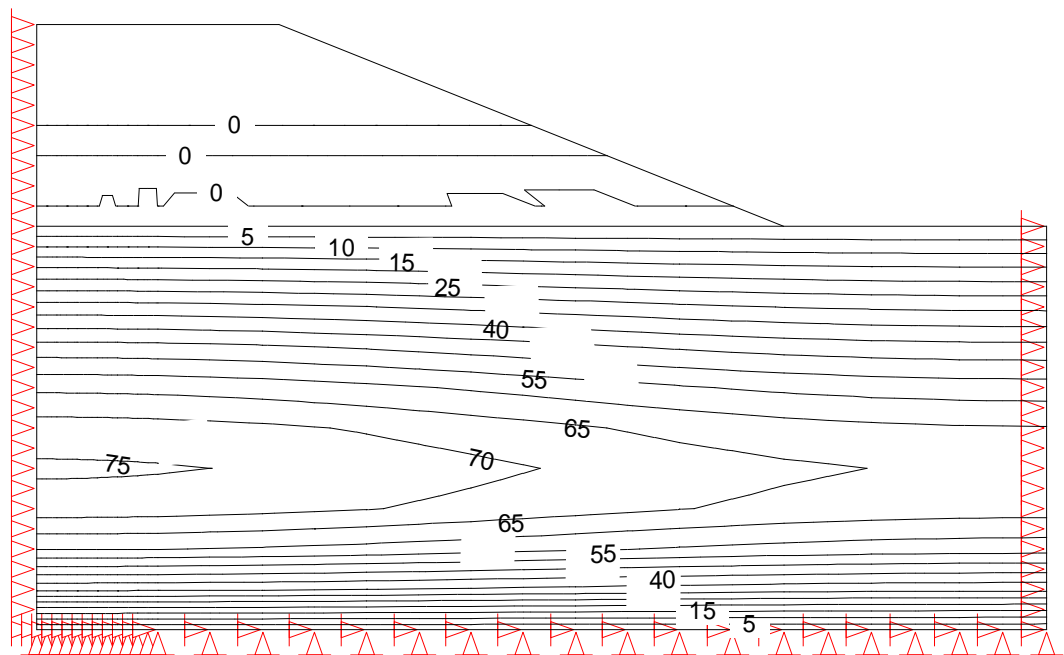


Fig. (6.28) Contour lines of pore water pressure (kPa) of fully saturated soil after 190 days.

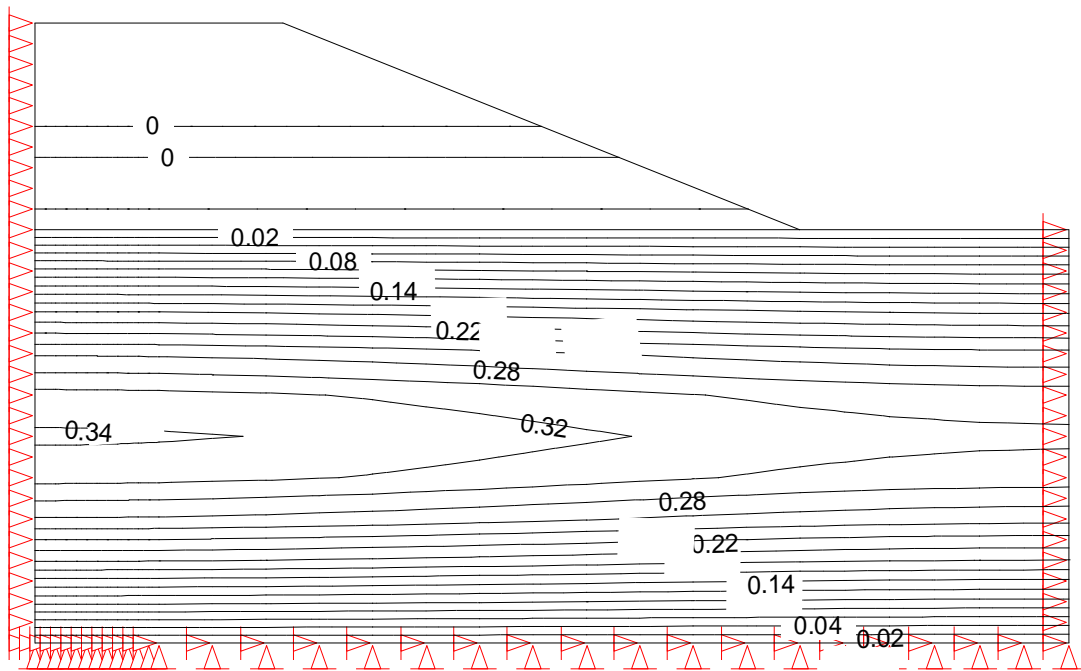


Fig. (6.29) Contour lines of pore water pressure (kPa) of fully saturated soil after 2000 days.

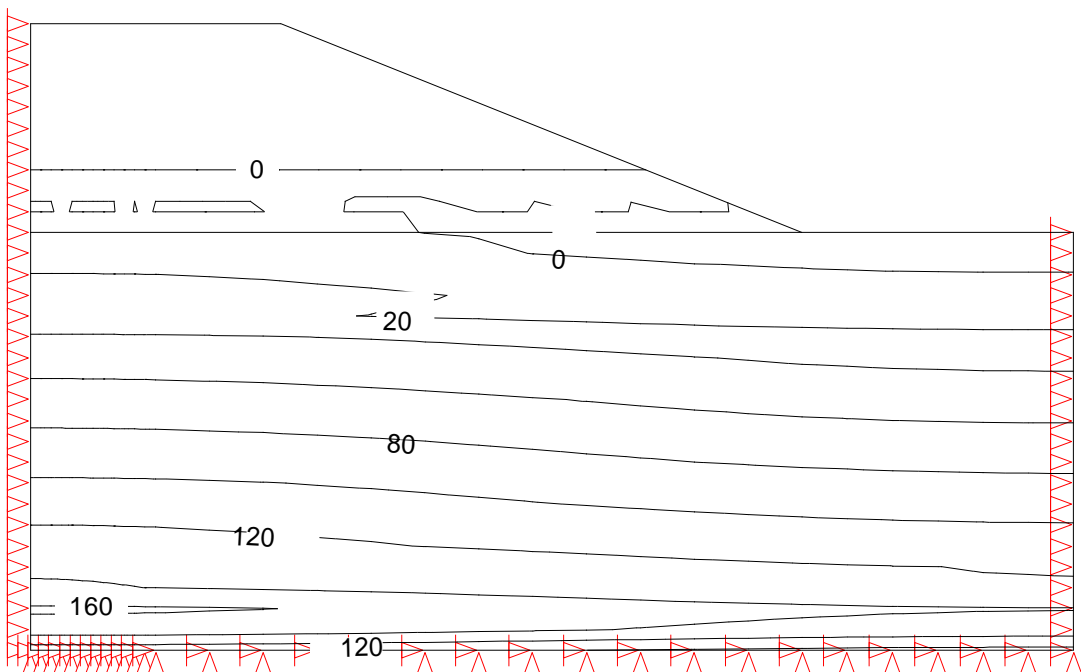


Fig. (6.30) Contour lines of pore water pressure (kPa) of partially saturated soil with water table at (2 m) from the ground level after 1 day.

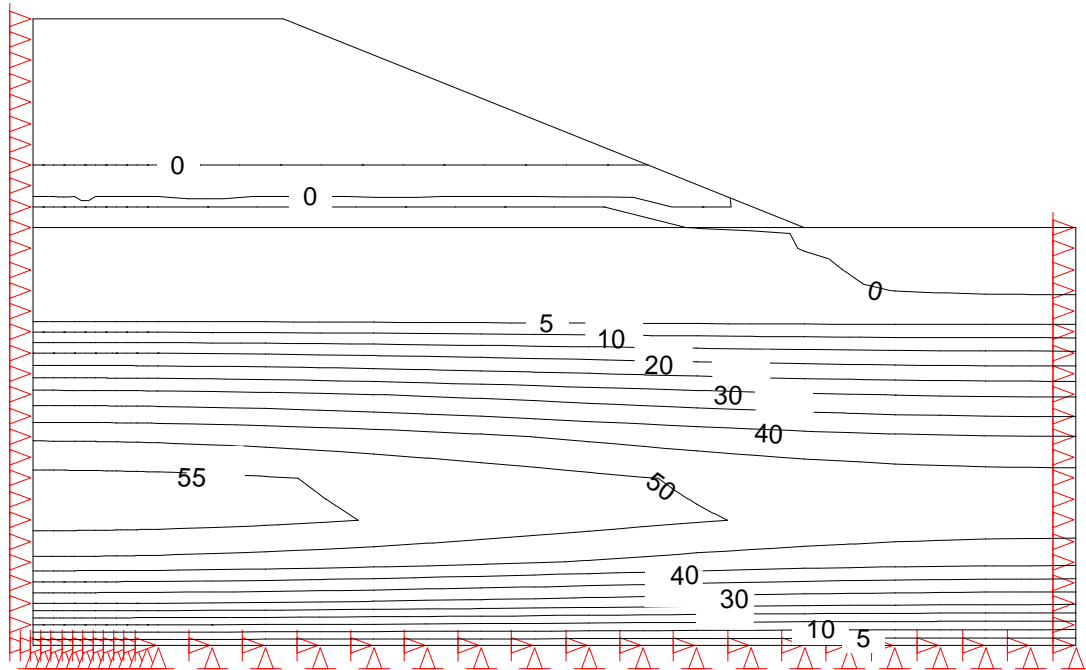


Fig. (6.31) Contour lines of pore water pressure (kPa) of partially saturated soil with water table at (2 m) from the ground level after 190 days.

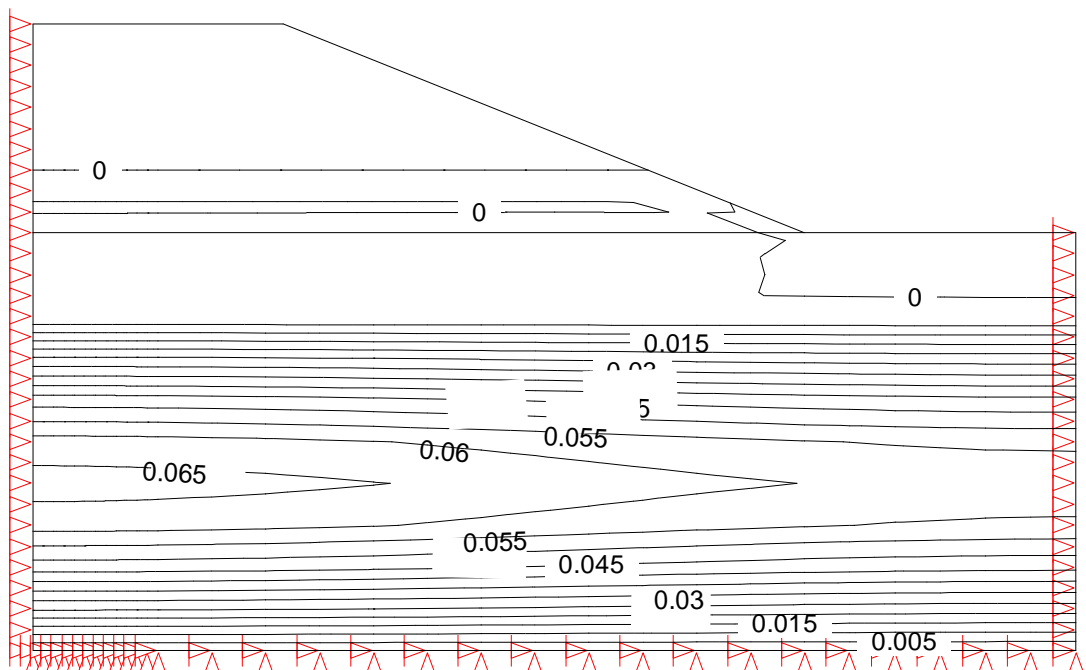


Fig. (6.32) Contour lines of pore water pressure (kPa) of partially saturated soil with water table at (2 m) from the ground level after 2000 days.

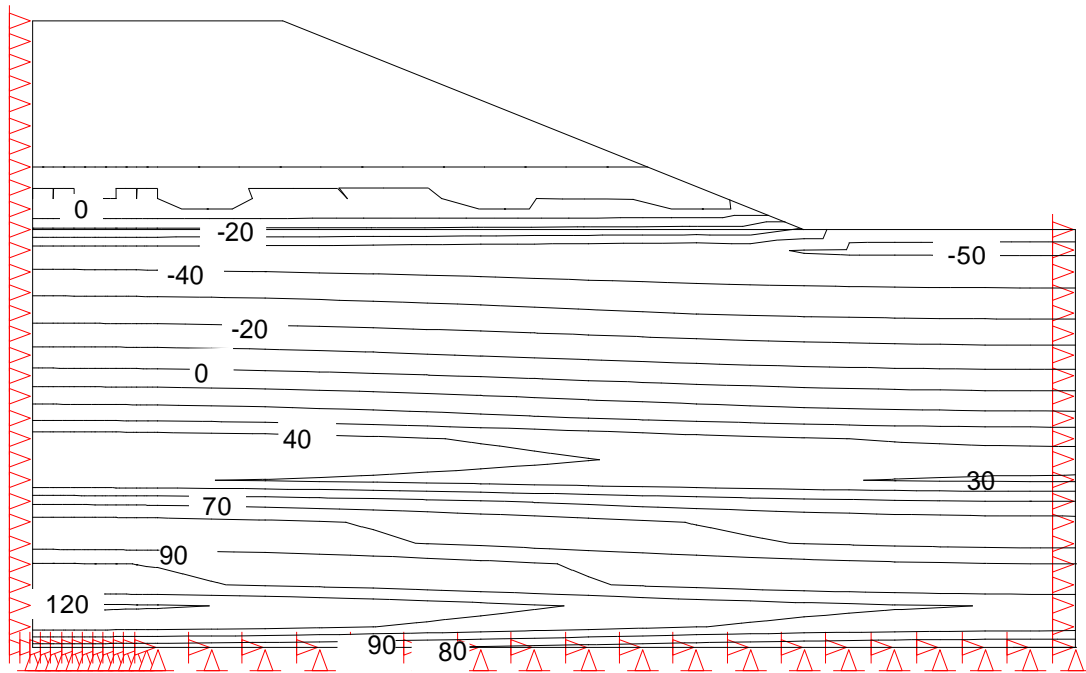


Fig. (6.33) Contour lines of pore water pressure (kPa) of partially saturated soil with water table at (6 m) from the ground level after 1 day.

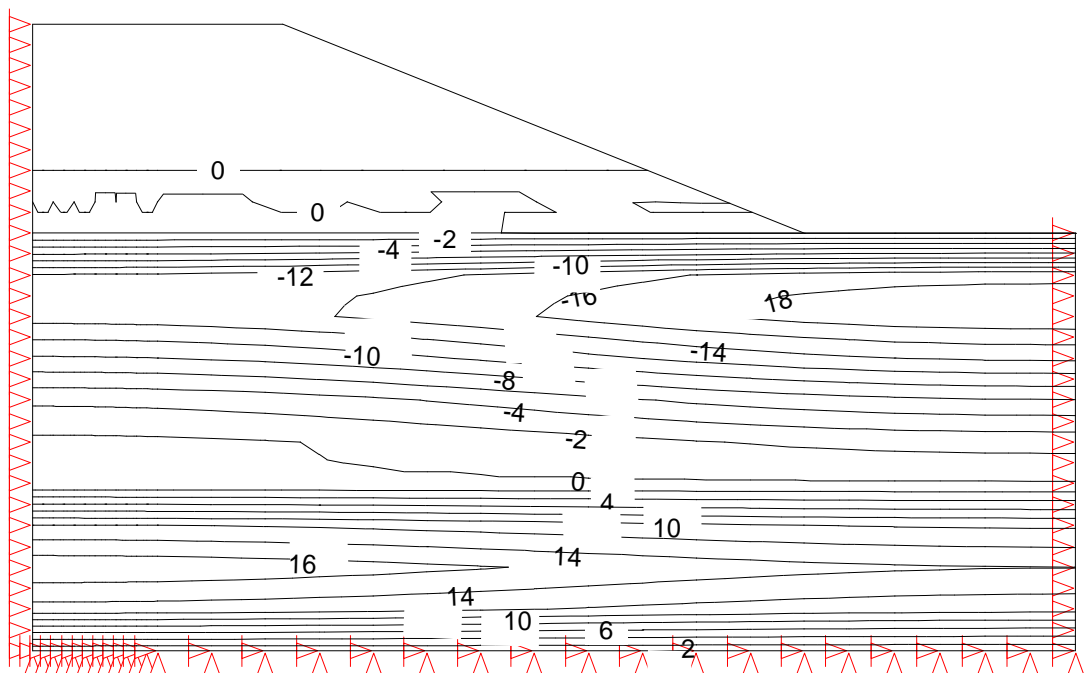


Fig. (6.34) Contour lines of pore water pressure (kPa) of partially saturated soil with water table at (6 m) from the ground level after 190 day.

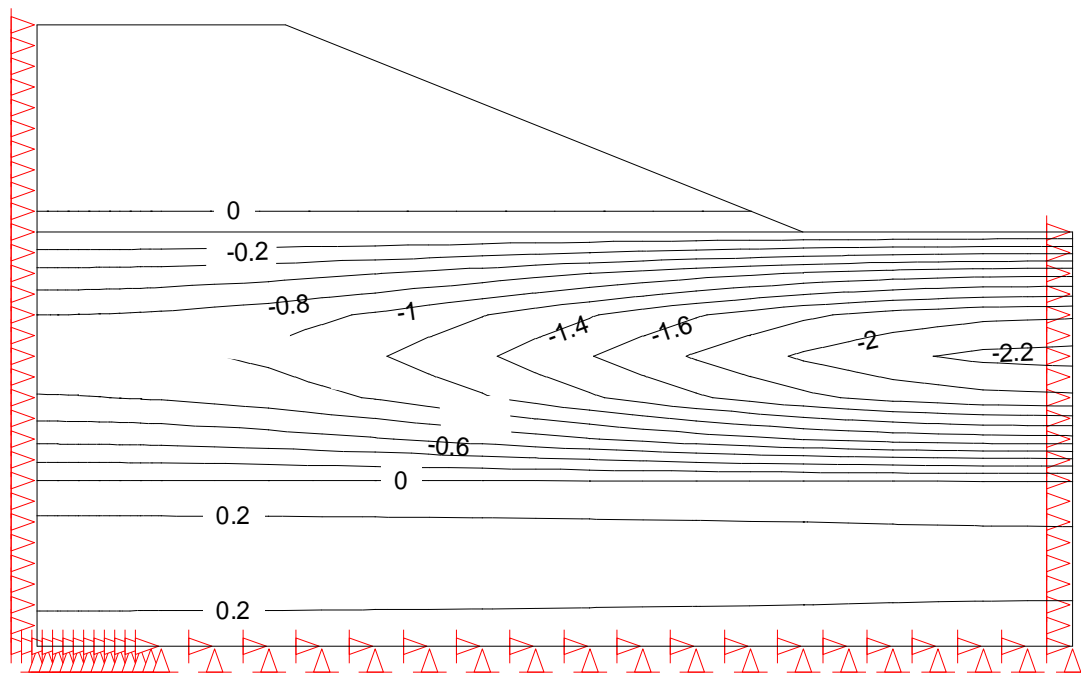


Fig. (6.35) Contour lines of pore water pressure (kPa) of partially saturated soil with water table at (6 m) from the ground level after 2000 day.

Figures (6.27), (6.28) and (6.29) reveal that the pore water pressure decreases with passage of time until reaching zero at the time (2000 days).

From Figures (6.30), (6.31) and (6.32) it is noticed that the behaviour of pore water pressure is similar to that in condition of fully saturated state, but with less pressure value when compared at a certain time. The value of pore water pressure is at lower limits at the upper and lower ends of soil layer. It was noticed that negative pore water pressures do not appear when the water drops to depth of (2 m) from the ground surface, which can be explained by the fact that the phenomenon of Mendel-Cryer effect caused increase the pore water pressure to level greater than the value of the suction pressure, and this leads to disappearance of the negative pressure.

In all these figures, it can be noticed that the pore water pressure is maximum at the middle of the clay layer due to two-way drainage condition except at early time (1 day) at which near the bottom boundary, the maximum pore water pressure is obtained.

This may be attributed to the algorithm of convergence adopted by the program and the method of defining the drainage condition in the program SEEP/W. this case is also noticed when drawing the isochrones of pore water pressure at different times.

A comparison between Figures (6.28), (6.31) and (6.34) and Figures (6.29), (6.32) and (6.35) shows that as the soil tends to become unsaturated, the excess pore water pressure decreases at a certain time. The decrease in pore water pressure becomes apparent when the degree of saturation further decreases.

6.5.5 Contour Lines of Vertical Displacement

Figures (6.36) to (6.47), show the contour lines of vertical displacement through the embankment and its foundation under different conditions of water table and at different times.

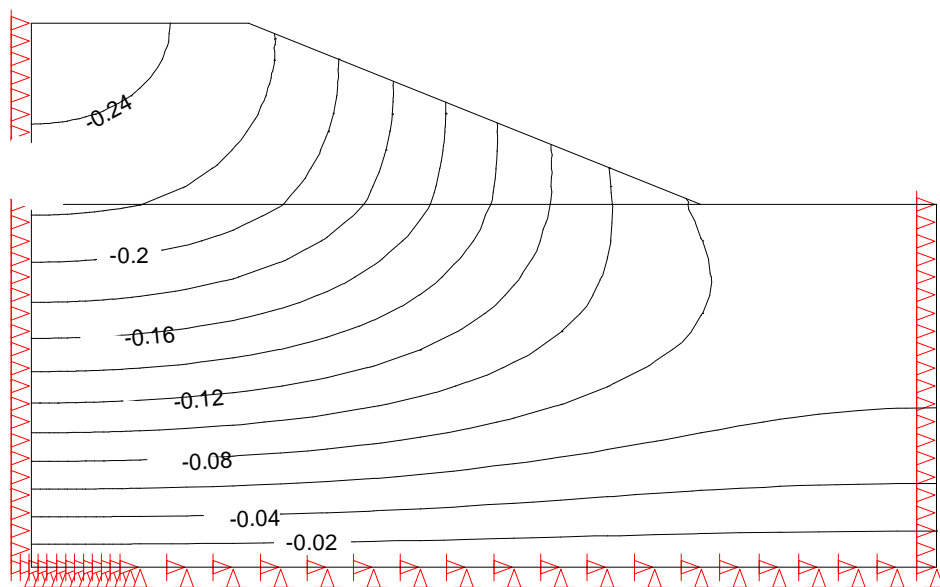


Fig. (6.36) Contour lines of vertical displacement (m) of fully saturated soil after 1 day.

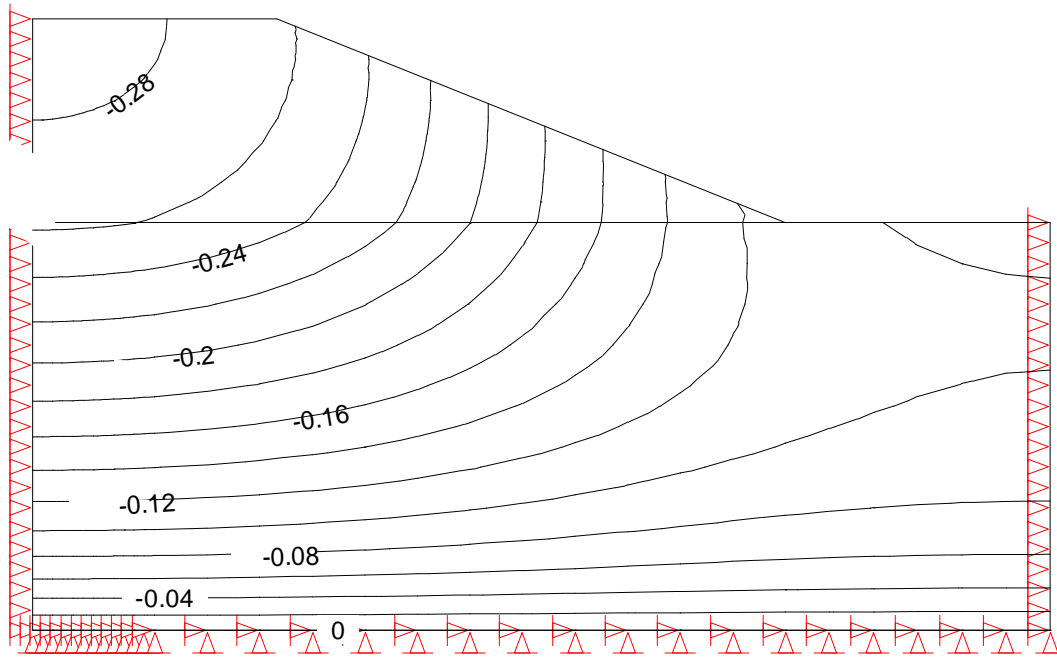


Fig. (6.37) Contour lines of vertical displacement (m) of fully saturated soil after 190 days.

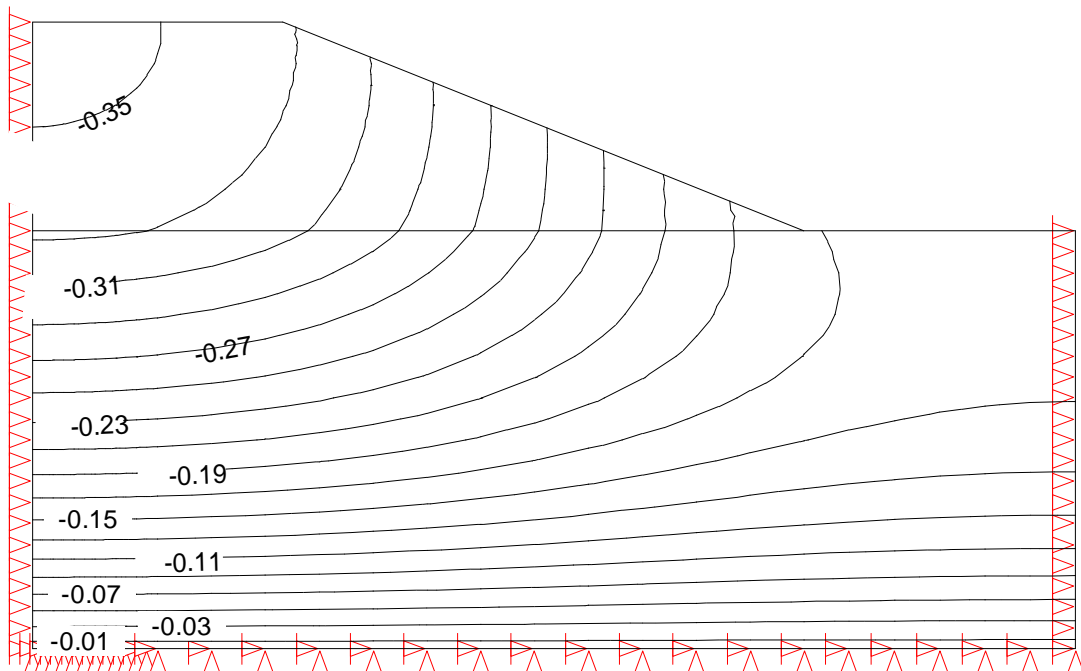


Fig. (6.38) Contour lines of vertical displacement (m) of fully saturated soil after 1500 days.

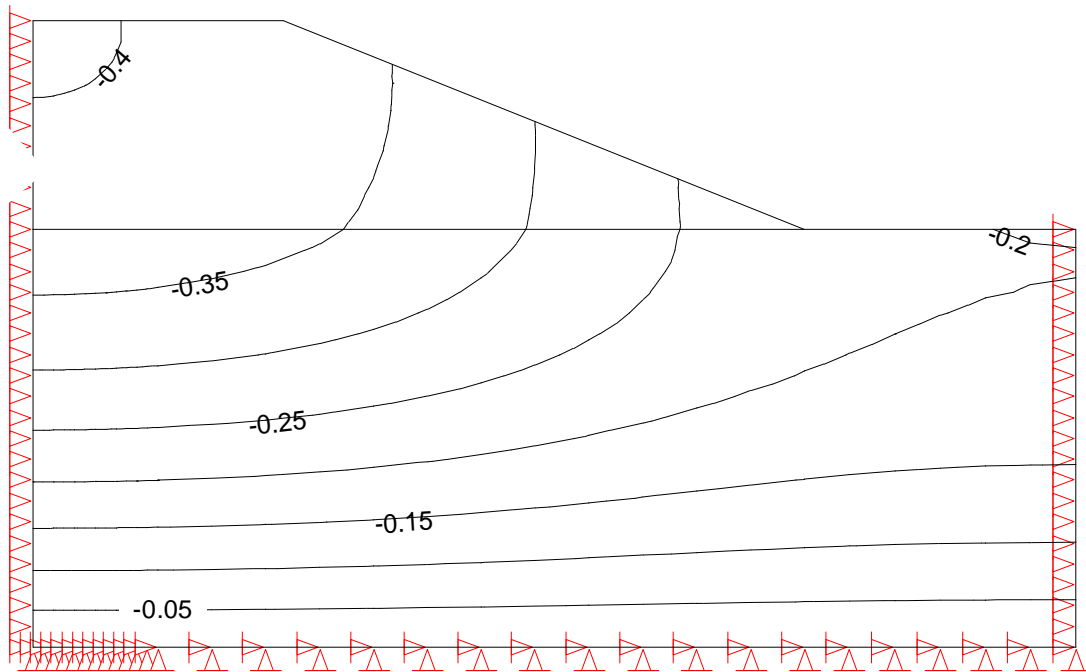


Fig. (6.39) Contour lines of vertical displacement (m) of fully saturated soil after 5000 days.

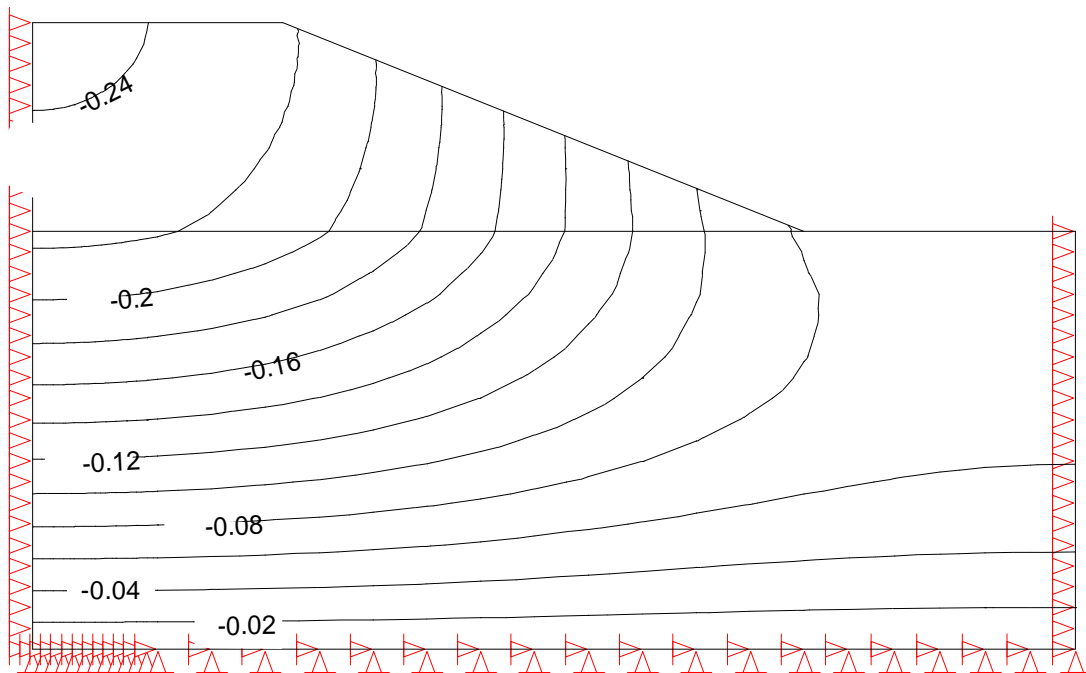


Fig. (6.40) Contour lines of vertical displacement (m) of partially saturated soil with water table at (2 m) from the ground level after 1 day.

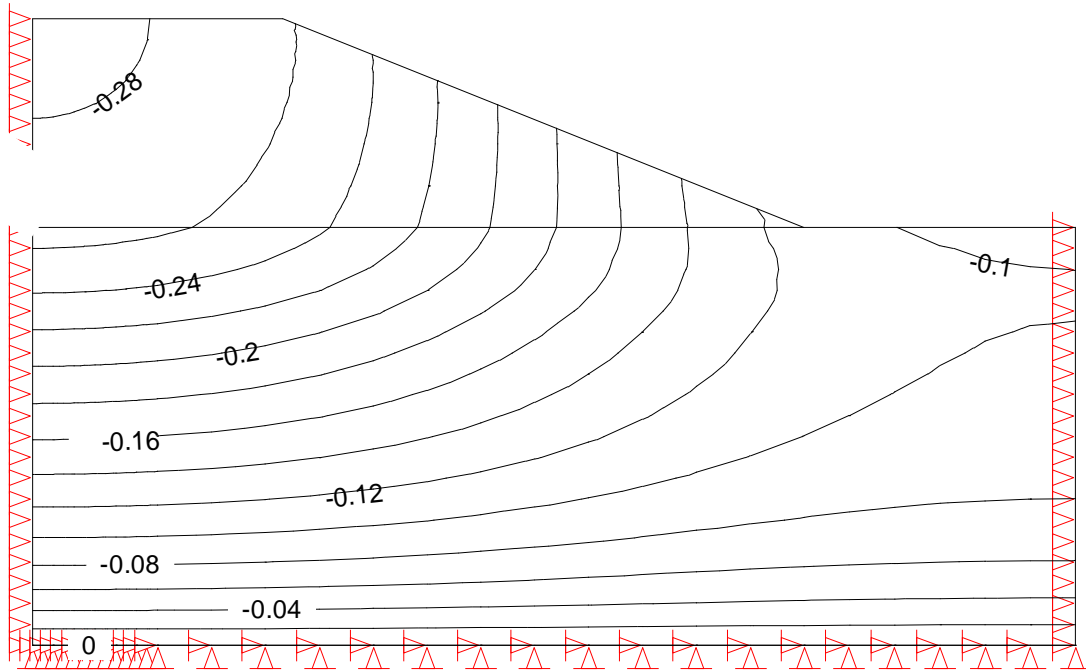


Fig. (6.41) Contour lines of vertical displacement (m) of partially saturated soil with water table at (2 m) from the ground level after 190 days.

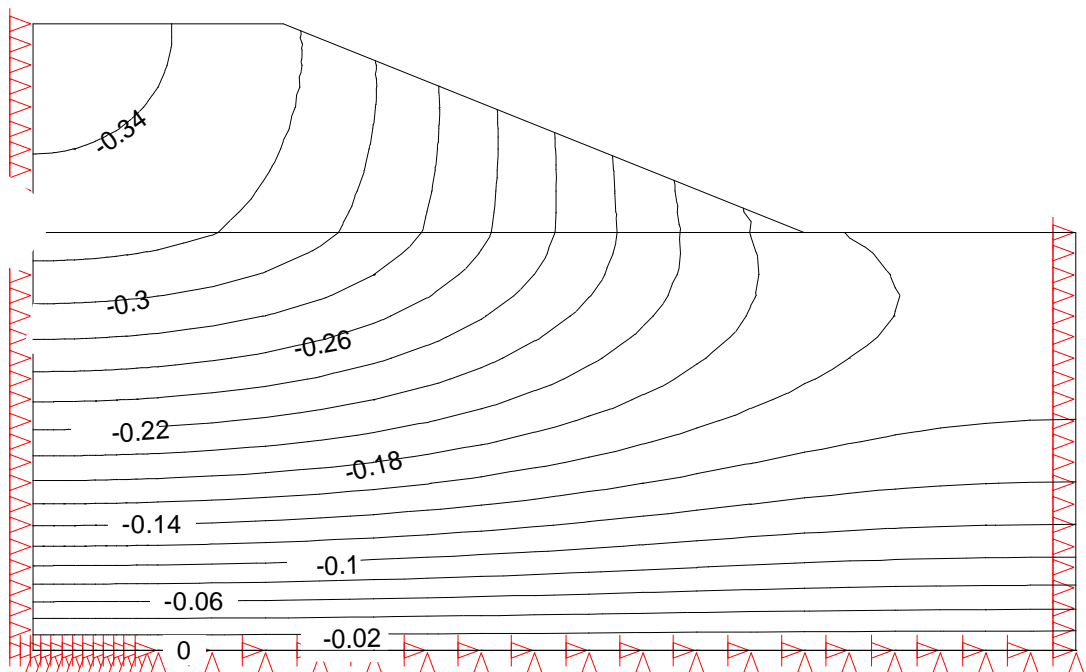


Fig. (6.42) Contour lines of vertical displacement (m) of partially saturated soil with water table at (2 m) from the ground level after 1500 days.

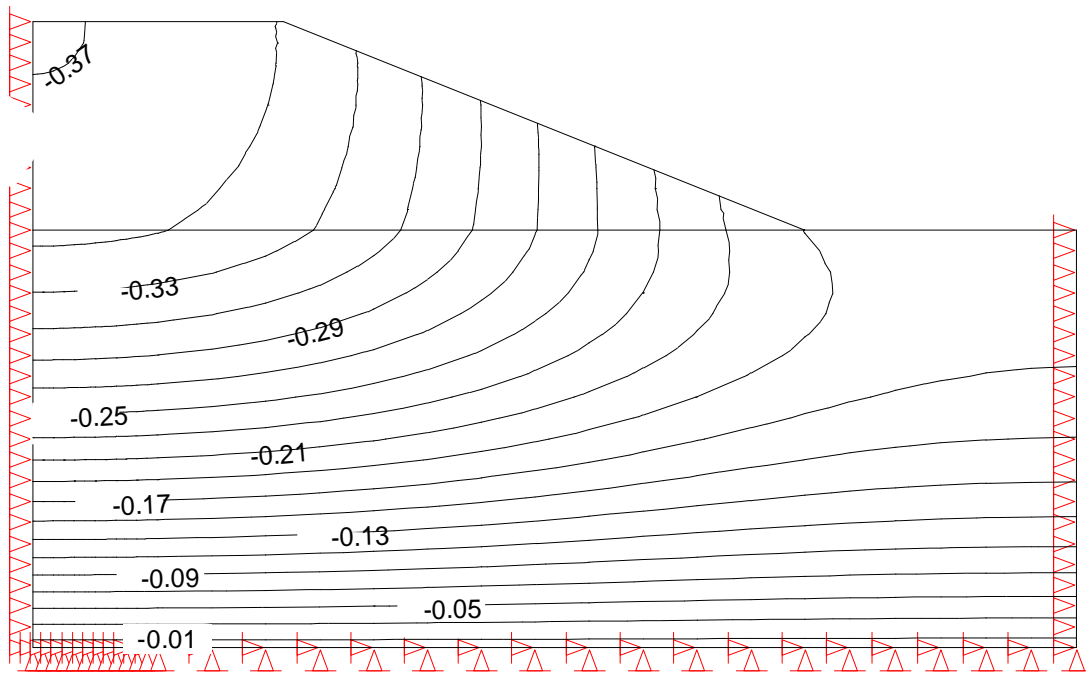


Fig. (6.43) Contour lines of vertical displacement (m) of partially saturated soil with water table at (2 m) from the ground level after 5000 days.

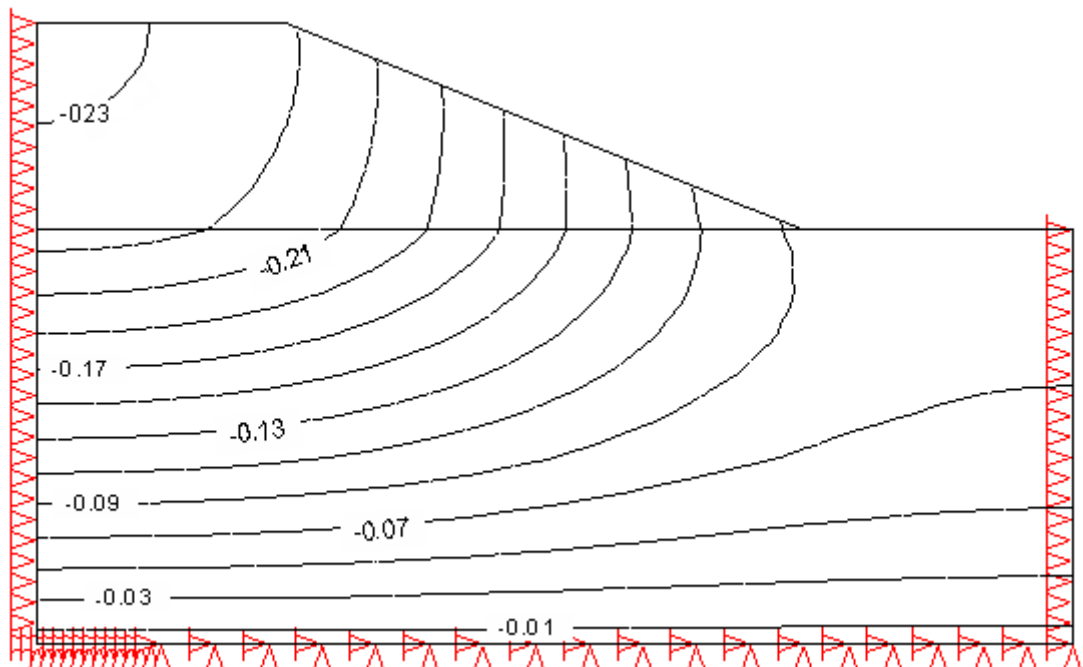


Fig. (6.44) Contour lines of vertical displacement (m) of partially saturated soil with water table at (6 m) from the ground level after 1 day.

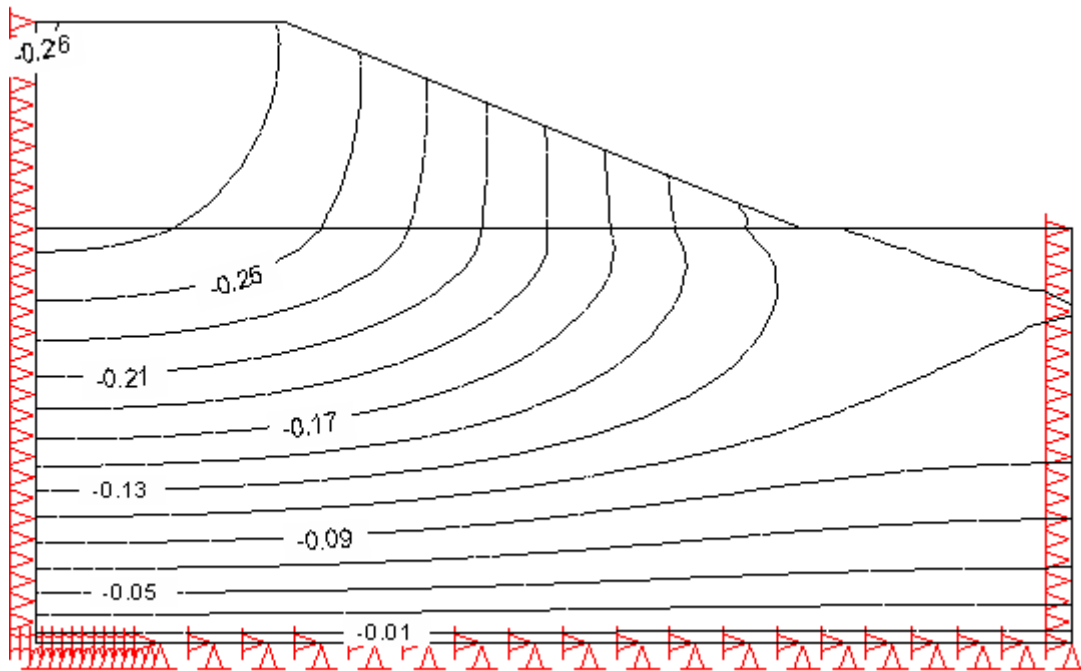


Fig. (6.45) Contour lines of vertical displacement (m) of partially saturated soil with water table at (6 m) from the ground level after 190 days.

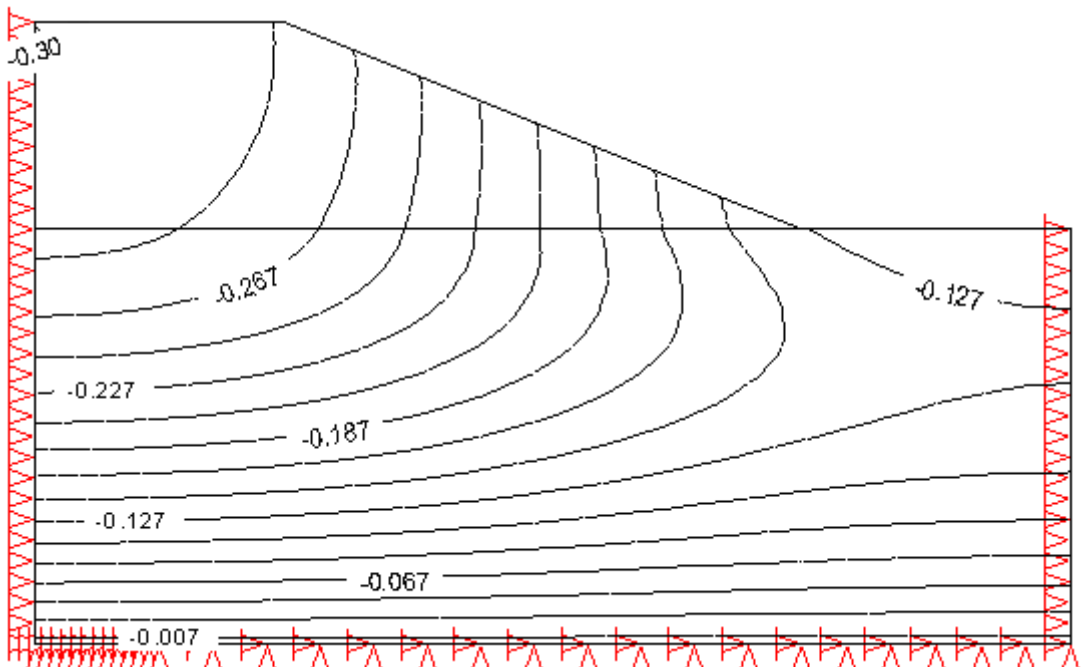


Fig. (6.46) Contour lines of vertical displacement (m) of partially saturated soil with water table at (6 m) from the ground level after 1500 days.

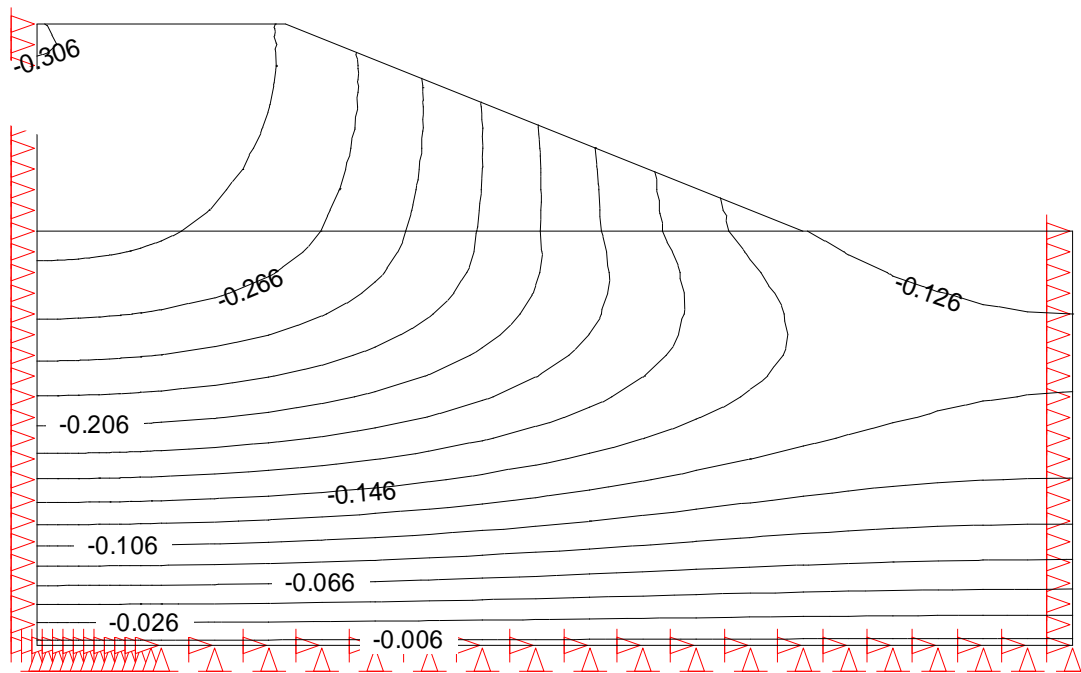


Fig. (6.47) Contour lines of vertical displacement(m) of partially saturated soil with water table at (6 m) from the ground level after 5000 days.

Figures (6.36) to (6.39) reveal that the vertical displacement will be at a maximum value at top of embankment and at a maximum value near the lower end of soil layer. It is also noticed that with passage of time, the vertical displacement is increased due to the dissipation of pore water pressure until reaching the end value at nearly the time of (5000 days).

Figures (6.40) to (6.43) show that the vertical displacement is increased with passage of time, but at later times like (1500 days) and above, its value decreases in comparison with its value in case of fully saturated. The value of vertical displacement is about (37 cm) which means that a decrease in settlement of the order of about (1.2 %) takes place when the soil is unsaturated .

Figures (6.44) to (6.47) illustrate that an increase in vertical displacement takes place with a passage of time but its maximum value is much less in case of fully saturated. The difference between the value of

vertical displacement after (1 day) and after (5000 days) would be low compared with condition of the fully saturated state. This means that in condition of partial saturation, as the depth of water is increased the problem of settlement decreases and the soil tends to behaves as if it were dry.

6.5.6 Contour Lines of Deviatoric Stress

Figures (6.48) to (6.56), show the contour lines of deviatoric stress through the embankment and its foundation under different conditions of water table and at different times.

Figures (6.48) to (6.50) reveal that the deviatoric stress increases as we go down inside the soil layers until reaching the maximum value at the lower end of soil layer. It is also clear that the value of deviatoric stress increases at a certain depth with passage of time until the time (190 days), after which the increase becomes slowly and the change does not exceed about (1 kN/m²) at the time (1500 days), and after that, the value of deviatoric stress becomes constant until the end of consolidation at the value of (118 kN/m²).

The above explanation is also applied to Figures (6.51), (6.52) and (6.53), but with a lower value of deviatoric stress in comparison with their values in case of fully saturated condition at the same time and location . The final values of deviatoric stress reach about (111.5 kN/m²).

It can be concluded that when the soil is unsaturated, the failure potential is less than that for fully saturated soil since that the deviatoric stress ($\sigma_1 - \sigma_3$) at all stages of consolidation is smaller.

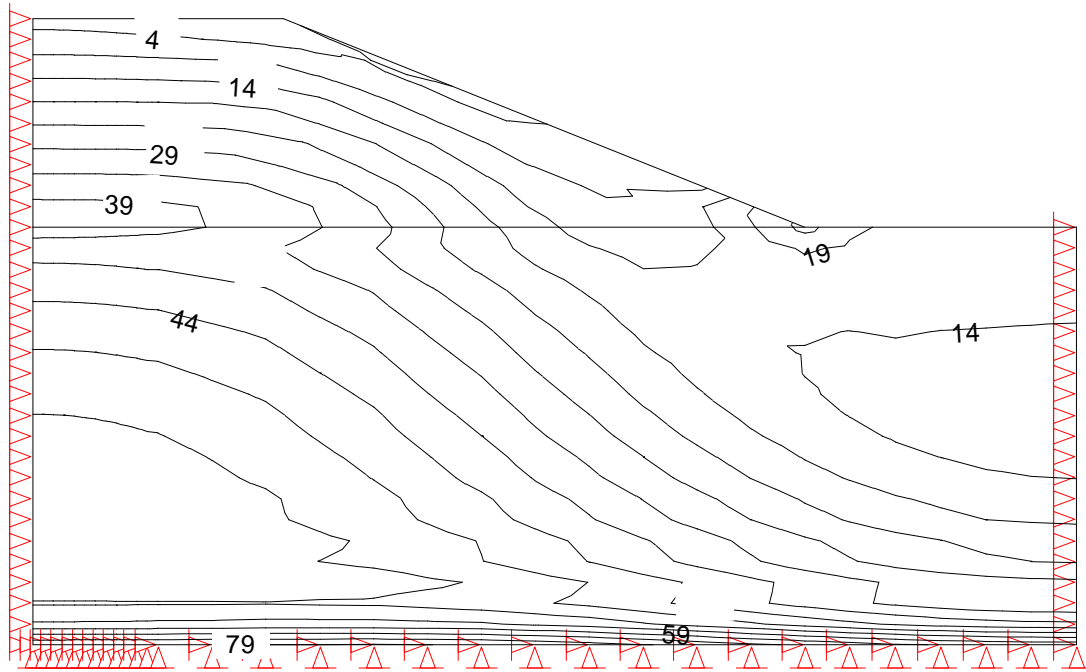


Fig. (6.48) Contour lines of deviatoric stress (kN/m^2) at fully saturated soil after 1 day.

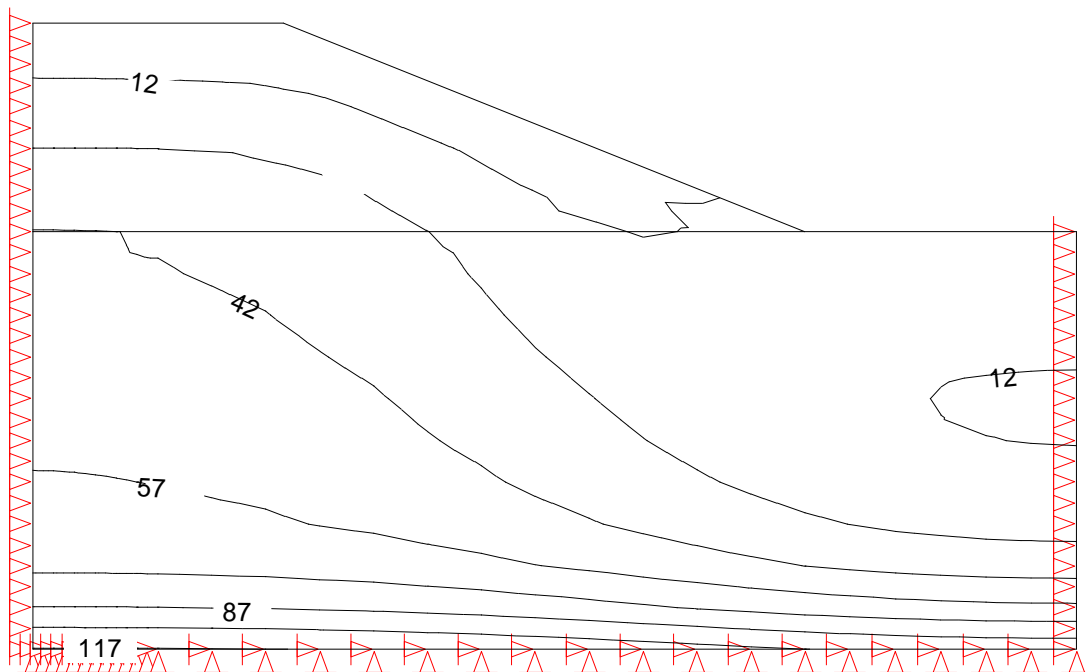


Fig. (6.49) Contour lines of deviatoric stress (kN/m^2) at fully saturated soil after 190 days.

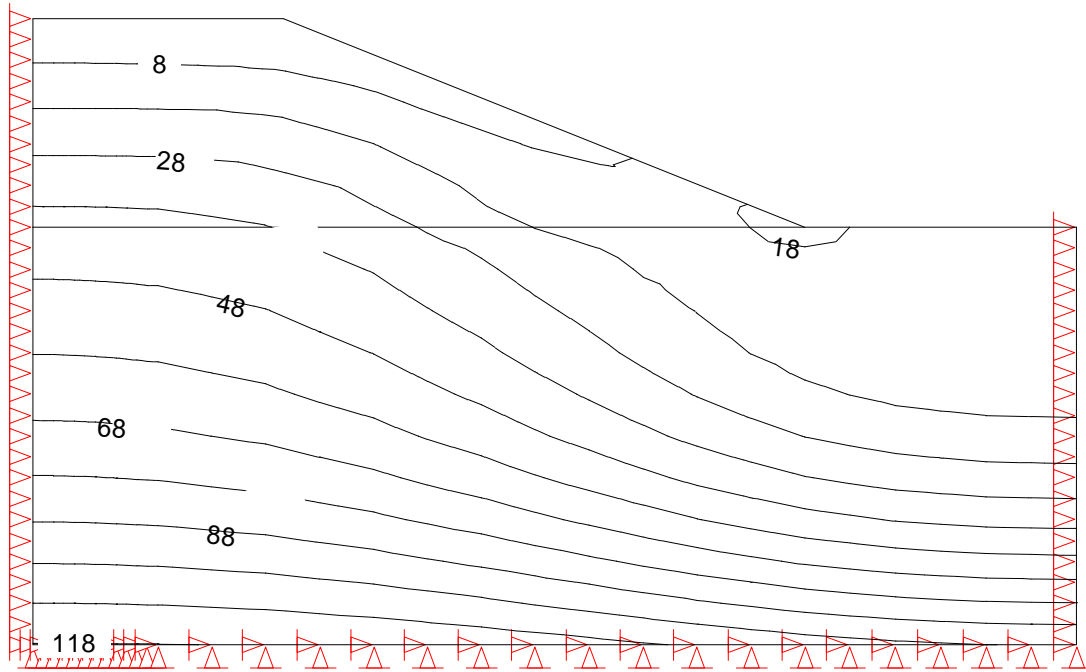


Fig. (6.50) Contour lines of deviatoric stress (kN/m^2) at fully saturated soil after 1500 days.

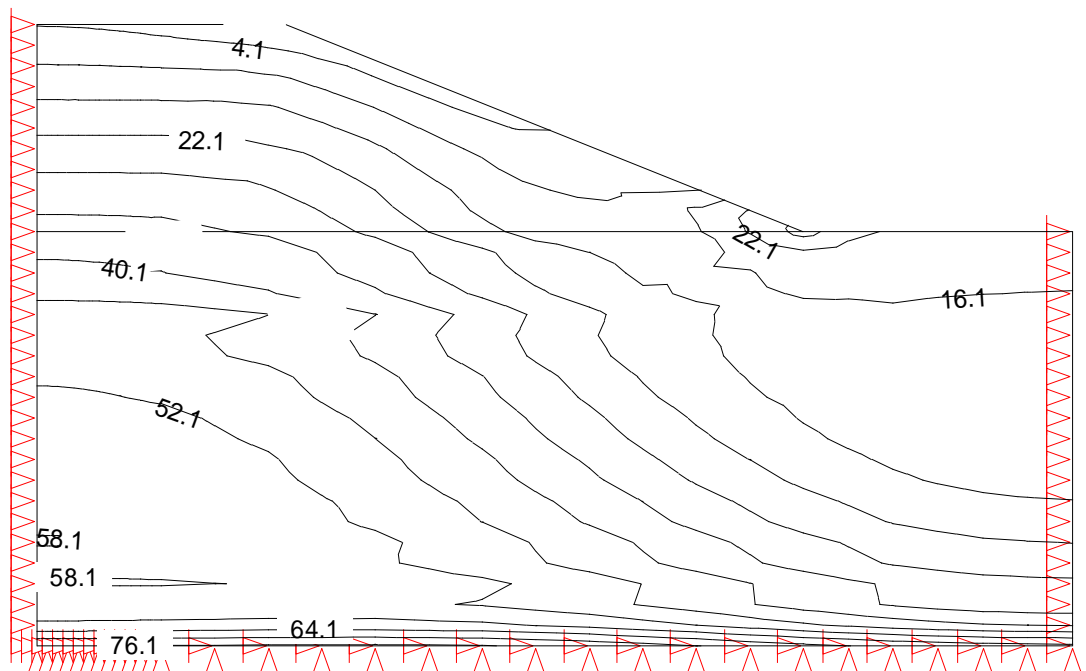


Fig. (6.51) Contour lines of deviatoric stress (kN/m^2) of partially saturated soil with water table at (2 m) from the ground level after 1 day.

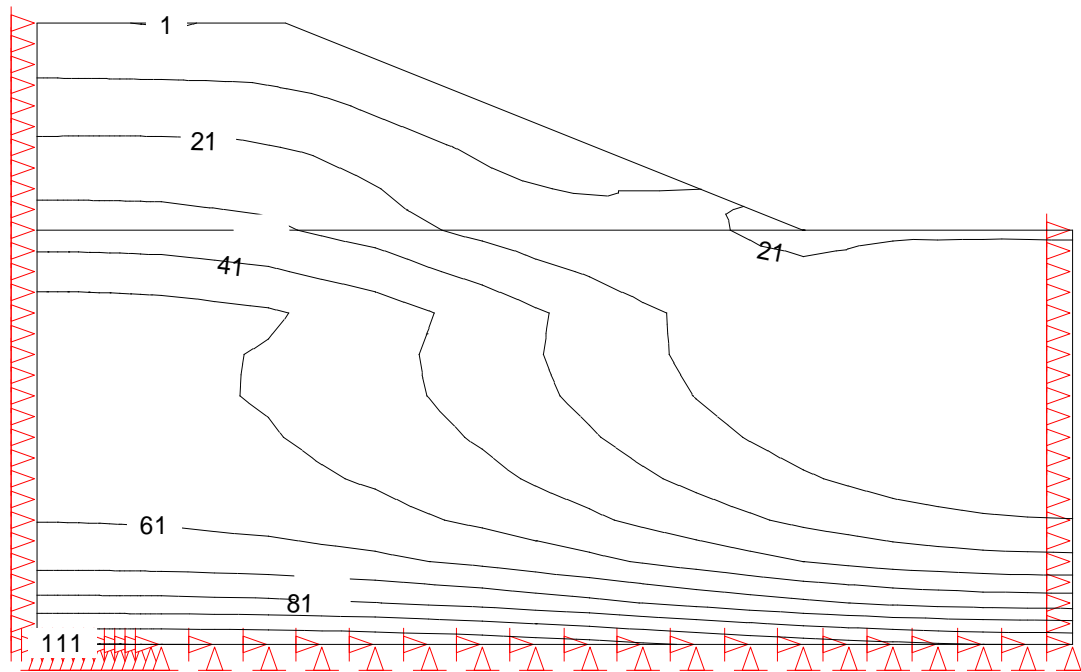


Fig. (6.52) Contour lines of deviatoric stress (kN/m^2) of partially saturated soil with water table at (2 m) from the ground level after 190 days.

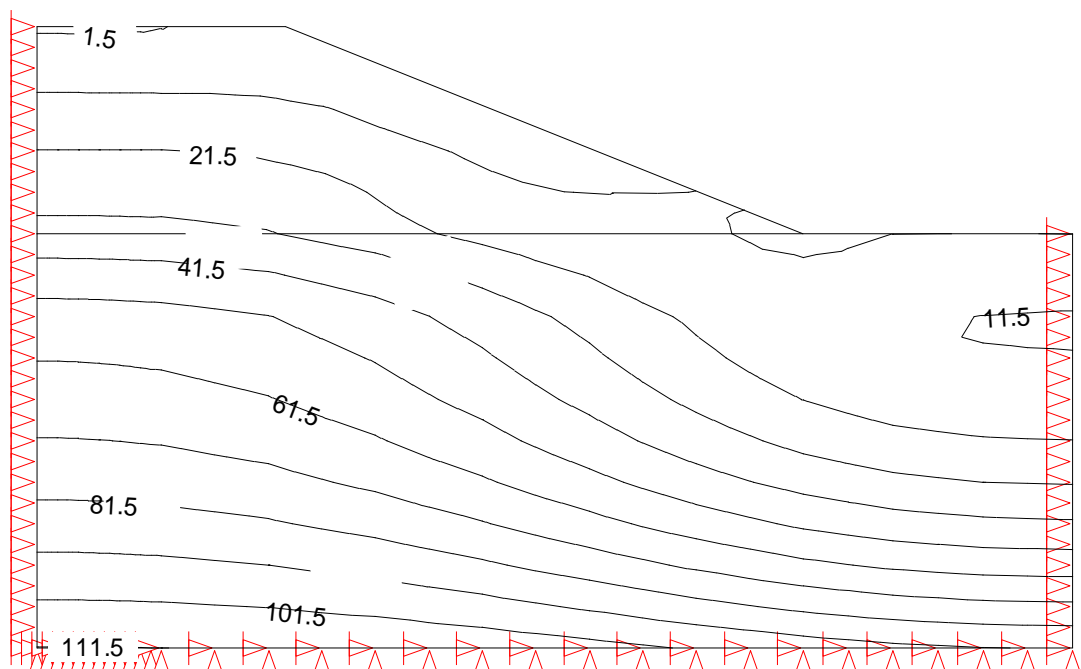


Fig. (6.53) Contour lines of deviatoric stress (kN/m^2) of partially saturated soil with water table at (2 m) from the ground level after 1500 days.

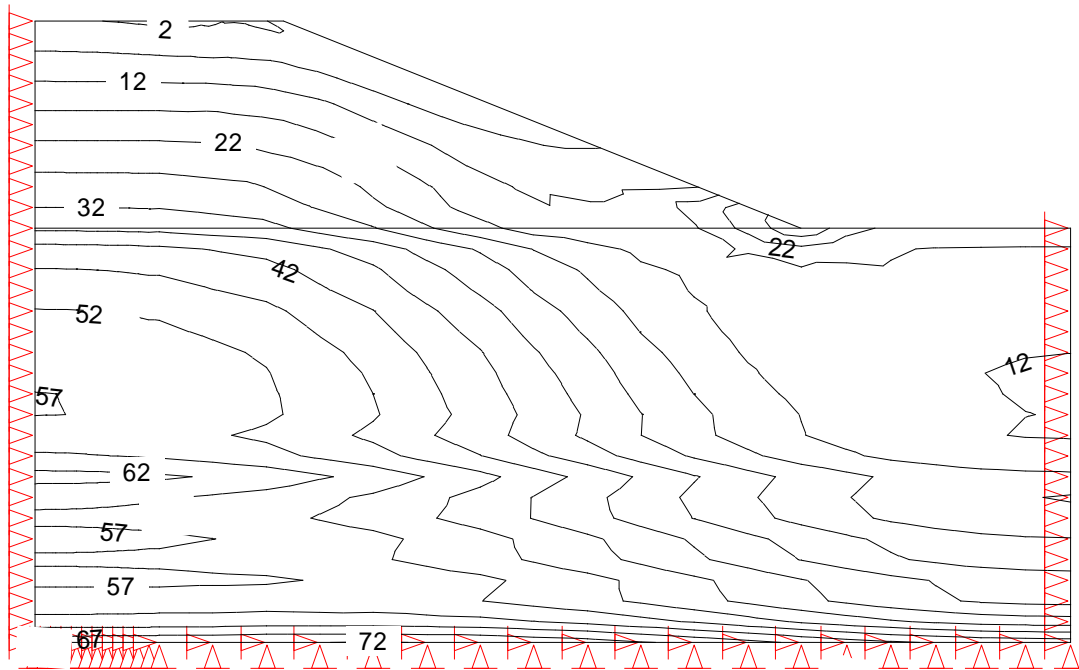


Fig. (6.54) Contour lines of deviatoric stress (kN/m^2) of partially saturated soil with water table at (6 m) from the ground level after 1 day.

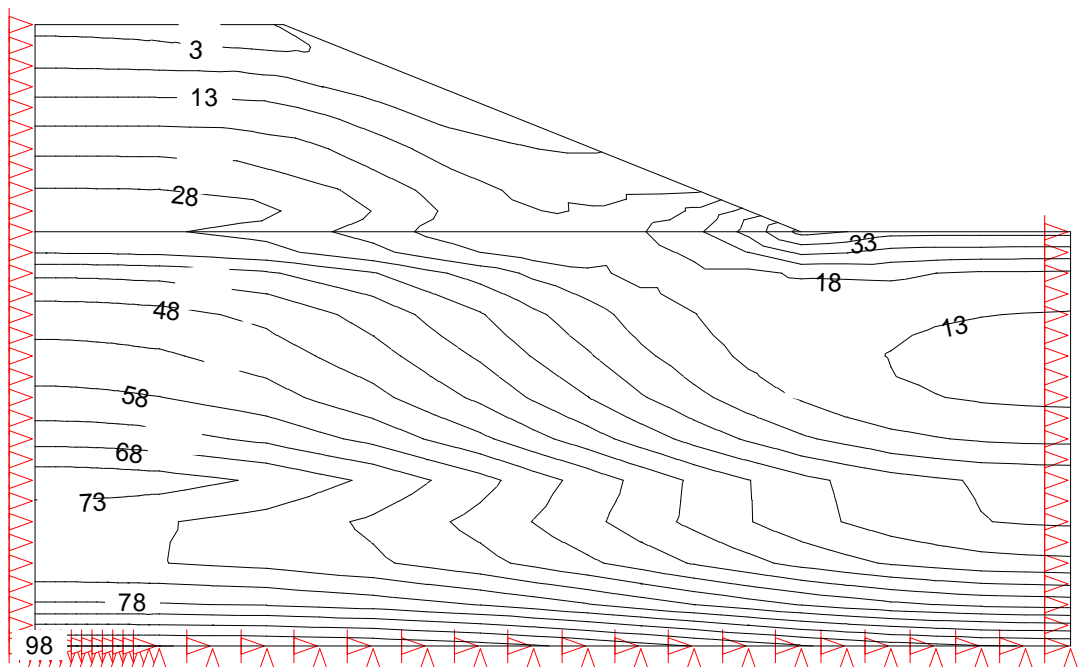


Fig. (6.55) Contour lines of deviatoric stress (kN/m^2) of partially saturated soil with water table at (6 m) from the ground level after 190 day.

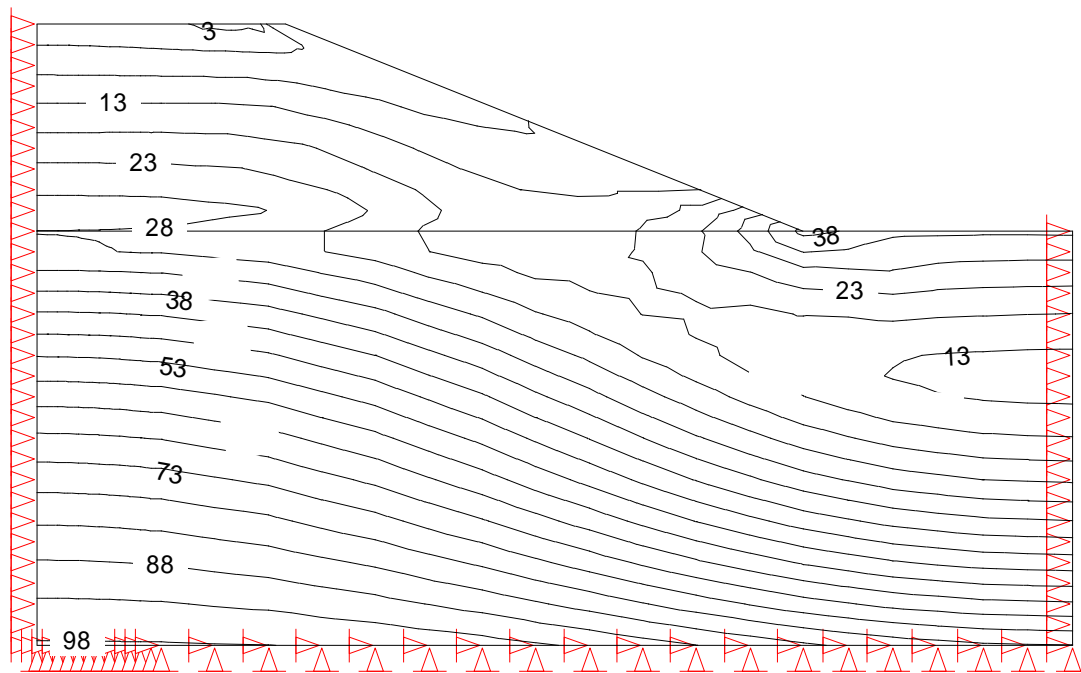


Fig. (6.56) Contour lines of deviatoric stress (kN/m^2) of partially saturated soil with water table at (6 m) from the ground level after 1500 day.

6.5.7 Vertical Displacement along Center Line of the Embankment

Figures (6.57) to (6.59), show the relation between the vertical displacement and the elevation of the soil under center line of the embankment at different times.

Figure (6.57) illustrates that at the time of applying the embankment weight, the vertical displacement will be close to zero along the centre line, and its value is increased with passage of time. This increase will be fast at the beginning until reaching the time of (800 days) where the value of vertical displacement will be about (90%) from its final value. At the time of (2000 days), the average degree of consolidation reaches about (97%) and after that, the soil needs about another (3000 days) to reach the final value of vertical displacement.

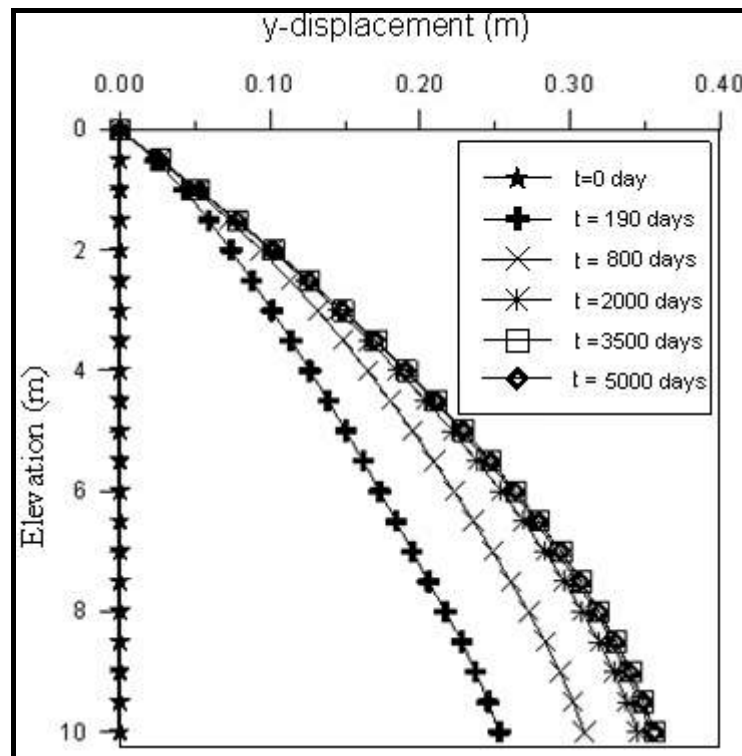


Fig. (6.57) Distribution of the vertical displacement along the center line of the embankment with time (fully saturated).

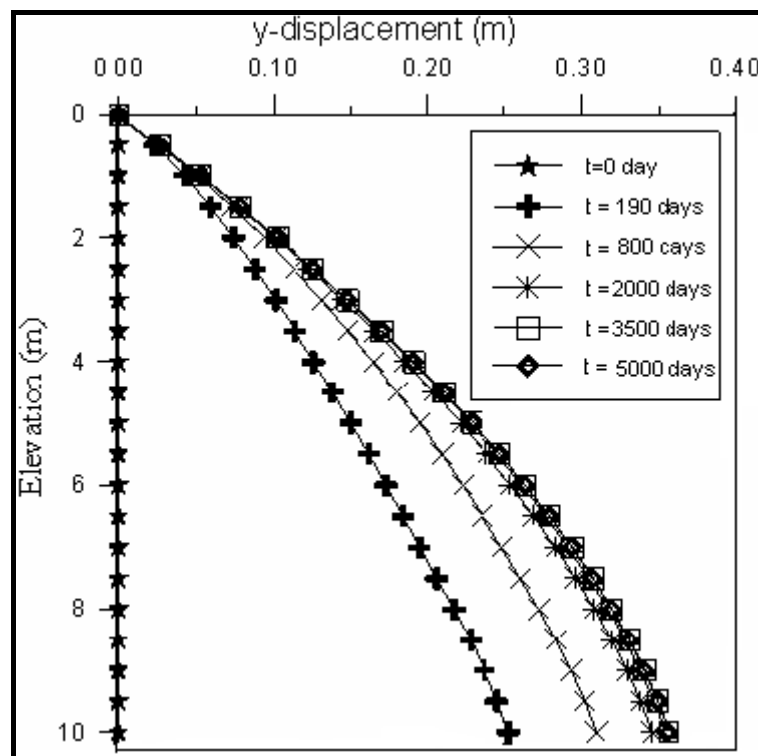


Fig. (6.58) Distribution of the vertical displacement along the center line of the embankment with time (W.T. at 2 m from the ground level).

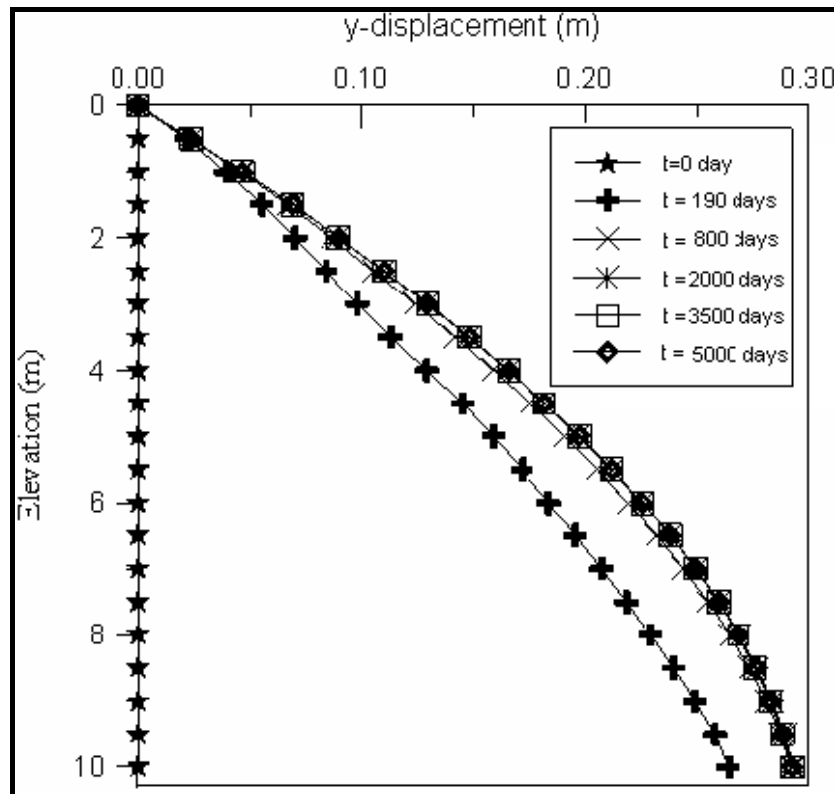


Fig. (6.59) Distribution of the vertical displacement along the center line of the embankment with time (W.T. at 6 m from the ground level).

In Figure (6.58), it is noticed that the soil in general behaves like in condition of fully saturated state but the difference is that the final value of vertical displacement will be less with minor differences, and the average degree of consolidation of (90%) of the soil is reached at the time of (800 days).

Figure (6.59) reveals that the drawdown of water table to depth of (6 m) from the ground level leads to decrease the value of vertical displacement, to a value of (29 cm). The figure also reveals that the average degree of consolidation of (90%) of the soil is reached at a time of (190 days). So, it is concluded that with drawdown of water level, the vertical displacement is decreased and the final settlement takes place with a faster time.

It can be concluded that the unsaturated zone absorbs a portion of the mechanical loading stress permanently.

6.5.8 Pore water pressure vs. hydraulic conductivity

Figures (6.60), (6.61) and (6.62) show the relationship between the pore water pressure and hydraulic conductivity at point A (in Figure 6.2) at different elevations of water table.

Figures (6.63), (6.64), and (6.65) show the relationship between the pore water pressure and hydraulic conductivity at point B (in Figure 6.2) at different elevations of water table.

In these figures, u_p refers to pore water pressure for the case of partially saturated soil while u_f refers to pore water pressure in the case of fully saturated soil.

Figure (6.60) reveals that at time of (1 day), the increase in hydraulic conductivity, has no effect on the percentage (u_p/u_f) and this is because that at this time, there is very small dissipation of pressure whatever the hydraulic conductivity value is. At a time of (70 days) and more, the condition of unsaturation has no effect for the case of low hydraulic conductivity of (10^{-5} m/day) and below, but when the hydraulic conductivity is greater than (10^{-5} m/day) and up to (10^{-3} m/day), the effect of partial saturation will appear at time (70 and 250 days). This condition can be explained as the dissipation of water pressure at a low hydraulic conductivity, there is no difference between the fully and partially saturated conditions, but at a higher hydraulic conductivity the remaining pressure at the state of fully saturated soil becomes more than that in case of partially saturated soil, and so that, the percentage (u_p/u_f) is decreased.

At time of (2500 days) and when the hydraulic conductivity is low, the percentage (u_p/u_f) will be high as there is no great difference between water pressure at both conditions of fully and partially saturated.. With increasing of hydraulic conductivity up to about (10^{-3} m/day), the

percentage (u_p/u_f) goes back to increase because the water pressure in both conditions of fully and partially saturation is reaching zero value.

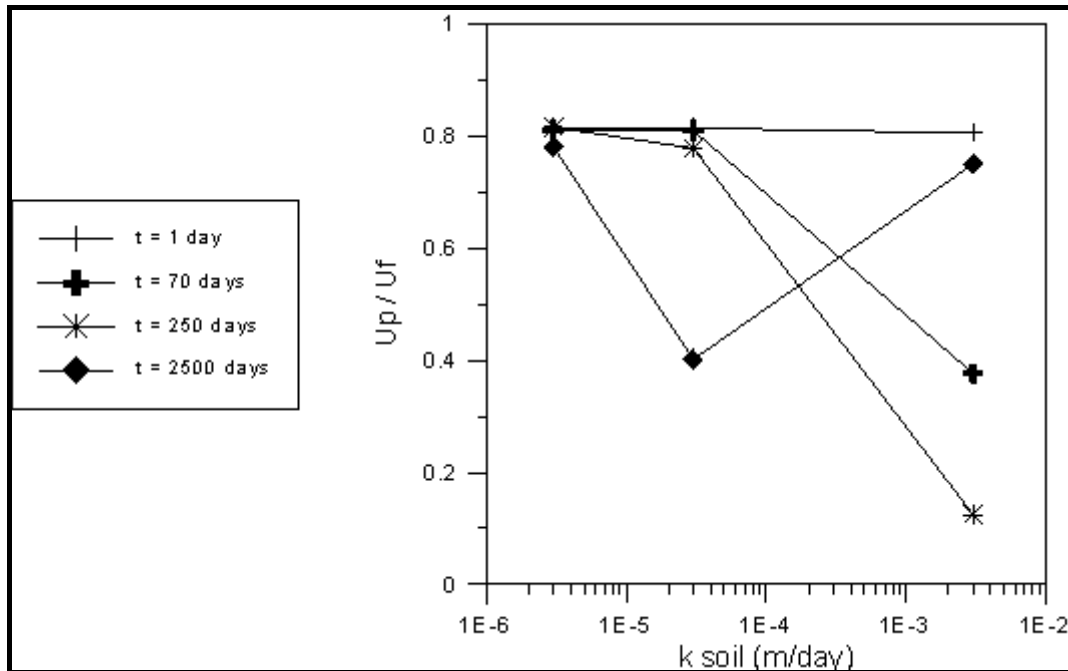


Fig. (6.60) The relation between (u_p/u_f) and soil hydraulic conductivity at point (A) when water table is at (2 m) from the ground level.

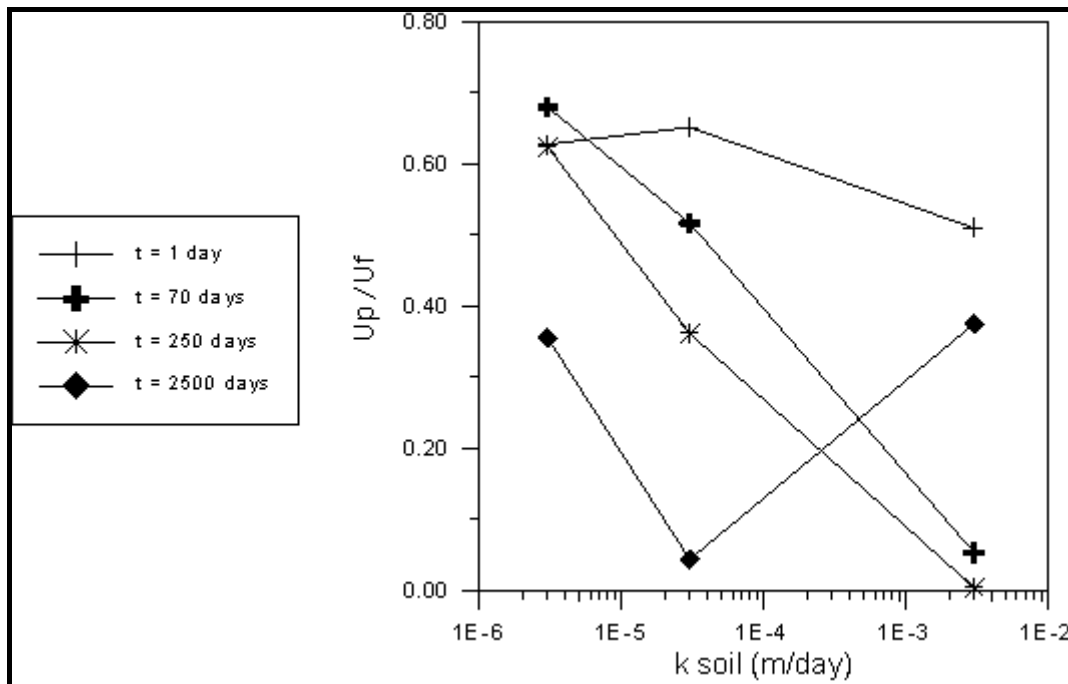


Fig. (6.61) The relation between (u_p/u_f) and soil hydraulic conductivity at point (A) when water table is at (4 m) from the ground level.

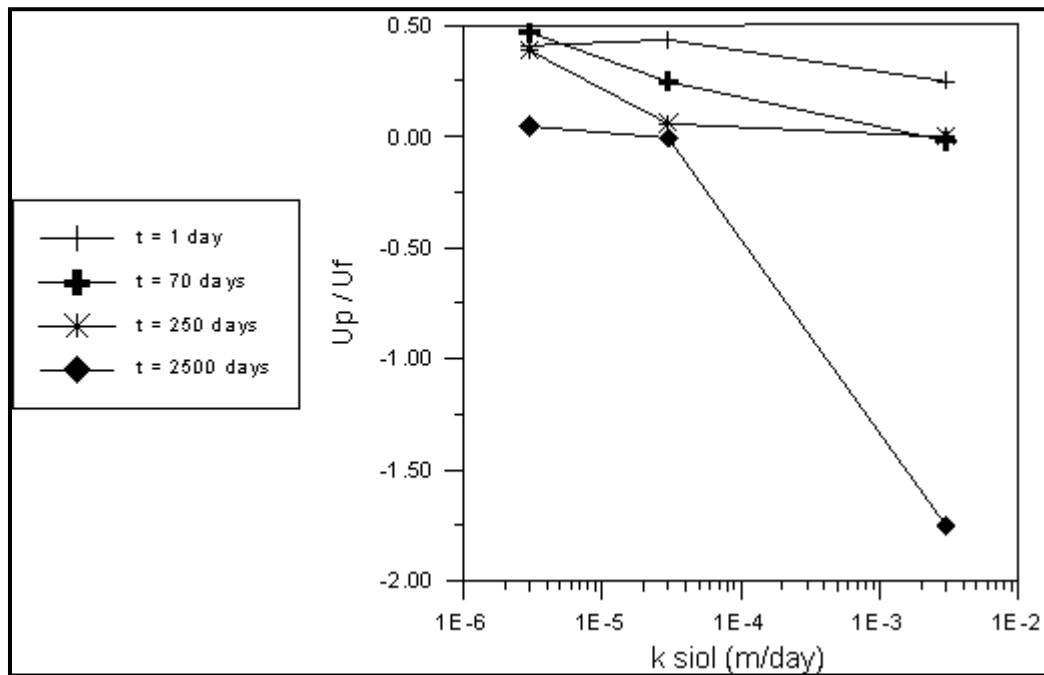


Fig. (6.62) The relation between (u_p/u_f) and soil hydraulic conductivity at point (A) when water table is at (6 m) from the ground level.

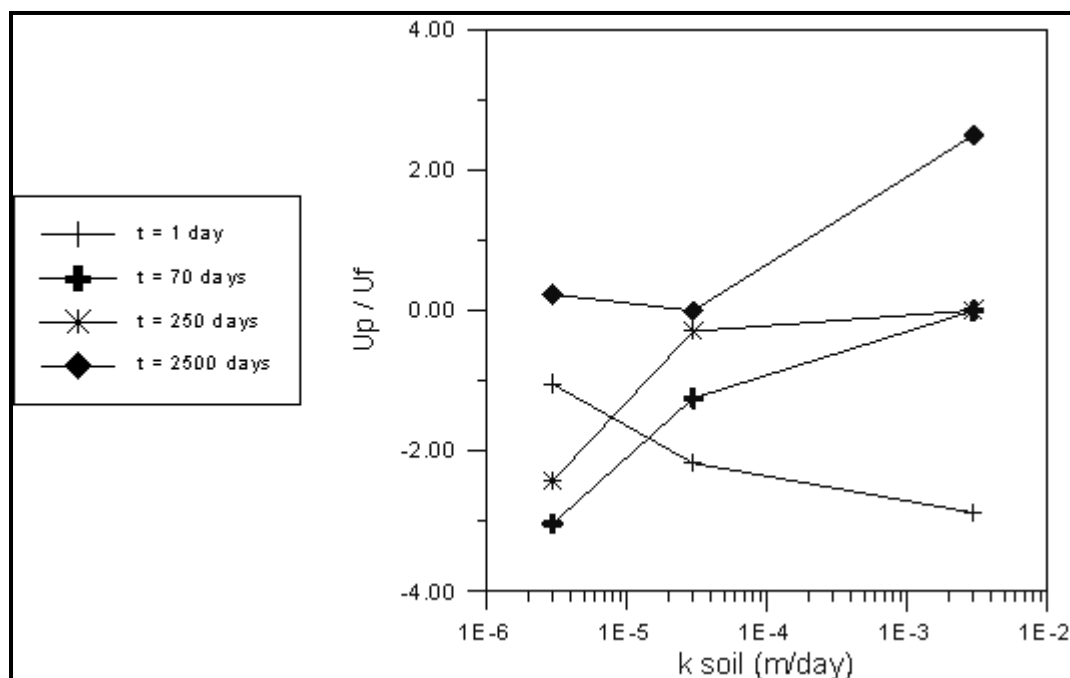


Fig. (6.63) The relation between (u_p/u_f) and soil hydraulic conductivity at point (B) when water table is at (2 m) from the ground level.

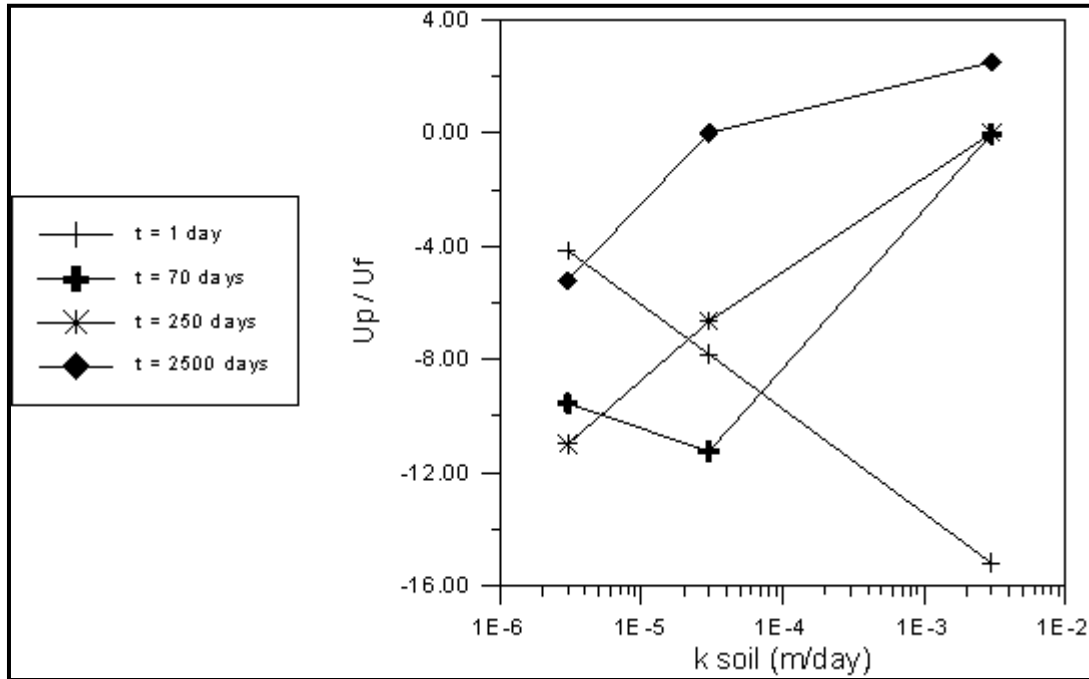


Fig. (6.64) The relation between (u_p/u_f) and soil hydraulic conductivity at point (B) when water table is at (4 m) from the ground level.

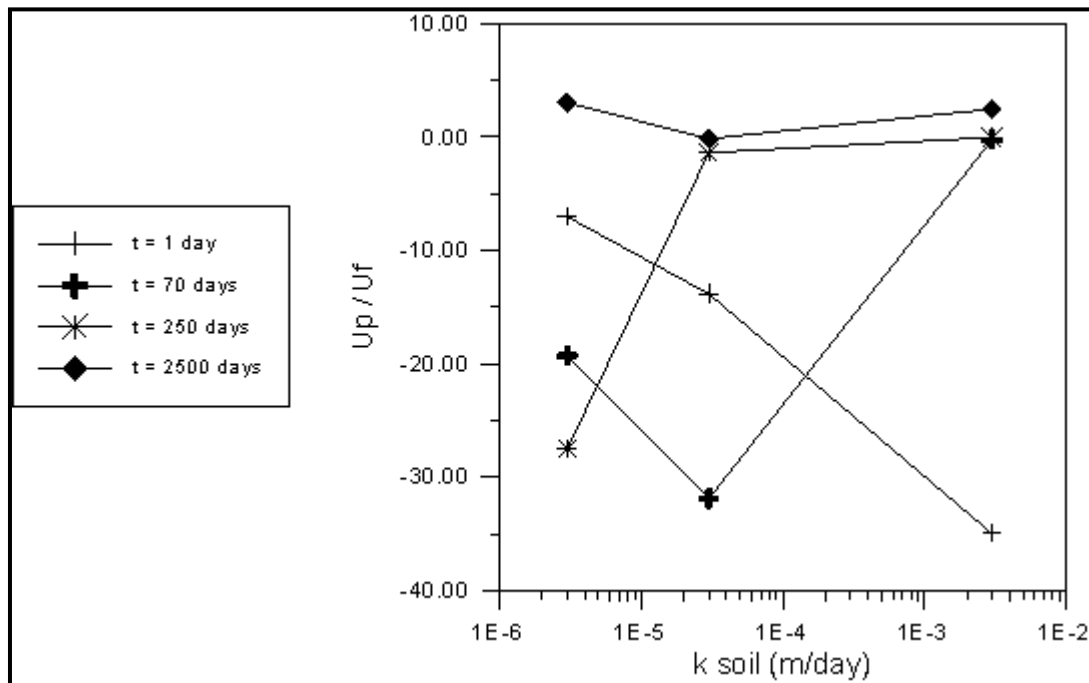


Fig. (6.65) The relation between (u_p/u_f) and soil hydraulic conductivity at point (B) when water table is at (6 m) from the ground level.

Figure (6.61) reveals that the increase of depth of water up to (4 m) below ground level leads to difference in the values of (u_p/u_f) at a certain time and hydraulic conductivity will be greater than when the water depth increases.

Figure (6.62) illustrates that the dropping of water level to depth of (6 m) leads to development of negative values of pore water pressures at later time, i.e. (2500 days) and at hydraulic conductivity greater than (10^{-5} m/day). However, at time (1-250 days), the behaviour of water pressure was exactly compatible with the behaviour for water depth of (2-4 m) below the ground level. The appearance of negative values at the water depth of (6 m) can be attributed to that point (A) is situated above the water level and this will lead to appearance of the effect of negative pressure.

Figures (6.63) to (6.65) reveal that the appearance of the percentage (u_p/u_f) in negative values at all water levels, can be attributed to that point (B) is situated on the ground level (surface) and so that, at all water levels there will be a negative pressure. It is noticed also that the value of (u_p/u_f) directs toward the positive values at times (70-250 days) with the increase of hydraulic conductivity value. Anyhow, reverse behaviour was noticed at time (1 day) as the increase in hydraulic conductivity leads to increase in value of (u_p/u_f) at the negative direction.

At time (2500 days) and for a depth of water of (2 m) from the ground level, the percentage (u_p/u_f) will be positive and directed to the increase with the increasing of hydraulic conductivity above (10^{-5} m/day). At depth of water of (4 m) from ground level, the percentage (u_p/u_f) begins with a negative value at a hydraulic conductivity of (10^{-6} m/day) and increasing towards the positive values with the increasing of hydraulic conductivity values. At depth of water of (6 m) from ground

level, the positive value will reappear again at all values of hydraulic conductivity.

6.5.9 Vertical displacement vs. hydraulic conductivity

Figures (6.66), (6.67) and (6.68), present the relationship between the vertical displacement and hydraulic conductivity at point (A) (shown in Figure 6.2) at different elevations of water table.

Figures (6.69), (6.70) and (6.6.71), show the relationship between the vertical displacement and hydraulic conductivity at point (B) (shown in Figure 6.2) at different elevations of water table.

In these figures, δ_{vp} and δ_{vf} refer to vertical displacement in the case of partially and fully saturated soil, respectively.

Figures (6.66) and (6.67) reveal that the value of $(\delta_{vp}/\delta_{vf})$ at time of (1 day) increases proportionally with the value of hydraulic conductivity, and then returns to decrease when the hydraulic conductivity approaches the value of $(10^{-5}$ m/day). However, at times of (70-250 days), the value of $(\delta_{vp}/\delta_{vf})$ is decreasing with increasing the value of hydraulic conductivity.

Figure (6.68) shows that at time of (1 day), the value of $(\delta_{vp}/\delta_{vf})$ is increased with increase in hydraulic conductivity, and this increase is much greater at the hydraulic conductivity of $(10^{-3}$ m/day). At times (70-250 days), the value of $(\delta_{vp}/\delta_{vf})$ is increased with increase in hydraulic conductivity up to $(10^{-5}$ m/day) and then decreases with increase in hydraulic conductivity. At time of (2500 days), $(\delta_{vp}/\delta_{vf})$ begins with a high value then decreases with the increase in hydraulic conductivity values.

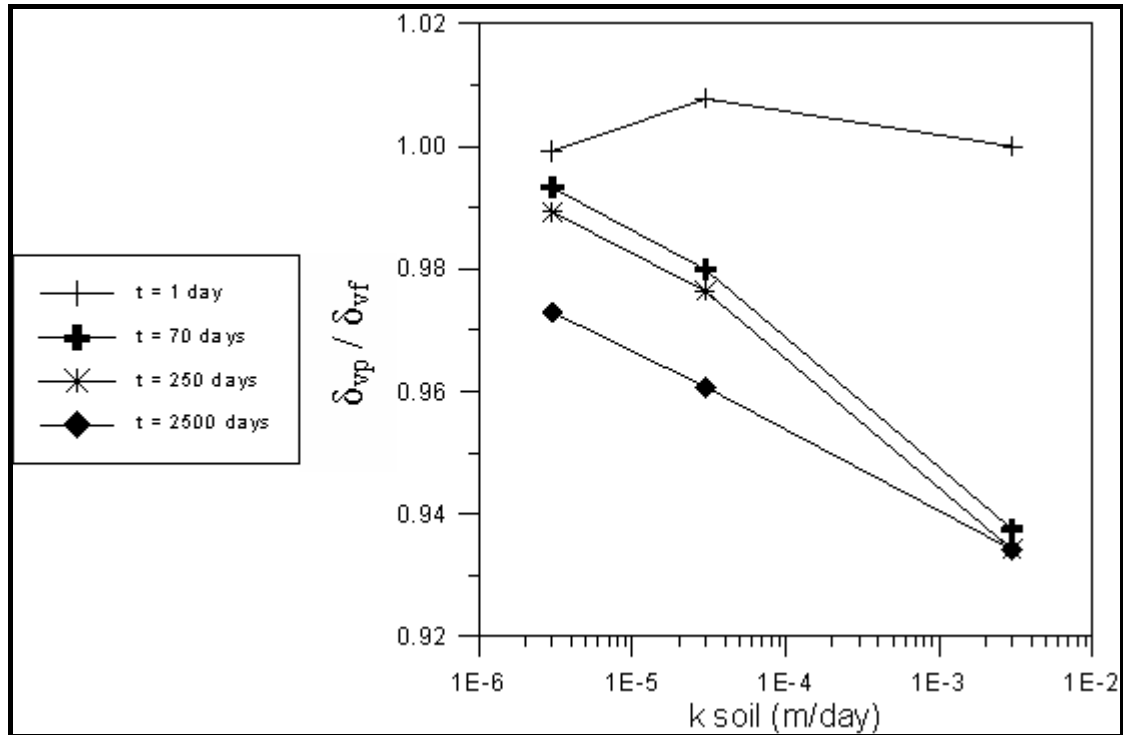


Fig. (6.66) The relation between $(\delta_{vp}/\delta_{vf})$ and soil hydraulic conductivity at point (A) when water table is at (2 m) from the ground level.

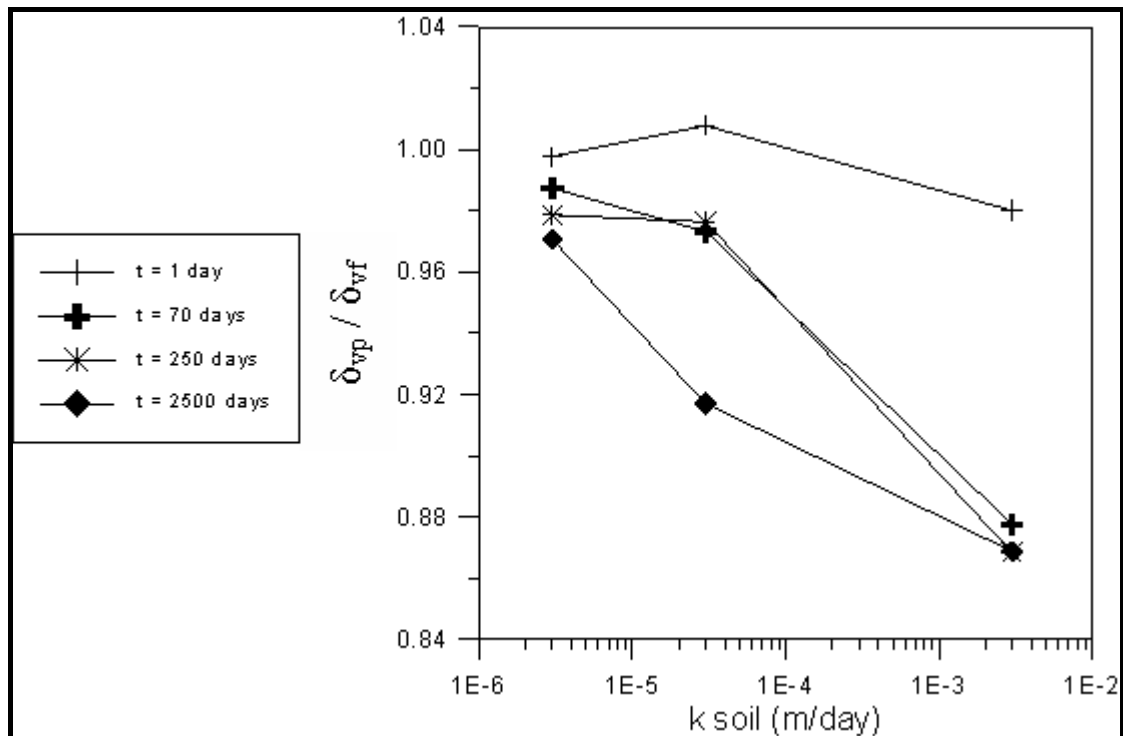


Fig. (6.67) The relation between $(\delta_{vp}/\delta_{vf})$ and soil hydraulic conductivity at point (A) when water table is at (4 m) from the ground level.

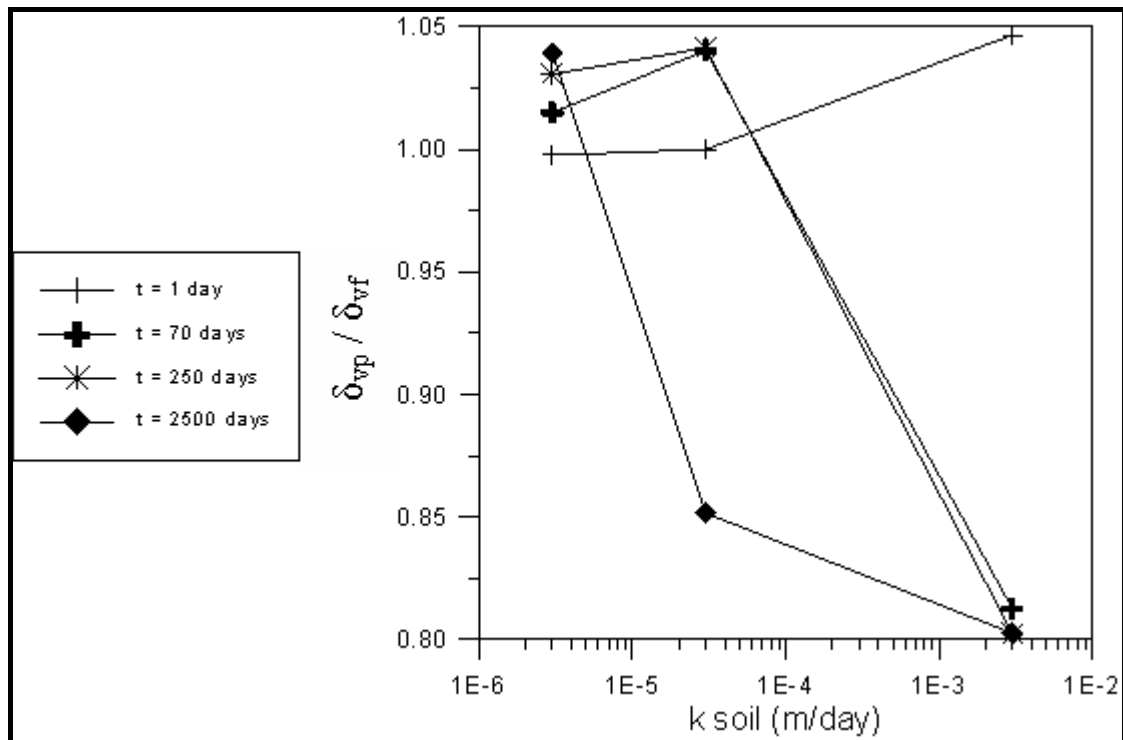


Fig. (6.68) The relation between $(\delta_{vp}/\delta_{vf})$ and soil hydraulic conductivity at point (A) when water table is at (6 m) from the ground level.

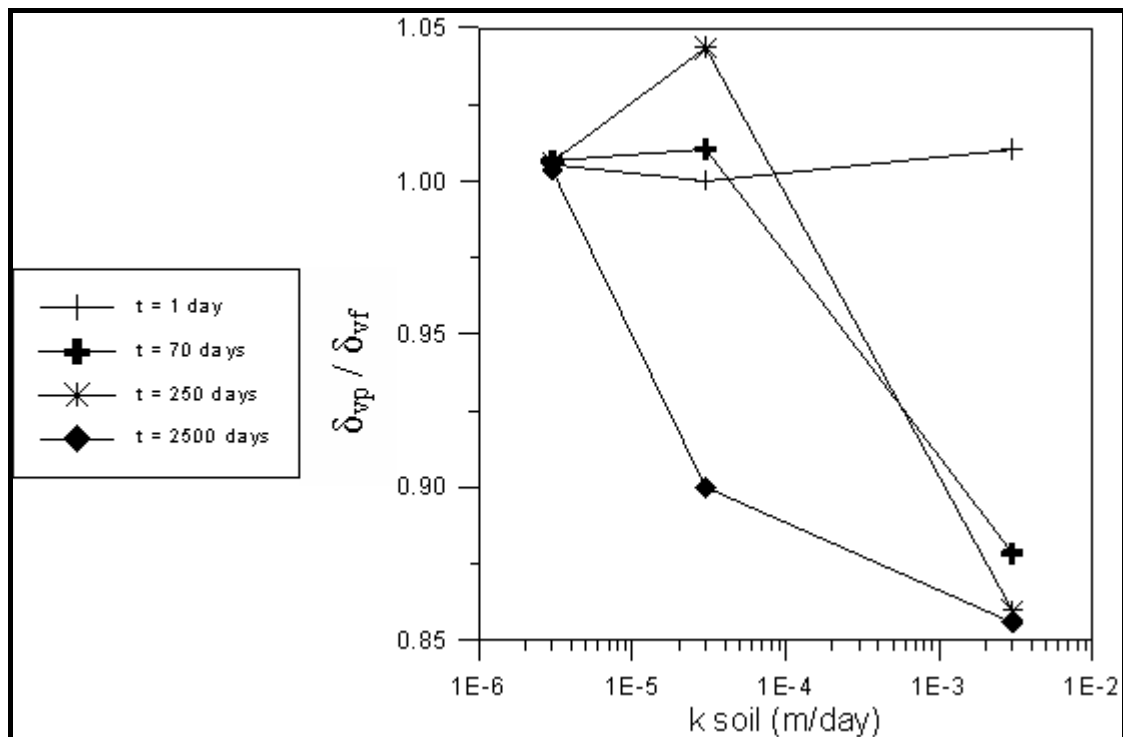


Fig. (6.69) The relation between $(\delta_{vp}/\delta_{vf})$ and soil hydraulic conductivity at point (B) when water table is at (2 m) from the ground level.

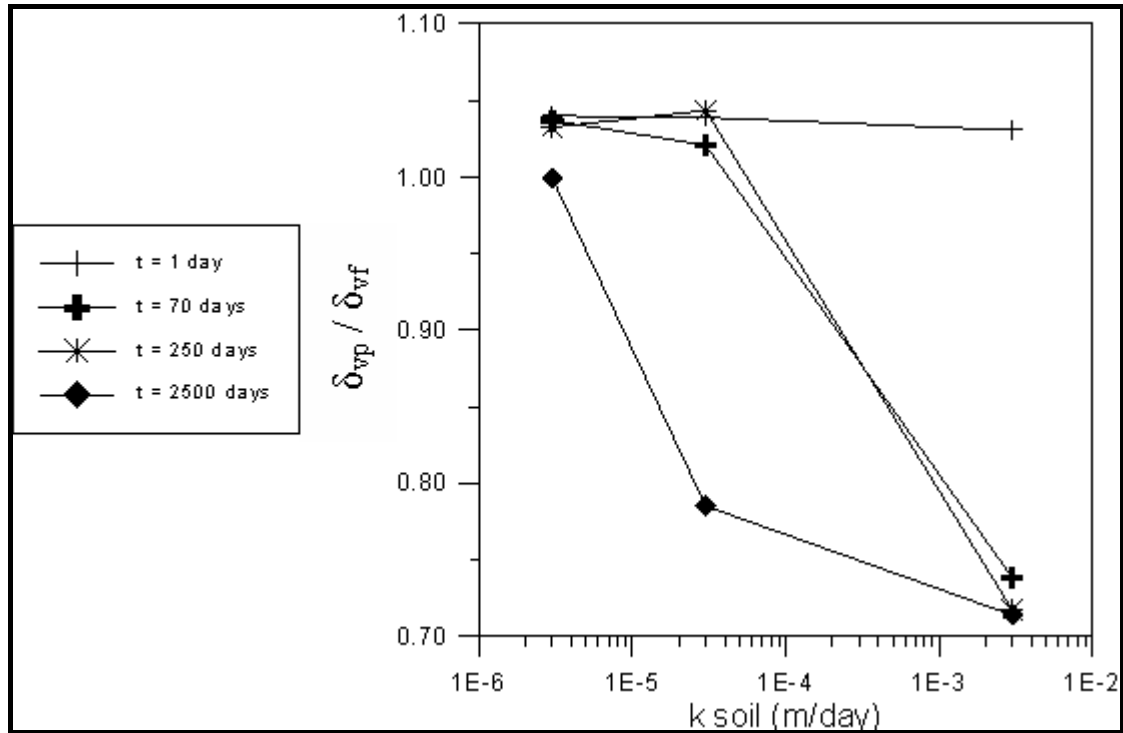


Fig. (6.70) The relation between $(\delta_{vp}/\delta_{vf})$ and soil hydraulic conductivity at point (B) when water table is at (4 m) from the ground level.

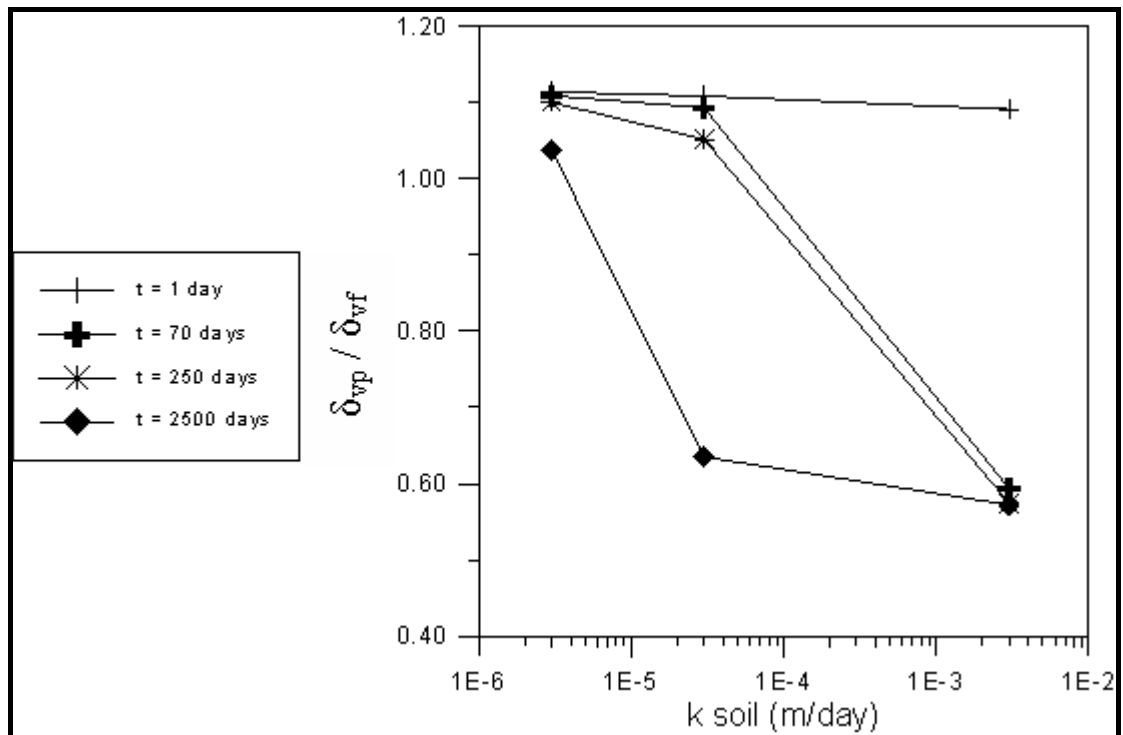


Fig. (6.71) The relation between $(\delta_{vp}/\delta_{vf})$ and soil hydraulic conductivity at point (B) when water table is at (6 m) from th

Figure (6.69) reveals that, at time of (1 day), the value of $(\delta_{vp}/\delta_{vf})$ decreases slightly when the hydraulic conductivity increases, but this value returns to increase when the hydraulic conductivity value passes the value of (10^{-5} m/day) but, however, with a slight increase. At times (70-250 days), the increase in hydraulic conductivity leads to increase in $(\delta_{vp}/\delta_{vf})$ up to the value of (10^{-5} m/day) and thereafter, the value is greatly decreased.

Figures (6.70) and (6.71) reveal that at time (1 day), there is no detected changes in the value of $(\delta_{vp}/\delta_{vf})$ with increasing value of hydraulic conductivity. At times (70-2500 days), the increase in hydraulic conductivity leads to a decrease in the value of $(\delta_{vp}/\delta_{vf})$. At time of (250 days) and when the water level is at (4 m), the value of $(\delta_{vp}/\delta_{vf})$ is increased slightly with increase of hydraulic conductivity of the soil. At a hydraulic conductivity of (10^{-5} m/day) , a the behaviour becomes opposite, as the value of $(\delta_{vp}/\delta_{vf})$ is decreased with increasing the value of hydraulic conductivity. Anyhow, this behaviour is not the case when the water level is at (6 m) below the ground level as the value of $(\delta_{vp}/\delta_{vf})$ is decreasing with increase of the hydraulic conductivity.

6.5.10 Pore water vs. time with H- modulus

Figures (6.72) to (6.74) illustrate different H-modulus functions. H1 is imported from the program SIGMA/W library for typical soils while H2 and H3 are assumed.

Figures (6.75) and (6.76) present the relationship between pore water pressure and time with change in H-modulus function at points (A) and (B) respectively .

Figure (6.75) reveals that the change in the modulus (H) has a considerable effect on the value of pore water pressure at early times.

Later, i.e. (after 200 days) this effect is decreased and the curves are compacted on each other after about (1000 days).

Figure (6.76) reveals that a complete compatibility of the curves on each other which leads to conclusion that, there is no great effect of the value of the modulus (H) on the water pressure at point (B).

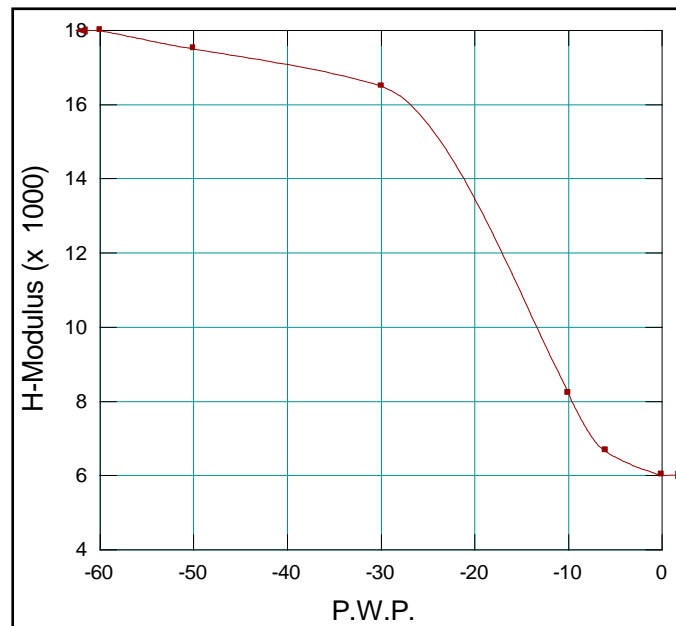


Fig. (6.72) H1-modulus function.

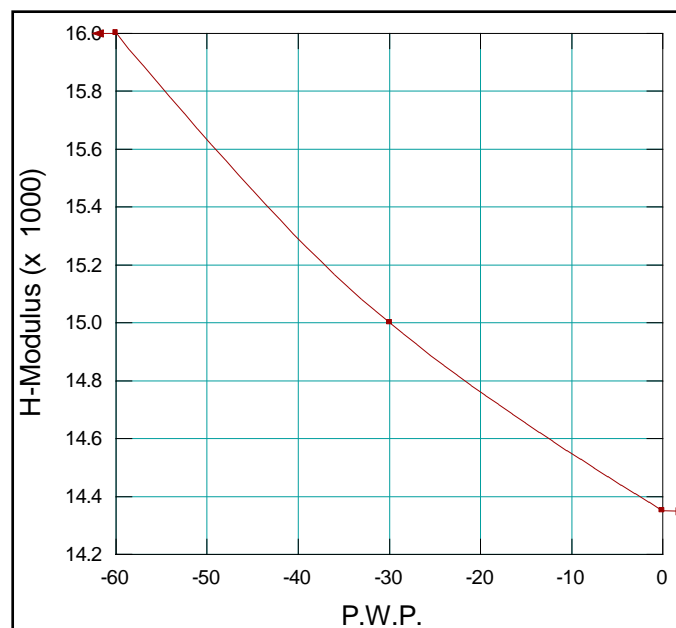


Fig. (6.73) H2-modulus function.

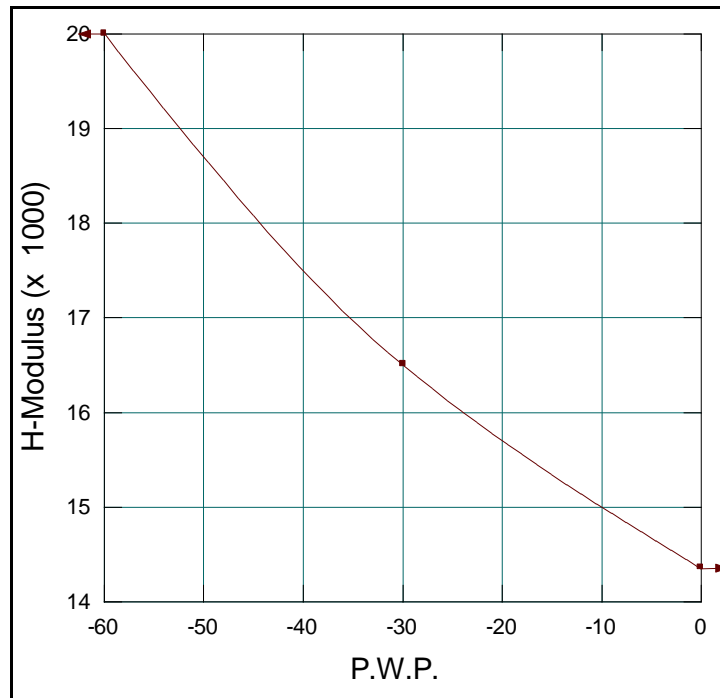


Fig. (6.74) H3-modulus function.

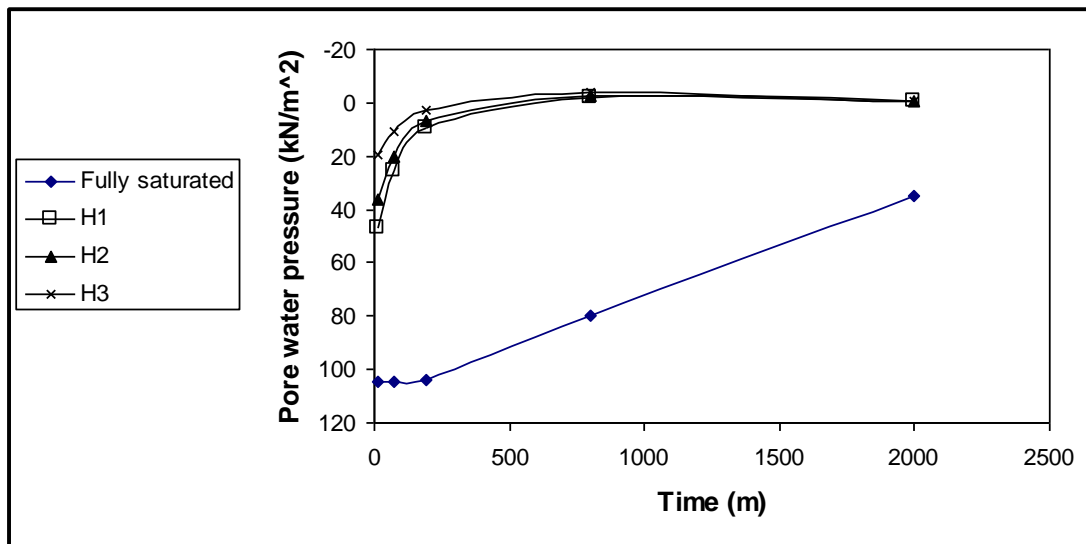


Fig. (6.75) The variation in pore water pressure with time at point (A) considering different H-modulus functions.

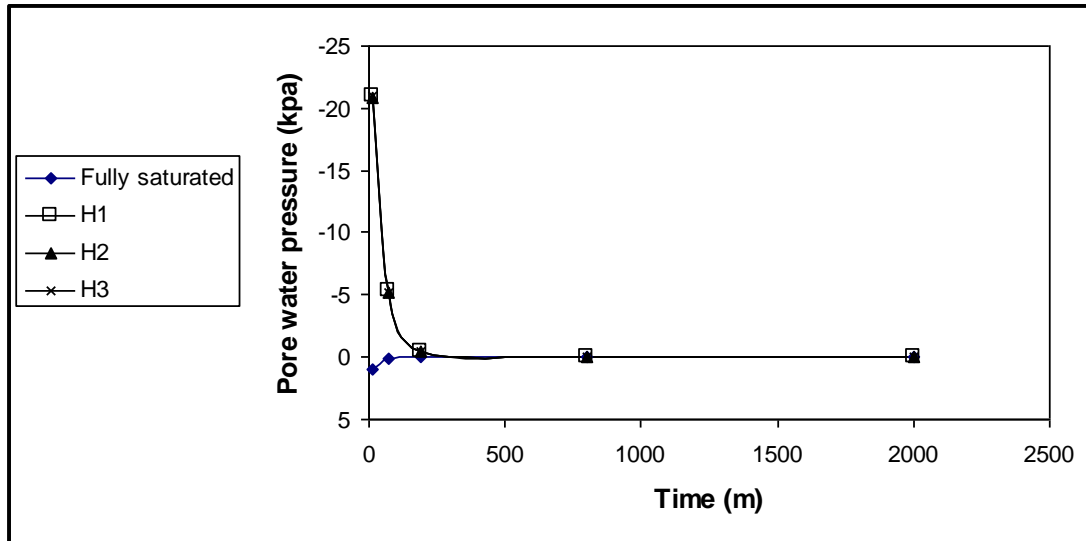


Fig. (6.76) The variation in pore water pressure with time at point (B) considering different H-modulus functions.

6.5.11 Vertical displacement vs. time with H- modulus

Figures (6.77) and (6.78) present the relationship between the vertical displacement and time at points (A) and (B) respectively considering different H-modulus functions.

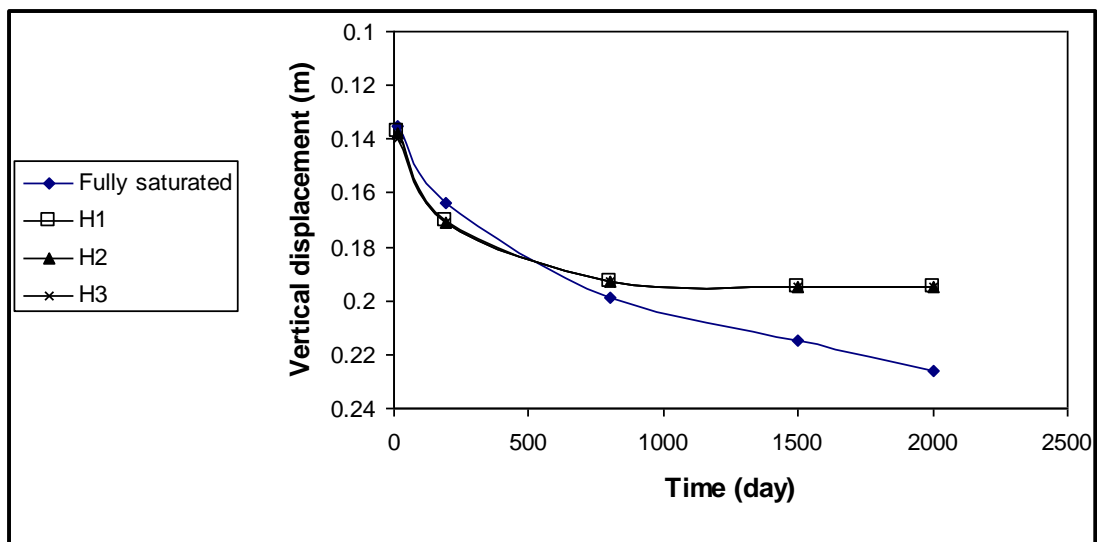


Fig. (6.77) The relation between vertical displacement and time at point (A) considering different H-modulus functions.

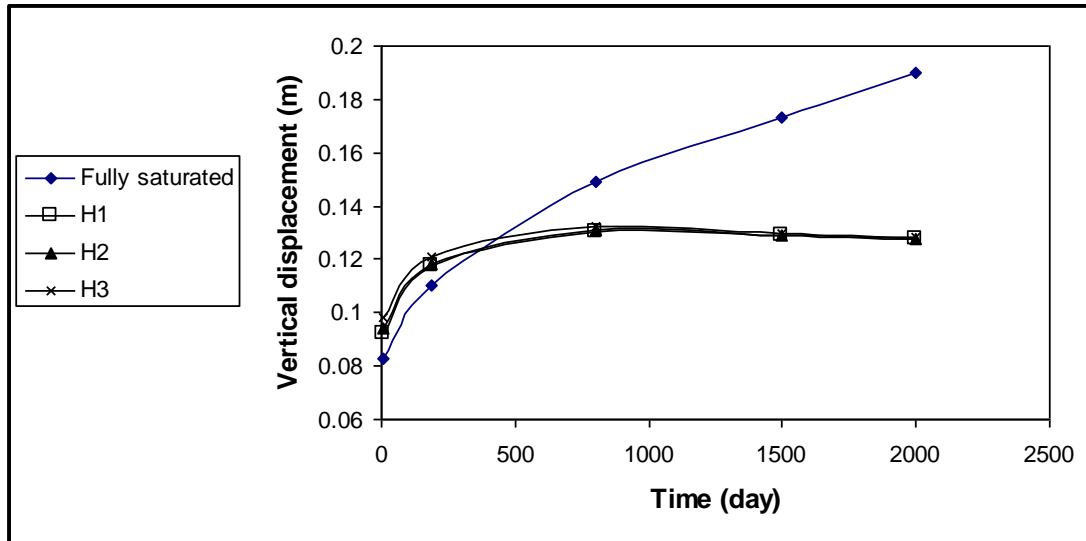


Fig. (6.78) The relation between vertical displacement and time at point (B) considering different H-modulus functions.

The change in the modulus (H) does not lead to occurrence of considerable changes in the vertical displacement, but there is a considerable difference between the values of vertical displacement of partially and fully saturated soils whatever the function of H-modulus is.

CHAPTER SEVEN

CONCLUSIONS AND RECOMMENDATIONS

CHAPTER SEVEN

CONCLUSIONS AND RECOMMENDATIONS

7.1 Conclusions

1. The effect of modulus of elasticity on the behaviour of unsaturated soil is apparent at early stages of consolidation and diminishes when the time proceeds. For example, at (10 days) the difference of (u_p/u_f) between modulus of elasticity of (2870 kN/m^2) and (20000 kN/m^2) is about (0.081) , while at time (2000 days) the difference becomes approximately zero.
2. When the clay layer consists of soft clay ($E_{\text{soil}} < 10000 \text{ kN/m}^2$), the effect of unsaturated soil is apparent, while effect of the modulus of elasticity diminishes when the soil is stiff. For example, at (10 days) the difference of $(\delta_{vp}/\delta_{vf})$ between modulus of elasticity of (2870 kN/m^2) and (10000 kN/m^2) is about (0.05) , while after modulus of elasticity of (10000) difference becomes approximately zero.
3. The phenomenon of Mendel-Cryer which leads to increase in the value of initial pore water pressure will eliminate part of negative pore water pressure at Aeration zone. The excess pore water pressure of fully saturated soil is greater than partially saturated soil and dissipation starts at fast rate and becomes slow with time .
4. The vertical displacement of fully saturated soil is greater than that of partially saturated soil. The vertical displacement is (36 cm) of fully saturated, while it is (29 cm) of partially saturated with water table at (6 m) from the ground level, this means about (19.44%) less than fully saturated case. The horizontal displacement of fully saturated soil is greater than partially saturated soil.

5. The effect of unsaturation becomes greater at the middle of the clay layer and near the center line of the embankment where more load concentrates than at its toe. At a certain depth of water and in case that all other parameters were fixed, the percentage of $(\delta_{hp}/\delta_{hf})$ would be maximum at the embankment toe rather than at the middle of clay layer.
6. The failure potential of unsaturated soil is less than that for fully saturated soil since the deviatoric stress $(\sigma_1 - \sigma_3)$ at all stages of consolidation is small.
7. The effect of hydraulic conductivity on the behaviour of unsaturated soil is apparent when the time proceeds. For example at time of (1 day), the increase of hydraulic conductivity, has no effect on the percentage (u_p/u_f) , while at a time of (70 days) and more, the condition of unsaturation has no effect on the case of low hydraulic conductivity of $(10^{-5}$ m/day) and below, but when the hydraulic conductivity is greater than $(10^{-5}$ m/day) and up to $(10^{-3}$ m/day), the effect of partial saturation will appear at time (70 and 250 days).
8. The change in the modulus (H) does not lead to occurrence of considerable changes in the vertical displacement, but there is a considerable difference between the values of vertical displacement of partially and fully saturated soils whatever the function of H-modulus is.

7.2 Recommendations

1. Finding experimentally the exact H-modulus function of Al-Mdaina embankment and finding its effect when the problem is resolved.

2. Resolving the problem using true layers of Al-Mdaina embankment.
3. Using other models for the soil, such as (nonlinear Elastic (Hyperbolic)).
4. Studying the relationship between the variation in hydraulic conductivity with suction.
5. Studying the effect of air coefficient of permeability on behaviour of partially saturated soil.

References

- Abdul Kareem E. Zainai (2002). "Solution of some problems of partially saturated soils using the finite element method", M.Sc. thesis, University of Baghdad.
- Adamson, A. W., and Gast, A. P. (1997). Physical chemistry of surfaces, 6th Ed., Wiley, New York.
- Alonso, E.E., Batlle, F., Gens, A. and Lloret, A. (1988). "Consolidation analysis of partially saturated soils application to earthdam construction" in "Numerical methods in geomechanics" Innsbruck , pp.1303-1308, edited by Swoboda. Publication Balkema.
- Alonso, E. E., Gens, A., and Josa, A. (1990). "A constitutive model for partly saturated soils." *Geotechnique*, 40(3), 405–430.
- Assouline, S., D. Tessier, and A. Bruand,(1998) A"conceptual model of the soil water retention curve", *Water Resour. Res.*, Vol. 34,pp. 223–231.
- Ba-Te, Zhang, L. Z., and Fredlund, D. G. (2005). "A general air-phase permeability function for airflow through unsaturated soils" *Proc.*, 2005 AS Geo-Frontiers, ASCE, Reston, Va.
- Ernest S. Berney, (2003). "The Thermodynamics of Three-Phase Partially Saturated Soil".
- Biot, M.A. (1941). "General theory of three-dimensional consolidation", *Journal of Applied Physics*(American Institute of Physics, Incorporated), pp. 155-164.
- Bishop, A. W., Alphan, I., Blight, G. E., and Donald, I. B. (1960). "Factors controlling the shear strength of partly saturated cohesive soils" *ASCE Research Conf. on Shear Strength of Cohesive Soils*, University of Colorado, Boulder, Colo., pp. 503–532.

-
- Blatz, J. A., and Graham, J. (2003). "Elastic-plastic modeling of unsaturated soil using results from a new triaxial test with controlled suction." *Geotechnique*, Vol. 53, No.(1), pp. 113–122.
 - Blight, G. E. (1971). "Flow of air through soils." *J. Soil Mech. Found. Div.*, 97(4), 607–624.
 - Brooks, R. H., and A. T. Corey, (1964). "Hydraulic properties of porous media", *Hydrol. Pap. 3*, Colorado State University, Fort Collins.
 - Childs, E. C., and Collis-George, N. (1950). "The permeability of porous materials", *Proc. R. Soc. London, Ser. A*, 201, pp. 392–405.
 - Chiu, T., and Shackelford, C. D. (1998). "Unsaturated hydraulic conductivity of compacted sand-kaolin mixtures", *Journal of Geotechnical and Geoenvironmental Engineering, ASCE*, Vol. 124, No.(2), pp. 160–170.
 - Christenson, H. G. (1988). "Adhesion between surfaces in undersaturated vapors—A re-examination of the influence of meniscus curvature and surface forces." *J. Colloid Interface Sci.*, 121(1), 170–178.
 - Daniel M. Tartakovsky, (2001). "Unsaturated hydraulic conductivity function based on a soil fragmentation process".
 - Dakshanamurthy, V., Fredlund, D.G. and Rahardjo, H., (1984). "Coupled three dimensional consolidation theory of unsaturated porous media", *Proceedings of the fifth International Conference on Expansive Soil*, Adelaide, South Australia, May 1984.
 - De Campos, T.M.P., Andrade, M.H.N. and Vargas Jr, E.A. (1992). "Unsaturated colluvium over rock slide in a forested site in Rio de Janeiro, Brazil In Landslides", *Proceedings of the Sixth International*

- Symposium, 10-14 February 1992, Christchurch, Volume 2, pp. 1357-1364. Ed D.H.Bell, pub Balkema.
- Derjaguin, B. V., and Churaev, N. V. (1981). “Structure of the boundary layers of liquids and its influence on the mass transfer in fine pores”, Progress in Surface and Membrane Science, edited by D. A. Cadenhead and J. F. Danielli, Academic, New York, pp. 69–130.
 - Donald, I. B. (1956). “Shear strength measurements in unsaturated non-cohesive soils with negative pore pressures”, Proc., 2nd Australia–New Zealand Conf. on Soil Mechanics and Foundation Engineering, Christchurch, New Zealand, pp. 200–205.
 - Ernest S. Berney, John F. Peters, Don M. Smith, THE THERMODYNAMICS OF THREE-PHASE PARTIALLY SATURATED SOIL.
 - Philip G. C. Smith (2003)" NUMERICAL ANALYSIS OF INFILTRATION INTO PARTIALLY SATURATED SOIL SLOPES
 - Fick, A. (1855). “Ueber diffusion.” Anu. der Phys. (Leipzig), 94, 59–86.
 - Fredlund, D. G., and Morgenstern, N. R. (1977). “Stress state variables for unsaturated soils”, Journal of Geotechnical Engineering Division, ASCE, Vol. 103, No.(5), pp. 447–466.
 - Fredlund, D. G., and Morgenstern, N. R. (1976). “Constitutive relations for volume change in unsaturated soils”, Canadian Geotechnical Journal, Vol. 13, No.(3), pp. 261–276.
 - Fredlund, D. G., Morgenstern, N. R., and Widger, R. A. (1978). “The shear strength of unsaturated soils”, Canadian Geotechnical Journal, Vol. 15, No.(3), pp. 313–321.
 - Fredlund, D. G., and Rahardjo, H. (1993). “The role of unsaturated soil behaviour in geotechnical practice”, Proceeding, 11th Southeast

-
- Asian Geotechnical Conference, Invited Keynote Address, Singapore, pp. 37–49.
- Fredlund, D. G. (2000). “The 1999 R. M. Hardy Lecture: The implementation of unsaturated soil mechanics into geotechnical engineering, R. M. Hardy Address”, Canadian Geotechnical Journal, Vol. 37, No.(5), pp. 963–986.
 - Fredlund, M. D., Stianson, J., and Rykaart, M., (2002a). “Application of automatic mesh refinement in the SVFlux and ChemFlux software packages”, Proceeding, 55th Canadian Geotechnical Conference., Niagara Falls, Ont., Canada, pp. 25–32.
 - Fredlund, M. D., Wilson, G. W., and Fredlund, D. G., (2002b). “Representation and estimation of the shrinkage curve”, Proceeding, 3rd International Conference on Unsaturated Soils, UNSAT 2002, Recife, Brazil, pp. 145–149.
 - Fredlund, M. D., Wilson, G. W., and Fredlund, D. G. (2002c). “Use of grain-size distribution for the estimation of the soil-water characteristic curve”, Canadian Geotechnical Journal, Vol. 39, No.(5), pp. 1103–1117.
 - Freeze, R. A., and Cherry, J. A. (1979). "Groundwater", Prentice-Hall, Englewood Cliffs, N.J.
 - Forsyth, P.A. (1988). "Comparison of the single-phase and two-phase numerical model formulation for saturated-unsaturated groundwater flow". Computer Methods in Applied Mechanics and Engineering, vol. 69, pp. 243-259.
 - Forsyth, P.A., Wu, Y.S. & Pruess, K. (1995) ‘Robust numerical methods for saturated unsaturated flow with dry initial conditions in heterogeneous media’. Advances in water resources, vol. 18, pp. 25-38.

-
- G. N. Smith, and Ian G. N. Smith, (1998). "Elements of Soil Mechanics".
 - Gan, J. K.M., Fredlund, D. G., and Rahardjo, H. (1988). "Determination of the shear strength parameters of an unsaturated soil using the direct shear test", Canadian Geotechnical Journal, Vol. 25, No.(8), pp. 500–510.
 - Gan, J. K.M., and Fredlund, D. G. (1996). "Shear strength characteristics of two saprolitic soils", Canadian Geotechnical Journal, Vol. 33, No.(4), pp. 595–609.
 - Gioda, G and Desideri, A. (1988). "Some numerical techniques for free-surface seepage analysis", in "Numerical methods in Geomechanics", edited by Swoboda , Balkema, pp. 71-84.
 - Gibson, R. E. (1953). "Numerical solution for some problems in the consolidation of clay. Proc. Inst. Civ. Engrs, Part 1, London.
 - Gibson, R. E. (1958). "The progress of consolidation in a clay layer increasing in thickness with time".
 - Israelachvili, J. N. (1991). "Intermolecular and surface forces", 2nd Ed., Academic, New York.
 - Jommi, C. (2000). "Remarks on the constitutive modeling of unsaturated soils", Experimental Evidence and Theoretical Approaches in Unsaturated Soils, edited by A. Tarantino and C. Mancuso, eds., Balkema, Rotterdam, The Netherlands, pp. 139–153.
 - Kim, J.M. (2000). "A fully coupled finite element analysis of water table fluctuation and land deformation in partially saturated soils due to surface loading", International Journal for Numerical Methods in Engineering, vol. 49, pp. 1101-1119.
 - Lam, L, Fredlund, D.G. and Barbour, S.L. (1987). "Transient seepage model for saturated-unsaturated soil systems: a geotechnical

- engineering approach", *Canadian Geotechnical Journal*, vol. 24, pp. 565-580.
- Liakopoulos, A. C. (1965). "Theoretical solution of the unsteady unsaturated flow problem in soils." *Bull. Int. Assoc. Sci. Hydrol.*, 10, pp. 5–39.
 - Lim, P. C., Barbour, S. L., and Fredlund, D. G. (1998). "The influence of the degree of saturation on the coefficient of aqueous diffusion", *Canadian Geotechnical Journal*, Vol. 35, No.(5), pp. 811–827.
 - Lloret, A. and Alonso, E.E (1980). "Consolidation of unsaturated soils including swelling and collapse behaviour", *Geotechnique*, vol. 30, No.(4), pp. 449-477.
 - Lyklema, J. (2000). "Fundamental of interface and colloid science", Vol. 3, Academic, New York.
 - Maatouk, A., Leroueil, S., and La Rochelle, P. (1995). "Yielding and critical state of a collapsible unsaturated silty soil", *Geotechnique*, Vol. 45, No.(3), pp. 465–477.
 - Matsumoto, M., and Kataoka, Y. (1988). "Study on liquid–vapour interface of water. I. Simulational results of thermodynamic properties and orientational structure", *Journal Chemical Physics*, Vol. 88, No.(5), pp. 3233–3245.
 - Matyas, E. L., and Radakrishna, H. S. (1968). "Volume change characteristics of partially saturated soils", *Geotechnique*, Vol. 18, No.(4), pp. 432–448.
 - Melinda, F., Rahardjo, H., Han, K. K., and Leong, E. C. (2004). "Shear strength of compacted soil under infiltration condition", *Journal of Geotechnical Geoenvironmental Engineering*, Vol. 130, No.(8), pp. 807–817.

-
- Mualem, Y. (1976). "Hysteretical models for prediction of the hydraulic conductivity of unsaturated porous media", *Water Resources Res.*, Vol. 12, No.(6), pp. 1248–1254.
 - Newman, G. P. (1996). "Heat and mass transfer in unsaturated soils during freezing", M.Sc. thesis, University of Saskatchewan, Saskatoon, Sask., Canada.
 - Ng, A.K.L. and Small, J.C. (2000). "Use of coupled finite element analysis in unsaturated soil problems", *International Journal for Numerical and Analytical Methods in Geomechanics*, Vol. 24, pp. 73-94.
 - Ng, C.W.W. and Pang, Y.W. (2000). "Influence of stress-state on soil-water characteristics and slope stability", *Journal of Geotechnical and Geoenvironmental Engineering*, ASCE. vol. 126, No.(2), Feb 2000.
 - Nishimura, T., and Fredlund, D. G. (2001). "Failure envelope of a desiccated, unsaturated silty soil", *Proceedings, XVth International Conference on Soil Mechanics and Foundation Engineering*, Istanbul, Turkey, pp. 615–618.
 - Pentland, J., Gitirana, G., Jr., and Fredlund, D. G. (2001). "Use of a general partial equation solver for solution of heat and mass transfer problems in geotechnical engineering", *Proceedings, 4th Brazilian Symposium on Unsaturated Soils, UNSAT 2001*, Porto Alerge, RS, Brazil, pp. 29–36.
 - Pham, H. Q., Fredlund, D. G., and Barbour, S. L. (2003). "Estimation of the hysteretic soil-water characteristic curves from the drying boundary curve", *Proceedings, 56th Canadian Geotechnical Conf.*, Vol. 2, Winnipeg, Canada, pp. 115–121.

-
- Pham, H. Q. (2005). "Volume-mass constitutive relations for unsaturated soils", Ph.D. thesis, University of Saskatchewan, Saskatoon, Sask., Canada.
 - Philip G. S., (2003). "numerical analysis of infiltration in to partially saturated soil slopes", Ph.D. thesis, University of London, London, England.
 - Schuurman, E. (1966). "The compressibility of an air/water mixture and a theoretical relation between the air and water pressures", *Geotechnique*, Vol. 16, No.(4), pp. 269–281.
 - Scott, R. K. (1963), "Principles of soil mechanics". Addison Wesley, Reading, Mass.
 - SEEP/W, (Version 5) (2002). "Manuel for Finite Element Seepage Analysis".
 - SIGMA/W, (Version 5) (2002). " Manuel for Finite Element Stress and Deformation Analysis".
 - Shmuel Assouline (2001)" Unsaturated hydraulic conductivity function based on a soil fragmentation process".
 - Skempton, A.W. and Bjerrum, L. (1957). "A contribution to settlement analysis of foundations on clay". *Geotechnique*. vol.(7), No.(4), pp. 168- 178.
 - T. William Lambe and Robert V. Whitman, (1979). "Soil Mechanics".
 - Terzaghi, K. (1943). *Theoretical soil mechanics*, John Wiley, NewYork.
 - Thieu, N. T. M., Fredlund, M. D., Fredlund, D. G., and Vu, H. Q. (2001). "Seepage modelling in a saturated/unsaturated soil system", *Proceedings, International Conference on Management of the Land and Water Resources*, Hanoi, Vietnam, pp. 49–56.

-
- Toll, D. G. (1990). "A framework for unsaturated soil behavior", *Geotechnique*, Vol. 40, No.(1), pp. 31–44.
 - Townsend, R. M., and Rice, S. A. (1991). "Molecular dynamic studies of the liquid-vapour interface of water." *Journal Chemical Physics*, Vol. 94, No.(3), pp. 2207–2218.
 - Van Genuchten, M. T.,(1980) "A closed-form equation for predicting the hydraulic conductivity of unsaturated soils", *Soil Sci. Soc. Am. J.*, Vol. 44, pp. 892–898.
 - Vanapalli, S. K., Fredlund, D. G., Pufahl, D. E., and Clifton, A. W. (1996). "Model for the prediction of shear strength with respect to soil suction." *Canadian Geotechnical Journal*, vol.33, No.(3), pp. 379–392.
 - Watson, K. K., and Sardana, S. A. (1987). "Numerical study of the effect of hysteresis on post-infiltration redistribution", *Proc., Int. Conf. on Infiltration Development and Application*, Water Resources Center, Univ. of Hawaii, Manoa, Honolulu, pp. 241–250.
 - Wheeler, S. J., and Sivakumar, V. (1995). "An elasto-plastic critical state framework for unsaturated soil", *Geotechnique*, Vol. 45, No.(1), pp. 35–53.
 - Wong, T.T., Fredlund, D.G. and Krahn, J. (1998). "A numerical study of coupled consolidation in unsaturated soils". *Canadian Geotechnical Journal*, Vol. 35, pp. 926-937.
 - Zienkiewicz, O.C. and Taylor, R.L., (1989). "The Finite Element Method", 4th Edition, Vol. 1. McGraw-Hill.

خلاصة البحث

المسالة الثنائية الطور الأكثر شيوعا في الأوساط المسامية هي جريان الهواء والماء. وهذا على سبيل المثال يوجد في المناطق غير المشبعة، عندما ينفذ الماء خلال مسامات مشبعة جزئيا إلى الماء الأرضي. جريان السائل في المنطقة غير المشبعة يسيطر عليه بواسطة مركبة من الجاذبية والخاصية الشعرية وقوى اللزوجة.

السلوك الميكانيكي للترب المشبعة جزئيا يمكن أن يكون مختلف جدا عن سلوك الترب المشبعة كليا. لقد ثبت منذ زمن طويل انه لمثل هذه الترب فان التغير في الامتصاص لا يكون له نفس تأثير التغير في الإجهاد المسلط، وكنيجة لذلك فان مبدأ الجهد الفعال لا يكون قابل للتطبيق. لذلك النماذج التكوينية التقليدية والتي تستند على هذا المبدأ تكون محدودة الاستخدام عند تحليل المسائل الجيوتكنيكية المتضمنة وجود مناطق تربة مشبعة جزئيا.

في هذه الأطروحة تم العامل مع مسألة سدة المدينة التجريبية. استخدم برنامجا العناصر المحددة ($SIGMA/W$) و ($SEEP/W$) ، وتم استخدام عناصر رباعية الأضلاع بثماني عقد لتمثيل هيكل التربة و ضغط ماء المسام. دراسة معاملات أجريت و معاملات متعددة غيرت قيمها لإيجاد تأثير هذه العوامل على سلوك التربة المشبعة جزئيا. هذه العوامل تتضمن معامل مرونة التربة (E) و معامل النفاذية (k) ومعامل التربة غير المشبعة (H).

توصل البحث إلى إن تأثير معامل المرونة على سلوك التربة غير المشبعة يظهر في المراحل الأولى من عملية الانضمام ويتلاشى مع تقدم الزمن. وعندما تتكون طبقة التربة من طين رخو يكون تأثيره واضح في التربة غير المشبعة بينما يتلاشى هذا التأثير عندما تكون التربة قوية.

وتبين أن الزيادة في ضغط ماء المسام في حالة الإشباع الكلي تكون اكبر منها في حالة الترب المشبعة جزئيا. بالإضافة إلى إن الانضمام العمودي في حالة التربة المشبعة كليا يكون اكبر منه في حالة التربة المشبعة جزئيا.

كما تم التوصل إلى أن احتمالية الفشل في التربة غير المشبعة تكون اقل منها للتربة المشبعة كلياً بما أن إجهاد الانحراف ($3\sigma-1\sigma$) في كل مراحل الانضمام اصغر.

خصائص الانضمام في الترويج غير المشروعة

رسالة مقدمة إلى قسم هندسة البناء والإنشاءات في الجامعة التكنولوجية وهي

جزء من متطلبات نيل درجة الماجستير في علوم الهندسة المدنية في قسم

هندسة البناء والإنشاءات

من قبل

فiras جواد كاظم

(بكالوريوس هندسة البناء والإنشاءات)

2003

أيار 2008 ميلادي

جمادى الأولى 1429 هجرية